Subcellular localization and dynamics of transmembrane and membrane associated proteins in *Corynebacterium glutamicum*

Gustavo Benevides Martins

Dissertation

Zur Erlangung des Doktorgrades der Naturwissenschaften

(Dr. rer. nat.)

an der Fakultät für Biologie der

Ludwig-Maximilians Universität München

July 2019

Subcellular localization and dynamics of transmembrane and membrane associated proteins in *Corynebacterium glutamicum*

PhD thesis by Gustavo Benevides Martins

Supervised by Professor Dr. Marc Bramkamp

Ludwig-Maximilians Universität

Biology, Department I

Die vorliegende Doktorarbeit wurde im Zeitraum von April 2015 bis April 2019 an der Ludwig-Maximilians-Universität München in Martinsried durchgeführt.

"É necessário fazer outras perguntas, ir atrás das indagações que produzem o novo saber, observar com outros olhares através da história pessoal e coletiva, evitando a empáfia daqueles e daquelas que supõem já estar de posse do conhecimento e da certeza."

Mario Sergio Cortella

Eidesstattliche Erklärung

Hiermit versichere ich an Eides statt, dass ich die vorliegende Arbeit selbstständig verfasst habe, keine als die angegebenen Quellen und Hilfsmittel benutzt wurden und alle Zitate kenntlich gemacht sind. Des Weiteren versichere ich, nicht anderweitig ohne Erfolg versucht zu haben, eine Dissertation einzureichen oder mich einer Doktorprüfung zu unterziehen. Die vorliegende Dissertation liegt außerdem keiner anderen Prüfungskommission vor.

I hereby confirm that I have written the accompanying thesis by myself, without contributions from any sources other than those cited in the text. This also applies to all graphics, drawings and images included in this thesis. Moreover, I declare that I have not submitted or defended a dissertation previously without success. This thesis has not been presented to any other examining board.

München, 21. Juni 2019

_____

Gustavo Benevides Martins

Index

List of publications

I. **Martins, G. B.**, **Giacomelli, G., Goldbeck, O., Seibold, G. M., Bramkamp, M.** 2019. Substrate-dependent cluster density dynamics of *Corynebacterium glutamicum* phosphotransferase system permeases. Mol Microbiol, **111**(5):1335-1354

Contributions to Publications

I. G.B.M. and M.B. designed the study and wrote the manuscript, G.B.M. constructed the plasmids, strains, as well as cell wall-deficient cells, performed all the biochemical assays, fluorescence microscopy and data analysis, G.G. designed and performed the PALM analysis and wrote its methodology, O.G. constructed and characterized the strains CGM007, CGM008 and CGM009 and provided fluorescence microscopy images of strain CGM009, G.S. reviewed the manuscript.

Abbreviations

ABC	ATP binding cassette
AMP	Adenosine monophosphate
BHI	Brain heart infusion
cAMP	cyclic AMP
CCR	carbon catabolite repression
CL	Cardiolipin
CTF	Corrected total fluorescence
CWD	Cell wall-deficient
DCS	D-Cycloserine
EI	Enzyme I
EII	Enzyme II
FRAP	Fluorescence recovery after photobleaching
HPLC	High Performance Liquid Chromatography
HPr	Histidine-containing phosphocarrier protein
KW	Kruskal-Wallis
LB	Lysogeny Broth
mRNA	Messenger Ribonucleic acid
MS	Mechanosensitive
NB	Nutrient broth
OD	Optical density
PALM	Photoactivated Localization Microscopy
PCR	Polymerase chain reaction
PEP	Phosphoenolpyruvate
PG	phosphatidyl-glycerol
PI	phosphatidyl-inositol
PPP	Pentose phosphate pathway
PSF	Point spread function
PTS	Phosphotransferase system
PVDF	Polyvinylidene difluoride
RFU	Relative fluorescence unit

RC   Respiratory chain

RT   Room temperature

SDHA   Succinate Dehydrogenase Complex Flavoprotein Subunit A

SDS-PAGE   Sodium dodecyl sulfate- Polyacrylamide gel electrophoresis

SW   shapiro-wilk

TBS   Tris-buffered saline

TM   Transmembrane

Abstract

The cytoplasmic membrane of *Corynebacterium glutamicum* comprises 660 predicted membrane integral proteins of various functional categories, including transport, signal transduction, protein translocation, proteolysis and energy metabolism. Being an important industrial producer of amino acids, studying the membrane proteome of this organism is relevant for a better understanding of its fundamental processes and possible targeted optimizations. Here, we analyzed the subcellular localization of different transmembrane and membrane-associated proteins of *Corynebacterium glutamicum*, including the fructose specific PtsF and the glucose specific PtsG transporters, the respiratory chain complex II component SdhA, the small-conductance mechanosensitive channel YggB, and the polar/septa scaffold DivIVA. Using widefield and single molecule localization microscopy, we discovered that PtsG and PtsF form membrane embedded clusters with no defined positions. A similar pattern was observed for SdhA, which curiously, seem to colocalize with PtsF in our widefield microscopy experiments. Size, number and fluorescence of the observed PTS clusters change upon presence or absence of the transported substrate. In presence of the transport substrate, clusters significantly increased in size. Photo-activated localization microscopy (PALM) data revealed that, in presence of different carbon sources, the number of EII proteins per cluster remains the same, however the density of these clusters reduces. Our work reveals a simple mechanism for efficient membrane occupancy regulation. Clusters of PTS EII transporters are densely packed in absence of a suitable substrate. In presence of a transported substrate, the EII proteins in individual clusters occupy larger membrane areas. This mechanism allows for efficient use of the limited membrane space under varying growth conditions without need of protein removal and re-synthesis. Clustering was also observed in YggB, that localized in a punctate pattern of different intensities at the membrane. By changing the NaCl concentration in medium, ranging from 0 mM to 170 mM, we could observe *C. glutamicum* cells under different degrees of osmotic

stress, ranging from hypoosmotic to low hyperosmotic. The extreme studied treatments resulted in impaired growth, which suggests that the cells were indeed under constant osmotic stress. Under such conditions, no changes in YggB-mNeonGreen foci number or fluorescence were observed, hinting that *yggB* expression is constitutive and that prolonged exposure to osmotic stress does not result in the recruitment of more channels to the membrane. Finally, we studied the dynamics of DivIVA in cells of various shapes, including L-form cells with different morphologies by performing widefield microscopy and fluorescence recovery after photobleaching (FRAP) experiments with a strain expressing DivIVA-mCherry. DivIVA is a membrane-associated protein that serves as a scaffold for different proteins related to cell division and cell growth. Cell division in bacterial L-forms is unlike the coordinated and precise division observed in cell-walled bacteria. It takes place randomly, not necessarily linked to the divisome and is highly influenced by perturbations in the surrounding environment. Due to this, it is not uncommon to find L-form cells with multiple, parts of, or no chromosomes. Still, in these cells, DivIVA continues to localize in regions of negative curvatures, characterized as bumps in the cytoplasmic membrane. In completely spherical cells, with no regions of higher negative curvature, DivIVA localize as larger foci. Our FRAP results demonstrated that in regions of bumps, the diffusion rate of DivIVA-mCherry is similar to the one observed for poles of rod-shaped cells, but with a significant lower half-time recovery. Furthermore, the diffusion rate on smooth surfaces was more than double, and the half-time recovery less half as the one observed in bumps. This suggests that DivIVA is significantly more mobile in such regions. Moreover, using novel microscopy techniques, the work presented on this thesis shed a light on unexplored facets of membrane protein compartmentalization in *Corynebacterium glutamicum*.

Zusammenfassung

Die Zytoplasmamembran von *Corynebacterium glutamicum* beherbergt 660 annotierte Membranintegralproteine, die verschiedene Funktionen in Transport, Signaltransduktion, Proteintranslokation, Proteolyse und Energiestoffwechsel wahrnehmen. Da *C. glutamicum* eine wichtige Rolle in der industriellen Aminosäureproduktion spielt, ist die Untersuchung des Membran-Proteoms wichtig für ein besseres Verständnis grundlegender Prozesse und gezielter Optimierung der Produktionsprozesse. In dieser Arbeit wurde die subzelluläre Lokalisation verschiedener Transmembran- und membranassoziierter Proteine von *C. glutamicum* analysiert. Dazu gehörten der Fructose-spezifische PtsF- und der Glucose-spezifische PtsG-Transporter, die Komponente SdhA des Komplexes II der Atmungskette, der mechanosensitive Kanal YggB und das am Zellpol lokalisierte Gerüstprotein DivIVA. Unter Verwendung von Weitfeld- und Einzelmolekül-Lokalisationsmikroskopie konnte gezeigt werden, dass PtsG und PtsF in Membranen eingebettete Cluster ohne definierte Positionen bilden. Ein ähnliches Muster wurde für SdhA beobachtet, das in Weitfeldmikroskopie-Experimenten interessanterweise mit PtsF zu kolokalisieren scheint. Größe, Anzahl und Fluoreszenz der beobachteten PTS-Cluster änderten sich bei Anwesenheit oder Abwesenheit des transportierten Substrats. In Gegenwart des transportierten Substrats nahm die Größe der Cluster signifikant zu. Daten der photoaktivierbaren Lokalisationsmikroskopie (PALM) ergaben, dass in Gegenwart verschiedener Kohlenstoffquellen die Anzahl der EII-Proteine pro Cluster konstant bleibt, die Dichte dieser Cluster jedoch abnimmt. Diese Arbeit zeigt einen einfachen Mechanismus zur effizienten Regulierung der Membranbelegung. Cluster von PTS-EII-Transportern sind in Abwesenheit eines geeigneten Substrats dicht gepackt. In Gegenwart eines transportierten Substrats besetzen die EII-Proteine in einzelnen Clustern größere Membranflächen. Dieser Mechanismus ermöglicht die effiziente Nutzung des begrenzten Membranraums unter verschiedenen Wachstumsbedingungen, ohne dass Proteine entfernt und erneut synthetisiert werden müssen. Clusterbildung wurde auch bei YggB beobachtet, das in einem punktförmigen Muster unterschiedlicher Intensität an der Membran lokalisiert war. Durch Änderung der NaCl-Konzentration im Medium im Bereich von 0 mM bis 170 mM konnten wir *C. glutamicum*-Zellen unter osmotischem Stress beobachten, der von hypo- bis leicht hyperosmotisch reichte. Unter Extrembedingungen ließ sich ein negativer Effekt auf

Zusammenfassung

das Wachstum beobachten, was darauf hindeutet, dass die Zellen tatsächlich einem konstanten osmotischen Stress ausgesetzt waren. Auch unter solchen Bedingungen wurden keine Änderungen der Anzahl an YggB-mNeonGreen-Foci oder der Fluoreszenz beobachtet, was darauf hindeutet, dass die *yggB*-Expression konstitutiv ist und dass eine längere Exposition gegenüber osmotischem Stress nicht zur Rekrutierung weiterer YggB-Kanäle an die Membran führt. Schließlich wurde die Dynamik von DivIVA in Zellen verschiedener Formen, einschließlich L-Formen mit unterschiedlichen Morphologien, untersucht. Hierfür wurde ein DivIVA-mCherry-exprimierender Stamm sowohl mittels Weitfeldmikroskopie, als auch mittels Fluorescence Recovery After Photobleaching (FRAP) analysiert. DivIVA ist ein membranassoziiertes Protein, das als Gerüst für verschiedene Proteine dient, die mit der Zellteilung und dem Zellwachstum zusammenhängen. Die Zellteilung in bakteriellen L-Formen unterscheidet sich von der koordinierten und präzisen Teilung, die bei Bakterien mit Zellwänden beobachtet wird. Sie findet zufällig statt, ist nicht notwendigerweise mit dem Divisom verbunden und wird stark von Störungen in der Umgebung beeinflusst. Aus diesem Grund ist es nicht ungewöhnlich, L-förmige Zellen mit mehreren, oder auch ganz ohne Chromosomen zu finden. Dennoch lokalisiert DivIVA in diesen Zellen weiterhin in Regionen mit negativen Krümmungen, die als „Ausbuchtungen" in der Zytoplasmamembran zu sehen sind. In vollständig kugelförmigen Zellen ohne Bereiche mit höherer negativer Krümmung lokalisiert DivIVA in größeren Foci. Unsere FRAP-Experimente zeigten, dass die Diffusionsrate von DivIVA-mCherry in Regionen mit hohes Membrankrümmung der von Polen stäbchenförmiger Bakterien ähnelt, jedoch mit signifikant geringerer Halbwertszeit in der Erholungsphase. Unsere Daten zeigen, dass die DivIVA Dynamik von der Zellgeometrie beeinflusst wird. Da DivIVA über die Rekrutierung des Zellwand-Synthese Apparates an der Ausbildung der Zellmorphologie beteiligt ist, stellt dieses System ein einfaches aber effektives Konzept der bakteriellen Selbstorganisation dar. Darüber hinaus war die Diffusionsrate auf wenig gekrümmten Oberflächen mehr als doppelt so hoch und die Halbwertszeit halb so hoch wie die Diffusionsrate in Regionen mit hohes Membrankrümmung. Dies deutet darauf hin, dass DivIVA in solchen Regionen wesentlich mobiler ist. zusammenfassend klären die in dieser Arbeit vorgestellten Daten mithilfe neuartiger Mikroskopietechniken noch nicht erforschte Facetten der Kompartimentierung von Membranproteinen in *Corynebacterium glutamicum* auf.

1   Introduction

1.1   The cytoplasmic membrane of *Corynebacterium glutamicum*

Corynebacterium glutamicum is a facultative anaerobic, gram-positive, non-motile, non-sporulating bacterium that in nature, inhabits mainly the surface layers of the soil. Members of the Corynebacterineae sub-order typically display a distinctive mycolic acid layer in the cell wall and a GC rich genomic DNA. It was discovered over 60 years ago as a natural producer of glutamate, and its significance in industry has been increasing over the years (Gourdon & Lindley 1999). Annually, over 2.6 million tons of L-glutamate and 1.96 million tons of L-lysine are produced through its industrial utilization (Heider *et al.* 2014). Hence the increased economic interest in metabolic engineering of strains to both enhance production of already secreted compounds, or to enable production of further amino acids or chemicals such as vitamins, ethanol, isobutanol, succinate and lactate (Litsanov, Brocker, & Bott 2012). *C. glutamicum* is also closely related to important pathogens such as *Mycobacterium tuberculosis*, *M. leprae* and *C. diphteriae*, and since fundamental aspects of bacterial cell biology are conserved within the Corynebacterianae, *C. glutamicum* serves as an excellent model organism to study spatio-temporal aspects of the bacterial cell cycle in this group of bacteria (Donovan *et al.* 2013; Bohm *et al.* 2017).

The cytoplasmic membrane of *C. glutamicum* is mainly composed of negatively charged phosphatidyl-glycerol, phosphatidyl-inositol and cardiolipin, and comprises circa 660 predicted membrane integral proteins (22% of the whole genome) of various functional categories, including transport, signal transduction, protein translocation, proteolysis and energy metabolism (Kalinowski *et al.* 2003). In several bacterial species, the lipid composition of the cytoplasmic membrane differs between cell poles and the rest of the cell envelope (Laloux & Jacobs-Wagner 2014). Due to its intrinsic curvature, poles are enriched with cardiolipins (CL). CL are anionic diphosphatidylglycerols composed of a small hydrophilic tip and a big

hydrophobic base. The phosphate head group provides the interface for the cytosol while the unsaturated fatty acyl chains provide the hydrophobic core (Claypool 2009). This structure makes it energetically favorable for CL molecules to localize at highly negatively curved bilayers such as bacterial cell poles inner membranes (Mileykovskaya *et al.* 2003; Huang and Ramamurthi 2010), and some proteins are known to interact preferentially with anionic phospholipids (Mileykovskaya *et al.* 2003; Renner & Weibel 2012; Laloux & Jacobs-Wagner 2014). Thus, proteins with affinity for cardiolipins bind more frequently to the cell poles. In this sense, the lipid composition of the cytoplasmic membrane in the cell poles can function as a partial sign for protein localization. Moreover, CL has been shown to have a predisposition to be organized into clusters (Epand and Epand 2009), tending to form microdomains, whose organization are driven by lipid-protein interactions and exist in specific regions of high membrane curvature. Membrane microdomains facilitate distinct protein and lipid assemblies, such as chromosomal and cell division-related events (Mileykovskaya & Dowhan 2005; Matsumoto *et al.* 2006).

Most polar proteins are recruited to the cell poles via interaction with a protein or a complex already present at the pole (Laloux and Jacobs-Wagner 2014). Some proteins can serve as polar landmarks for other proteins, which can themselves recruit others (Laloux & Jacobs-Wagner 2014). DivIVA is a cytoplasmic protein that works as a polar/septa scaffold in processes related to cell growth and cell division. It is highly conserved in Gram-positive bacteria, and in *B. subtilis*, it is responsible for the polar localization of the division inhibitor, MinC/MinD via interaction with MinJ (Edwards & Errington 1997). In *C. glutamicum*, it has been shown to interact with the transglycosylase RodA (Sieger *et al.* 2013; Arora *et al.* 2018). Furthermore DivIVA interacts with ParB in order to tether chromosomal origins to the cell poles (Donovan *et al.* 2013). DivIVA localizes in areas with negative curvature, and although single DivIVA molecules are too small to sense any membrane curvature, it has been shown that its monomers oligomerize *in vitro* and *in vivo*, forming dimers, which in turn form tetramers that can further

assemble in larger structures, finally achieving cooperative, long-range sensor of membrane curvature multimers (Muchova *et al.* 2002; Stahlberg *et al.* 2004). Although both CL and DivIVA preferentially localize at regions of negative curvature, they differ in the mechanism for such localization: while CL localize in these regions due to its primary structure, DivIVA uses 'molecular bridging', where the mutual interaction between DivIVA oligomers, their large size, plus their affinity for membranes, stabilize DivIVA clusters by 'bridging' opposing membranes (Lenarcic *et al.* 2009). *C. glutamicum*, like other Actinobacteria but unlike other rod-shaped bacteria, grows by apical insertion of peptidoglycan, where DivIVA plays a crucial role: it recruits the cell wall synthesis machinery to the cell poles (Letek *et al.* 2008; Sieger *et al.* 2013; Donovan & Bramkamp 2014; Sieger & Bramkamp 2014). A DivIVA deplete strain resulted in cells absent of polar growth; with consequent coccoid morphology (Letek *et al.* 2008), which demonstrates that DivIVA is required for cell elongation and acquisition of a rod shape during growth.

Bacterial cell growth is highly influenced by the carbon source present in medium and its concentration, and different carbon sources may lead to different morphologies, when cells try to regulate their surface/volume (S/V) ratio in order to reach the maximum efficiency for respiration rate (Zhuang *et al.* 2011). This was proposed for *E. coli* (Zhuang *et al.* 2011) and observed in our own experiments with *C. glutamicum*, showing that cells grown in glucose are smaller than cells grown in medium containing fructose, acetate, or mixed carbon sources.

1.2 Carbohydrate metabolism of *C. glutamicum*

In industry, the main feedstock used in most of the established industrial fermentation processes are molasses and starch hydrolysates, which contain a broad spectrum of simple carbohydrates, but mostly glucose, fructose and sucrose. Regulation of sequential carbohydrate usage and transport of carbohydrates is often governed by enzyme complexes termed

phosphoenolpyruvate-dependent carbohydrate:phosphotransferase systems (PTS) (Lengeler 2000; Deutscher *et al.* 2006; Gorke & Stulke 2008; Lengeler & Jahreis 2009; Deutscher *et al.* 2014; Lengeler 2015). Interestingly, some bacteria are known to co-ferment different carbohydrates with *Corynebacterium glutamicum* being a prominent example (Wendisch *et al.* 2000; Frunzke *et al.* 2008). In *C. glutamicum*, as in several other bacteria, these sugars are taken up and phosphorylated during transport into the cell mainly via PTS. This means that worldwide amino acid production using this organism depends heavily on the PTS transport activities. Therefore, studies concerning the functioning of PTS are of industrial relevance (Ikeda 2012).

In addition to the aforementioned carbon sources, *C. glutamicum* effectively metabolizes acetate for amino acid production (Woo *et al.* 2010). Acetate is taken up by diffusion and/or via the MctC transporter (encoded by *mctC*, cg0953), which is also responsible for the uptake of pyruvate and propionate (Jolkver *et al.* 2009). Once in the cytoplasm, acetate is converted into acetylphosphate by acetate kinase (encoded by *ackA*, cg3047), and subsequently converted into acetyl-coenzyme A (Acetyl-CoA) by phosphotransacetylase (encoded by *pta*, cg3048). The presence of acetate in medium was shown to up-regulate the transcription of *ackA* and *pta* (Wendisch *et al.* 1997; Reinscheid *et al.* 1999). Later it was discovered that this regulation is mainly mediated by the global regulators RamA and RamB, which will be further discussed later on (Auchter *et al.* 2011).

1.3 The phosphotransferase system (PTS)

The PTS utilizes the energy provided by phosphoryl group translocation to take up specific carbohydrates via active transport and convert them into their respective phosphoesters. This process is dependent on the phosphoryl transfer proteins Enzyme I (EI) and histidine-containing phosphocarrier protein (HPr), as well as on the sugar-specific Enzyme II (EII) complexes, which are divided into the domains Enzyme IIA (IIA), Enzyme IIB (IIB), and its

transmembrane permease Enzyme IIC (IIC) which may be supplemented by a fourth domain Enzyme IID (IID), as seen in the mannose PTS of *E. coli* (Erni and Zanolari 1985; Erni, Zanolari, and Kocher 1987; Huber and Erni 1996). The passage of specific sugar through the membrane is catalyzed by the transmembrane domain, but all three domains function together (Neidhardt and Curtiss 1996). Generally, there are four classes of Enzymes II: glucose, mannitol, mannose and lactose/chitobiose (Cai *et al.* 2003; Clore & Venditti 2013). The arrangement of EII varies according to the transporter and taxon, where IIA can be soluble or fused to the IIB and/or IIC subunits (Cai *et al.* 2003; Clore & Venditti 2013). Three-dimensional structures of all soluble protein-protein complexes of the PTS were solved by Clore and Venditti (Clore & Venditti 2013) using multidimensional NMR spectroscopy.

Phosphorylation of incoming sugars occurs concomitantly to its translocation accross the cytoplasmic membrane by IIC. The phosphoryl group is transfered from PEP via a phosphotransfer cascade starting with EI, followed by HPr, and EII. The order of proteins downstream of HPr tend to vary between different sugars, but generally IIA accepts the phosphoryl group from HPr and transfers it to histidine or cysteine residues of IIB, and finally IIC catalyzes the coupled translocation and phosphoryl transfer from IIB to the transported sugar. The phosphorylation state of these proteins can be indicators of the sugar supply, and different PTS proteins are known to be involved in different signal transduction strategies that link the availability of sugars to the activity of transport proteins, transcriptional regulators and metabolic enzymes.

1.4 The phosphotransferase systems of *C. glutamicum*

C. glutamicum PTS consists of two common energy-coupling cytoplasmic proteins, Enzyme I and HPr, which are encoded by *ptsI* (cg2117) and *ptsH* (cg2121) respectively, and a series of sugar-specific enzyme II (EII) complexes embedded in the cytoplasmic membrane. The EII of *C.*

glutamicum are divided into three protein domains, EIIA, EIIB and EIIC, and the organization of these domains differs between the PTS. *ptsG* (cg1537) encodes the glucose-specific membrane integral EIIBCA transporter, while *ptsS* (cg2925) encodes the sucrose-specific EIIBCA, and *ptsF* (cg2120) the fructose-specific EIIABC. A fourth PTS belongs to the L-ascorbate-type family (encoded by *rmpC*, cg3365) and was characterized by Hvorup *et al.* (Hvorup, Chang, and Saier 2003). The strain *C. glutamicum* R, unlike the strains ATCC 13032 and ATCC 13869, possesses a β-glucoside-specific PTS EIIBCA (gene *bglF*), which renders the strain capable of efficiently utilize methyl β-glucoside and the β-glucosides salicin and arbutin (Kotrba *et al.* 2001).

The fructose EII has the domain order IIA-IIB-IIC (Fig. 1), a typical arrangement found in the fructose/mannitol family, and shares 46% identity to the EII^{Fru} of *Streptomyces coelicolor* (Bertram *et al.* 2004). In the genome of *C. glutamicum*, *ptsF* is flanked by the genes that encode 1-phoshofructokinase (*pfkB*) and *ptsH*; and ptsI is located 2186 bp upstream of *ptsF*. PtsG (II^{Glc}) was first described as a mannose-specific PTS II^{Man} (*ptsM*) (Lee *et al.* 1993; Lee *et al.* 1994). Later it was discovered that *C. glutamicum* lacks a specific PTS for mannose, and its uptake is mediated by PtsG and PtsF (Sasaki *et al.* 2011). Both PtsG and PtsS share 47% amino acid sequence similarity (Moon *et al.* 2007) and have the same IIB-IIC-IIA domain order (Fig. 1).

1.5   Glucose metabolism

Glucose is taken up by IIC^{Glc} and concomitantly phosphorylated by IIB^{Glc}, resulting in Glucose-6-phosphate (G6P). The metabolic pathways for metabolism of G6P subsequently to PTS uptake are the glycolysis and the pentose phosphate pathway (PPP), which run in parallel and perform distinct functions: glycolysis is the preferential and most energy efficient pathway to metabolize carbohydrates, yielding 2 mols of pyruvate, 2 mols of ATP and 2

mols of NADH per mol of initial glucose, and the PPP fulfills the purposes of generating NADPH, which is necessary for reductive biosynthetic reactions, and ribose-5-phosphate (R5P), an important precursor for many biomolecules, including DNA, RNA, ATP, coenzyme A (CoA), flavin adenine dinucleotide (FAD) and histidine. The partitioning of carbon flux between the PPP and glycolysis will depend on the intracellular NADPH demand. During exponential cell growth, larger amounts of NADPH and R5P are needed for fatty acid and nucleotide synthesis, respectively. Glycolytic intermediates can then be diverted toward the non-oxidative phase of PPP by the expression of *pyk* which encodes pyruvate kinase (pyk). Pyk creates a bottleneck in the glycolytic pathway, allowing intermediates to be utilized by the PPP to synthesize NADPH and R5P. This process is further enabled by triosephosphate isomerase (TPI, encoded by *tpi*) inhibition by phosphoenolpyruvate (PEP), the pyk substrate (Eikmanns 1992). PTS-independent glucose uptake in *C. glutamicum* ATCC 13032 is mediated by the inositol uptake systems IolT1 and IolT2 (Ikeda *et al.* 2011; Lindner *et al.* 2011). In a *Δhpr* strain, where PTS-mediated uptake is not possible, cell growth in minimal medium with glucose as sole carbon source was heavily impaired (0.04 h^{-1} versus 0.37 h^{-1} in WT) but not completely abolished. In a *Δhpr ΔppgK* strain, the growth was even slower (0.03 h^{-1}). In a *Δhpr ΔiolT1 ΔiolT2* strain, no growth was possible, indicating that the PTS, IolT1, or IolT2 is required for cell growth in glucose minimal medium (Lindner *et al.* 2011). Interestingly, Ikeda *et al.* (Ikeda *et al.* 2015) found a suppressor mutant of a *C. glutamicum* ATCC 31833 *Δhpr ΔiolT1 ΔiolT2* strain that is capable of consuming glucose via the β-glucoside PTS (EII^{Bgl}, encoded by *bglF*). The presence of a EII^{Bgl} in *C. glutamicum* was first described in a WT strain *C. glutamicum* R, that unlike WT ATCC 13032 and ATCC 13869, can naturally metabolize the β-glucosides salicin and arbutin (Kotrba *et al.* 2001).

1.6   The pentose phosphate pathway

The pentose phosphate pathway (PPP) provides a way to oxidize glucose to generate NADPH, an important reducing agent in biosynthetic reactions, and ribose-5-phosphate, an essential component of nucleotides and nucleic acids. The pathway is divided in two phases (oxidative and non-oxidative) that will occur according to the necessities of the cells.

The first phase of the PPP is the oxidative breakdown of glucose to release CO_2 and generate NADPH. It begins with the dehydrogenation of Glucose 6-phosphate by glucose 6-phosphate 1-dehydrogenase (encoded by *zwf*, cg1778), which transfers a hydride ion from G6P onto an $NADP^+$, forming NADPH and releasing a hydrogen ion. This forms glucono-1,5-lactone-6P, which is then hydrolyzed by 6-phosphoglucono lactonase (*devB*, cg1780) into gluconate 6P. Next, 6-phosphogluconate dehydrogenase (*gnd*, cg1643) catalyzes the oxidative decarboxylation of gluconate-6P into ribulose-5P. In this step, a CO_2 molecule is released and another $NADP^+$ is reduced to NADPH. Finally, RB5P is converted to ribose 5-phosphate (R5P) by ribose 5-phosphate isomerase B (*rpi*, cg2658).

When the NADPH demand increases, cells can convert R5P produced in the first phase of the PPP into glycolytic intermediates via the non-oxidative phase of the PPP. In the first step of this phase, R5P is converted back into its isomer RB5P by RPI. Phosphate 3-epimerase (rpe, cg1801) then catalyzes the conversion of RB5P into xylulose 5P (X5P). In the second step, a X5P transfers a two-carbon group onto a R5P, generating a heptose sedoheptulose 7P (S7P) and a triose glyceraldehyde 3P (GA3P), a reaction catalyzed by transketolase (tkt, cg1774). The third step is the conversion of S7P and GA3P into erythrose 4P (E4P) and one of the final products F6P by transaldolase (tal, cg1776). Importantly, erythrose 4-phosphate, is the precursor for the synthesis of aromatic amino acids and aromatic vitamins. Last, TKT catalyses the reaction between 1x E4P and 1x X5P to generate another F6P and a GA3P. Therefore, the final yield of the non-oxidative

phase of the PPP per 3x ribose 5P, is 2x fructose 6P and 1x glyceraldehyde 3P.

1.7   Fructose and sucrose metabolism

After being translocated to the cytoplasm by PtsF, fructose is phosphorylated into Fructose-1-phosphate (F1P) by its subunit IIB^{Fru}, and subsequently converted into Fructose-1,6-biphosphate (F1,6BP), a process catalyzed by fructose-1-phosphate kinase (PfkB, encoded by *pfkB*, cg2119). F1,6BP is then split by fructose-bisphosphate aldolase (encoded by *fda*, cg3068) into glyceraldehyde-3-phosphate (GA3P) and dihydroxyacetone phosphate, continuing the glycolytic pathway. Kiefer *et al.* (2004), employing a metabolic flux analysis of *C. glutamicum* ATCC 21526, reported that 92.3% of fructose is taken up by PtsF, and the remaining 7.7% are taken up by PtsG, which leads to the conversion to F6P, and further phosphorylation into F1,6BP by PfkA. Therefore, PtsG plays an assisting role in fructose uptake. Additionally, the *myo*-inositol permeases IolT1 and IolT2 have been shown to transport fructose and glucose in *C. glutamicum* PTS deficient strains, as previously stated (Baumchen *et al.* 2009; Lindner *et al.* 2011).

Sucrose is taken up and phosphorylated into sucrose 6-phosphate (S6P) by PtsS. S6P is then hydrolyzed into glucose 6-phosphate (G6P) and fructose by sucrose 6-phosphate hydrolase (encoded by *scrB,* cg2927). G6P is further metabolized as previously described, however, unlike many sucrose-utilizing bacteria, *C. glutamicum* cannot phosphorylate fructose intracellularly (Dominguez and Lindley 1996). Therefore, to ensure its phosphorylation, the generated fructose is exported outside the cell by an unknown permease and enters the cell again via PtsF (Dominguez & Lindley 1996).
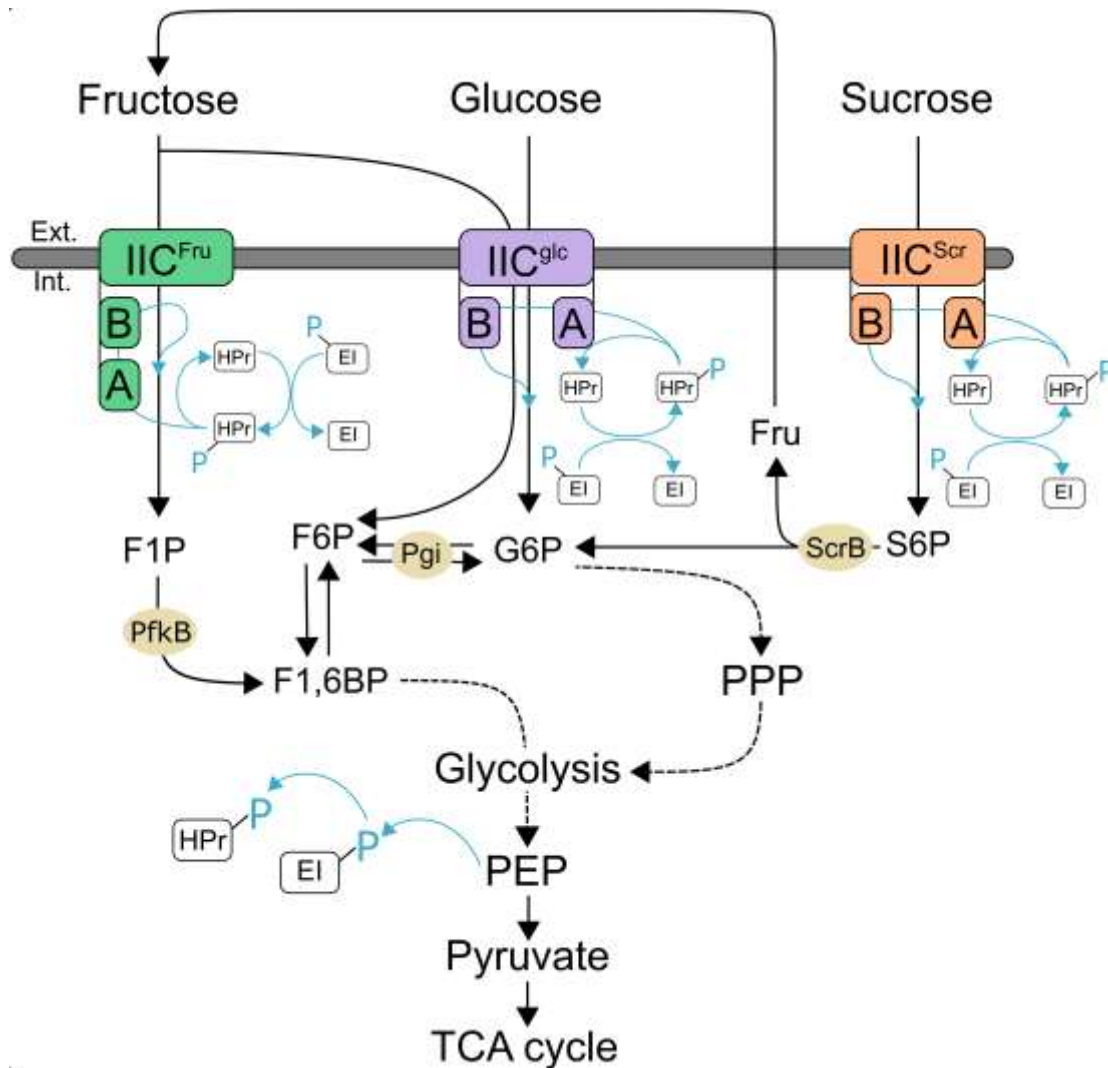
Figure 1. Schematic view of the sugar uptake mediated by the phosphoenolpyruvate-dependent phosphotransferase systems (PTS) in *Corynebacterium glutamicum*. Blue lines indicate phosphoryl group (PO_3^{2-}) transfer. F1P, fructose-1-phosphate; F6P, fructose-6-phosphate; F1,6BP, fructose-1,6-biphosphate; G6P, glucose-6-phosphate; Fru, fructose; S6P, sucrose-6-phosphate; PPP, Pentose phosphate pathway; PEP, phosphoenolpyruvate; scrB, beta-fructofuranosidase (putative S6P hydrolase); Pgi, glucose-6-phosphate isomerase; PfkB, 1-phosphofructokinase.

1.8   Regulation of PTS genes expression

The mechanism for control of PTS gene expression differs for the respective PTS genes. The transcriptional regulator SugR, encoded by *sugR* (cg2115) is a deoxyribonucleoside repressor (DeoR)-type regulator and is located in the fructose-PTS operon. It has been shown to repress not only *ptsF*, *ptsG* and *ptsS* expression in the absence of the transported sugar, but also the general PTS genes *ptsI* and *ptsH* (Engels and Wendisch 2007; Gaigalat *et al.* 2007; Engels, Lindner, and Wendisch 2008). Its activity is controlled by fructose 6-phosphate, which was shown to abolish binding of SugR to the *ptsG* promoter *in vitro*, and thus *ptsG* is derepressed during growth on sugars or under conditions of high concentrations of F6P (Engels and Wendisch 2007). RamA is a member of the LuxR family and acts as a central transcriptional activator or repressor of numerous genes encoding enzymes involved in cell wall synthesis, carbon uptake and central carbon metabolism, which include *mctC* (importer of acetate, propionate and pyruvate), *aceA* (isocitrate lyase), *aceB* (malate synthase), *ackA* (acetate kinase), *pta* (phosphotransacetylase), and the *sdhCAB* operon, that encodes succinate dehydrogenase (Bussmann *et al.* 2009; Schroder and Tauch 2010; Shah *et al.* 2018). It acts by binding to the promoters of targeted genes, and constitutes a feed-forward loop type of transcriptional motifs with other regulators such as GlxR, SugR, GntR1, and RamB. RamB is a negative transcriptional regulator of genes in the RamA regulon, thus acting as its antagonist. In acetate-grown cells, RamB was shown to be subject to positive regulation by RamA, and when glucose is used as source of carbon, *ramB* expression is subject to negative auto-regulation by RamB (Gerstmeir *et al.* 2004; Cramer *et al.* 2007).

The GntR-type transcriptional regulators GntR1 (cg2783) and GntR2 (cg1935) regulate gluconate catabolism by repressing *gnd* (6-phosphogluconate dehydrogenase), *gntP* (gluconate permease), and *gntK* (a

putative gluconate kinase) in absence of gluconate. At the same time, these regulators control glucose uptake by activating of *ptsG* expression in such conditions (Frunzke *et al.* 2008). A double mutant *ΔgntR1 ΔgntR2* ATCC 13032 strain showed slowed growth (0.16 h^{-1}) compared to WT (0.41 h^{-1}) and 60% lower glucose uptake rate in minimal medium with glucose as sole carbon source (Frunzke *et al.* 2008).

One of the molecular mechanisms for global transcription regulation in bacteria are sigma factors that are responsible for recognition and specific binding of RNA polymerase (RNAP) to gene promoters and are therefore, needed for initiation of transcription. Bacteria normally employ a primary sigma factor that is responsible for the transcription of most genes, especially those active during exponential growth. *C. glutamicum* has seven sigma factor-encoding genes: a primary sigma factor SigA, a non-essential primary-like SigB and 5 alternative SigC, SigD, SigE, SigH and SigM (Patek and Nesvera 2011). The sugar-specific EII genes PtsF, PtsG and PtsS, as well as the general components *ptsI* and *ptsH* have been shown to be subjected to regulation by SigA in cells in exponential growth (Patek & Nesvera 2011). In *C. glutamicum*, expression of *sigA* is regulated as a function of the growth phase, as the *sigA* mRNA is produced during exponential growth phase and its transcription stops when cells reach stationary phase. This supports the notion that SigA is the primary sigma subunit of corynebacterial RNA polymerase, which confers to the RNA polymerase holoenzyme, the specificity to recognize type I corynebacterial-like promoters (Oguiza, Marcos, & Martin 1997; Larisch *et al.* 2007; Patek & Nesvera 2011).

Post-transcriptional regulation of PtsG is governed by SgrS, a small Hfq-binding RNA that is induced by phosphosugar accumulation in the cytosol. It forms a ribonucleo-protein complex with Hfq and RNase E, resulting in translational repression and degradation of *ptsG* mRNA (Kawamoto *et al.* 2005; Maki *et al.* 2008). The catabolite repressor/activator FruR (also known as Cra), encoded by *fruR* (cg2118) down regulates the fructose-PTS operon in *Escherichia coli*, *Salmonella typhimurium* and *Pseudomonas putida* when

the sugar is not available (Saier & Ramseier 1996; Gaigalat *et al.* 2007; Chavarría *et al.* 2014). In *P. putida*, FruB acts by binding as a dimer to a single palindromic sequence within the *cra/fruB* intergenic region (which is different to those of *E. coli* and *S. typhimurium*), and that only F-1-Phosphate can lift such down regulation (Chavarría *et al.* 2014). In *S. pneumonia*, exogenous auto-inducer 2 (AI-2) induces *fruA* and *fruB*, which encode PtsF and 1-phosphofructokinase in that organism (Galinier & Deutscher 2017). Expression of enzyme I and HPr increases in the presence of different PTS sugars. In many bacteria, glucose is reported to be the most effective inducing sugar of *ptsI* and *ptsH* expression (Viana *et al.* 2000; Nothaft *et al.* 2003).

1.9   Carbon catabolite repression

Bacteria often are able to utilize a variety of different carbon sources and energy substrates, adapting their enzymatic equipment and thus their metabolism according to the availability of a given energy source. This adaptation is normally mediated by substrate-specific induction or repression of involved genes. When a mixture of different energy sources is present, many bacteria can first utilize a preferred substrate, such as glucose, which normally supports the best growth rate and/or growth yield. In this situation, genes required for the utilization of secondary carbon sources are not expressed and preexisting enzymes are often inactivated to prevent the waste of resources, and consumption of other additional sources will only take place when the preferred one is depleted. This phenomenon is known as carbon catabolite repression (CCR) (Deutscher 2008; Gorke & Stulke 2008). Although the physiological effects of CCR may be similar in different organisms, the underlying mechanisms leading to it may differ between species. In *E. coli*, as well as in other enteric bacteria, CCR is governed by the EIIA^{Glc} domain of PtsG. In absence of glucose in medium, EIIA^{Glc} remains in its phosphorylated state. In this form, EIIA^{Glc} activates the adenylate

cyclase, which in turn leads to an increase in the intracellular cyclic AMP (cAMP) concentration. Higher concentrations of cAMP activate the transcription activator CRP (cAMP receptor protein). CRP is a mediator of cAMP-dependent signaling; it recognizes specific operator sequences in the regulatory region of its targeted genes and is therefore, required for the expression of a vast number of catabolic genes/operons (Kohl and Tauch 2009). Whenever there is active glucose transport via PTS, EIIA^{Glc} donates the phosphoryl group to EIIB^{Glc}, that will in sequence, transfer it to glucose to form G6P. When this occurs, EIIA^{Glc} remains in its unphosphorylated state. Unphosphorylated EIIA^{Glc} inhibits the activity of several permease systems, preventing the use of other carbohydrates in the medium until glucose is fully depleted. Unphosphorylated EIIA^{Glc} is unable to activate adenylate cyclase, and additionally, it binds directly to either the respective permease (as seen in the lactose or melibiose permeases), or to the ATP-binding subunit of the ATP binding cassette (in the case of affected ABC transporters) (Deutscher *et al.* 2006; Gorke & Stulke 2008).

In *B. subtilis*, CCR is mediated by the transcription regulator carbon catabolite control protein (CcpA). CcpA binds directly to the DNA in presence of glucose, repressing several catabolic genes and activating the transcription of others (Blencke *et al.* 2003). Unlike in *E. coli*, the HPr of *B. subtilis* possesses a regulatory phosphorylation site Ser46 in addition to His15. In presence of glucose, HPr is phosphorylated during transport of the phosphoryl group to the sugar (HPr-Ser-P). HPr-Ser-P is the only form of HPr capable of interacting with CcpA, and is therefore, essential for its function as repressor of catabolic genes. Phosphorylation or dephosphorylation of HPr is mediated by HPr kinase phosphorylase (HPrK/P), and its antagonist functions are regulated by metabolites. High intracellular fructose 1,6-bisphosphate, Glucose 6-phosphate and ATP or PPi concentrations stimulate the kinase activity, as well as CcpA-(HPr-Ser46-P) binding to DNA, whereas the phosphorylase activity is stimulated when the Pi concentration is sufficiently high (Schumacher *et al.* 2007). In addition to glucose, other carbohydrates cause carbon catabolite repression in *B. subtilis*. These

substrates form a hierarchical order in their capacity to exert repression, suggesting that they trigger the formation of active CcpA complexes to different degrees (Singh *et al.* 2008).

After fully consuming a certain substrate, bacteria go through a short stationary phase, when the cellular machinery used to metabolize the following substrate is activated. This leads to a characteristic diauxic growth. Interestingly, *C. glutamicum*, simultaneously metabolizes glucose with fructose, sucrose, ribose, pyruvate, lactate, or acetate (Wendisch *et al.* 2000), and diauxic growth was described so far only for the mixture of glucose and glutamate, and glucose and ethanol in medium (Kramer *et al.* 1990; Kramer & Lambert 1990; Arndt *et al.* 2008). The *glxR* (cg0350) gene of *C. glutamicum* ATCC 13032 encodes the CRP homolog GlxR, a DNA transcription factor of the CRP-Frn protein family, and although this organism does not show diauxic growth for most carbon sources, a broad variety of *C. glutamicum* genes is under transcriptional control by GlxR (Kohl and Tauch 2009; Schroder and Tauch 2010), including genes involved in sugar uptake, glycolysis, gluconeogenesis, and different transport systems (Kohl and Tauch 2009).

1.10   Mechanosensitive channels

In nature, *C. glutamicum*, as a soil bacterium, is commonly subjected to various environmental conditions that lead to abrupt osmotic stresses (e.g. rainfall or droughts). An increase in osmolarity would normally lead to cell shrinkage due to dehydration, whereas a decrease would lead to cell inflation with water and eventual disruption. A strategy employed by this bacterium to compensate the osmotic imbalance are membrane proteins responsible for the uptake and excretion of compatible solutes. Under hyperosmotic conditions, cells fight against the efflux of water and consequent dehydration by a fast influx of K^+, followed by the accumulation of compatible solutes, most commonly betaine, trehalose, proline and glycine (Ruffert *et al.* 1997).

This accumulation can be achieved via biosynthesis or via uptake from the surrounding environment, being the latter preferred due to lower energy costs (Ruffert *et al.* 1997). *C. glutamicum* possesses four osmoregulator uptake systems for compatible solutes: BetP (*betP*, cg1016), EctP (*ectP*, cg2539), ProP (*proP*, cg3395) and LcoP (*lcoP*, cg2563) (Kramer and Morbach 2004), being the glycine betaine transporter BetP the most extensively studied. BetP is a symporter that co-transports two Na^+ ions together with one molecule of glycine betaine, thus being influenced both by the membrane potential and the Na^+ gradient (Farwick, Siewe, and Kramer 1995). Besides its transport function, BetP also functions as an osmosensor and osmoregulator (Kramer & Morbach 2004), and its activity is adapted to the actual extent of osmotic stress. In the absence of hyperosmotic conditions, BetP is inactive, whereas upon osmotic upshift, BetP switches to an activated state. Once the hyperosmotic stress has been compensated by accumulation of compatible solutes, uptake activity is reduced and fine regulated by not only the uptake systems, but as well as the passive mechanosensitive (MS) channels (Kramer & Morbach 2004).

MS channels are responsible for the efflux of compatible solutes, and in *E. coli*, can be divided into three categories according to their conductance: MscL, MscS and MscM for large, small or very small (mini) respectively. These channels function as emergency valves preventing cell lysis under hypoosmotic conditions, opening at different thresholds to allow a stepwise and proportional excretion of compatible solutes (Martinac *et al.* 1987; Berrier *et al.* 1996; Perozo & Rees 2003). The MscS homolog in *C. glutamicum* is YggB (*yggB*, cg1434), which plays a role not only in hypoosmotic stress, but it is also responsible for fine tuning the excretion of betaine in hyperosmotic conditions. Borngen *et al.* (2010) proposed that BetP and YggB work in a pump-leak model to accurately adjust the internal betaine concentration in response of osmotic stress (Fig. 2). Moreover, a strain containing YggB with a C-terminal truncation of 110 AA showed continuous glutamate production without induction, whereas overexpression of *yggB* from a plasmid resulted in increased glutamate production only upon induction by various triggers, and

16

deletion of *yggB* led to a decrease in glutamate production, with a residual production of 30% (Nakamura *et al.* 2007; Borngen *et al.* 2010). This suggests that YggB indeed exports glutamate as a compatible solute in response to osmotic stresses, and as *C. glutamicum* has been used as an industrial glutamate producer for over 60 years, characterization of mechanosensitive channels contributes to a better understanding of amino acid export systems.
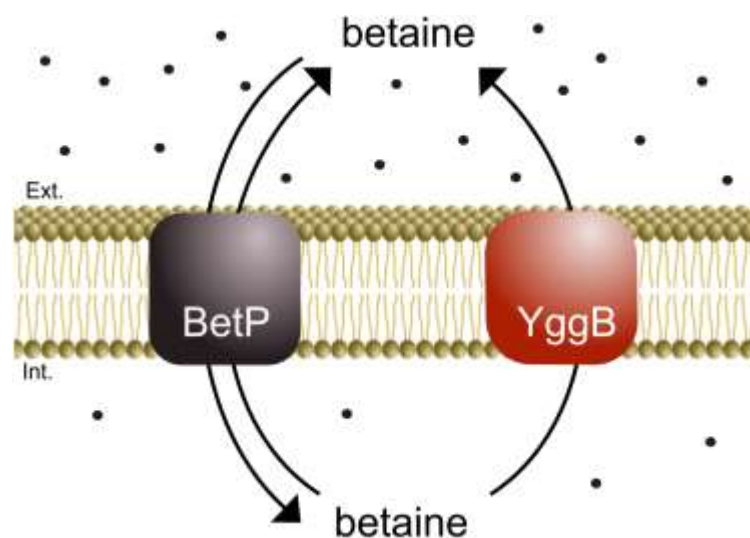
Figure 2. BetP and YggB work as a pump and leak system. Hyperosmotic stress leads to cell shrinkage due to loss of water. In this situation, the osmosensor and osmoregulator BetP is activated and takes up compatible solutes (here e.g. betaine) until the shift in osmolarity is compensated. Fine tuning of the solute concentration is aided by leaking through the small mechanosensitive channel YggB.

1.11 Respiratory chain proteins and membrane economy

The succinate dehydrogenase of *C. glutamicum* is composed of the flavoprotein SdhA (*sdhA*, cg0446), iron-sulfur protein SdhB (*sdhB*, cg0447), and the transmembrane anchor SdhCD (gene *sdhCD*, cg0445) (Kurokawa and Sakamoto 2005) (Fig. 3). The operon *sdhCAB* is flanked by cg0444, a transcriptional regulator of the MerR family employed in fatty acid utilization regulation, and cg0448, a hypothetical membrane protein with no function

defined to this date. The SQR is employed in two distinct functions: it catalyzes the oxidation of succinate to fumarate in the citric acid cycle, and transfers electrons to quinones in the cytoplasmic membrane during oxidative phosphorylation. SdhA has been shown to communicate with sulfur metabolism by regulating *cysR*, and thereby the expression of CysR, a protein responsible for the activation of genes involved in the assimilation of sulfate (Lee *et al.* 2014). SQR is subjected to some of the same regulators as the PTS, such as the repressor of *ptsF/G/I* GlxR (Kohl and Tauch 2009; Bussmann *et al.* 2009), the general repressor/activator of *ptsG/H* RamA (Cramer *et al.* 2006; Bussmann *et al.* 2009; Auchter *et al.* 2011) and its antagonist RamB (Gerstmeir *et al.* 2004; Bussmann *et al.* 2009), which plays a role in *ptsG/S* regulation, and finally the global transcription regulator SigA, that regulates transcription of *ptsF/G/H/I/S* (Patek and Nesvera 2011).
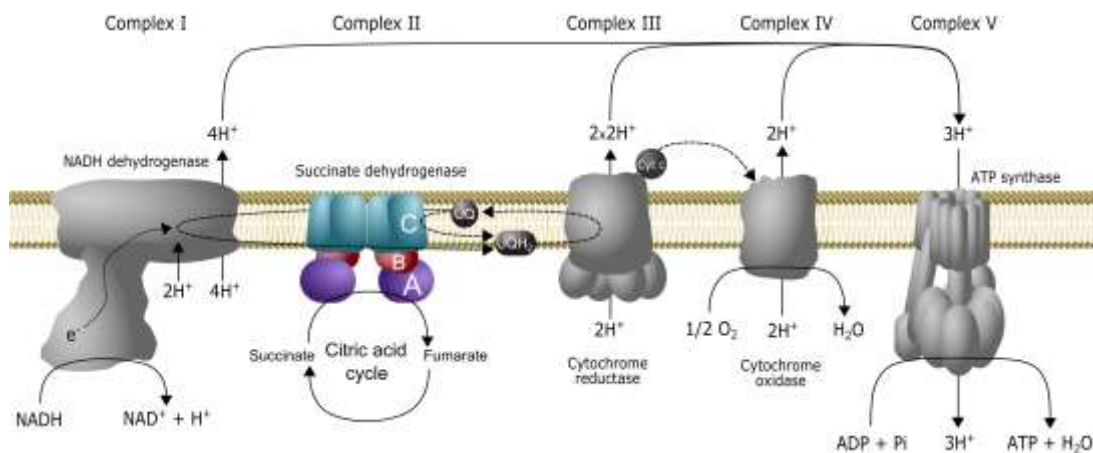
Figure 3. Succinate dehydrogenase arrangement in *C. glutamicum* respiratory chain. A indicates the flavoprotein SdhA, B indicates the iron-sulfur protein SdhB, C and D indicate the transmembranes domains SdhCD. UQ = Ubiquinone, UQH_2 = Ubiquinol, Cyt c = Cytochrome C.

C. glutamicum possesses a respiratory type of energy metabolism and can use either oxygen or nitrate as terminal electron acceptors, to allow respiration with or without oxygen (Koch-Koerfges *et al.* 2012). Since the

molar ATP yield from respiration with oxygen as final electron acceptor is nearly 15-fold higher than that from fermentation, ATP production via respiration is more efficient. However, at high catabolic rates, many facultative aerobic organisms employ fermentative pathways simultaneously with respiration, even in the presence of abundant oxygen to produce ATP. When this happens, the prokaryotic cytoplasmic membrane can become saturated with transmembrane proteins (Zhuang *et al.* 2011).

A previous study (Zhuang *et al.* 2011) hypothesized that because the cytoplasmic membrane is a finite space and a significant part must be composed of phospholipids in order to maintain its stability, fluidity and integrity, proteins must compete for the small fraction destined to protein expression. Hence, the outcome of a competition for membrane space between substrate transporters and respiratory enzymes influences respiration and fermentation, since both are localized on the membrane. In this scenario, sugar transporters and respiratory chain components would form separate domains that compete against each other, where increased substrate uptake rates require a decrease in the respiratory rate and vice versa, and bacteria manage the expression of transmembrane proteins economically so that the fitness is maximized while maintaining membrane integrity.

The specific cytoplasmic membrane available for transmembrane protein insertion is directly related to its surface area to volume (S/V) ratio, which is greatly affected by the cell morphology (Zhuang *et al.* 2011). In *C. glutamicum*, morphological control of S/V ratio may be a strategy in to obtain the desired rate of respiration, and this way, higher consumption of carbon, leading to a higher production of the desired metabolite. Therefore, a first step for potential biotechnological applications in this direction is to gather spatial information concerning sugar uptake systems and respiratory chain proteins.

1.12 Scope of this work

C. glutamicum has been used as a workhorse for the industrial production of a range of amino acids for over 60 years, and as a consequence, different aspects of its metabolism and proteome have been subject of intensive study in the past years. However, the subcellular localization of important membrane proteins is a gap present in the current knowledge that may act as a starting point for future biotechnological applications. The primordial aim of this thesis was to investigate, using novel microscopy techniques, proteins of distinct physiological relevance:

(I) The subcellular localization and occupancy of the glucose and fructose phosphotransferase systems PtsG and PtsF, which are responsible for the uptake and subsequent phosphorylation of their respective sugars, as well as the general PTS components EI and HPr.

(II) The spatial distribution of respiratory chain proteins compared to PTS, under the assumption that these complexes form separate domains in bacterial cell membranes.

(III) The localization and dynamics of transmembrane and membrane associated proteins, here represented by the MS channel YggB and the polar/septum scaffold DivIVA, by the use of techniques that allow the study of compartmentalization and membrane use.

2 Material and methods

2.1 Bacterial strains and cloning

Oligonucleotides, strains and plasmids used in this study are listed in Tables 1 and 2, respectively. Plasmids for integration of *C. glutamicum* genes of interest fused to the sequence of fluorophores were constructed with 500 base pairs homologous regions upstream and downstream of the 3′ end of the gene to be labeled with a fluorophore sequence in between.

For plasmids pK19mobsacB-mCherry-PtsF and pK19mobsacB-PAmCherry-PtsF, the upstream and downstream fragments were PCR amplified from *C. glutamicum* chromosomal DNA with primer pairs PtsF-upstr-fwd-HindIII/ PtsF-upstr-rev-XbaI and PtsF-N-ter-fwd-XmaI/ PtsF-N-ter-rev-EcoRI. mCherry or photoactivatable mCherry fluorescent proteins sequences were amplified with primer pair mCherry-fwd-XbaI/ mCherry-rev-XmaI.

For plasmids pK19mobsacB-mCherry-PtsG, pK19mobsacB-mNeonGreen-linker-PtsG, and pK19mobsacB-PAmCherry-linker-PtsG, the upstream and downstream fragments were PCR amplified from *C. glutamicum* chromosomal DNA with primer pairs PtsG-upstr-fwd-HindIII/ PtsG-upstr-rev-XbaI and PtsG-N-ter-fwd-XmaI/ PtsG-N-ter-rev-EcoRI. mCherry, mNeonGreen or photoactivatable mCherry fluorescent proteins sequences were amplified with primer pairs mNeonG-fwd-XbaI/ mNeonG-rev-XmaI-Linker and mCherry-fwd-XbaI/ mCherry-XmaI-linker-rev.

To construct pK19mobsacB-sdhA-mNeonGreen, the upstream and downstream fragments were PCR amplified from *C. glutamicum* chromosomal DNA with primer pairs SdhA-C-ter-fw-HindIII/ SdhA-C-ter-rev-XbaI and SdhA-down-fw-XmaI/ SdhA-down-rev-EcoRI. mNeonGreen fluorescent protein sequence was amplified with primer pairs mNeonG-fwd-XbaI/ mNeonG-XmaI-Rev-TAA.

21

To construct pK19mobsacB-yggB-mNeonGreen, the upstream and downstream fragments were PCR amplified from *C. glutamicum* chromosomal DNA with primer pairs YggB-C-ter-Sall-fw/ YggB-C-ter-XbaI-rev and YggB-down-BamHI-fw/ YggB-down-EcoRI-rev. mNeonGreen fluorescent protein sequence was amplified with primer pairs mNeonG-fwd-XbaI/ mNeonG-BamHI-Rev-TAA.

The resulting PCR fragments were digested with the respective restriction enzymes and consecutively ligated into pK19mobsacB vectors. Ligation products were then transformed into competent *E. coli* DH5α, and subsequent steps were carried out using standard cloning methods (Evans 1990). Last, all the constructed plasmids were verified by DNA sequencing.

The constructed plasmids were transformed into electro-competent wild-type *C. glutamicum* RES 167 via electroporation (600 Ω, 25 µF and 2.5 kV). Selection for integration of the fluorophore was performed as described before (Schafer *et al.* 1994). The final allelic replacements were confirmed by colony PCR and microscopy.

Table 1. Oligonucleotides used in this study. Upper case letters indicate gene-specific sequences. Underlined letters indicate restriction site sequences.

Oligonucleotide	Sequence	Restriction site
PtsG upstr fw HindIII	att<u>aagctt</u>TTTTGGCGGGCG	HindIII
PtsG upstr rev XbaI	ggg<u>tctaga</u>GTCAAACCTTTCTAAACG	XbaI
PtsG n-ter fwd XmaI	tata<u>cccggg</u>ATGGCGTCCAAA	XmaI
PtsG n-ter rev EcoRI	aggg<u>gaattc</u>GAGTGCAGGAATACATAAG	EcoRI
PtsF up fwd HindIII	aaa<u>aagctt</u>GCTGTCGATACCTCAGAC	HindIII
PtsF up rev XbaI	aaa<u>gtttct</u>AGAGCTGATTCTTTCAATCCTTTG	XbaI
PtsF N-ter fwd XmaI	gta<u>cccggg</u>ATGAATAGCGTAAATAATTCCTCGC	XmaI
PtsF N-ter rev EcoRI	atat<u>gaatt</u>CGCAACCGCCGCCGC	EcoRI
mCherry fwd XbaI	aaa<u>tctaga</u>ATGGTGAGCAAGGGCGAG	XbaI
mCherry rev XmaI	tta<u>cccggg</u>CTTGTACAGCTC	XmaI
mCherry XmaI link rv	aaa<u>cccggg</u>gaattcgccagaaccagcagcggagccagcggatc	XmaI

	cCTTGTACAGCTCGT	
mNG fwd Xbal	aaa<u>tctaga</u>ATGGTGAGCAAGGGCGAG	Xbal
mNG rev Xmal Link	aaa<u>cccggg</u>aattcgccagaaccagcagcggagccagcgCTT GTACAGCTCGTC	Xmal
mNG Xmal Rv TAA	cat<u>cccggg</u>TTACTTGTACAGCTCGTCCA	Xmal
mNG BamHI Rv TAA	aaa<u>ggatcc</u>TTACTTGTACAGCTCGTCCATG	BamHI
SdhA C-ter fw HindIII	att<u>aagctt</u>CAGCGATTGCG	HindIII
SdhA C-ter rev Xbal	taa<u>tctaga</u>CTTGTAGTTCCTTG	Xbal
SdhA dwn fw Xmal	tta<u>cccggg</u>TAATGAAACTTAC	Xmal
SdhA dwn rev EcoRI	tta<u>gaattc</u>AGCAACACATGC	EcoRI
sdhB upst HindIII fwd	aaa<u>aagctt</u>GCAGCGATTGCGC	HindIII
sdhB upstr Xbal rev	aaa<u>tctaga</u>TACTTGTAGTTCCTTGTCTGCAGTGGG	Xbal
sdhB N-ter Xmal fwd	aaa<u>cccggg</u>ATGAAACTTACACTTGAGATCT	Xmal
sdhB N-ter EcoRI rev	aaa<u>gaattc</u>GCAACACATGCGCC	EcoRI
HPr-N_fwd	caagcttgcatgcctgcaggGCCTGGCATTCGTCTCCG	-
Hpr-mVenus_fwd	gacactttccATGGCTTCCAAGACTGTAAC	-
Hpr-mVenus_rev	agagcgttgtTCACTTGTACAGCTCGTC	-
HPr-C_fwd	gtacaagtgaACAACGCTCTGCTTGTTAAAAG	-
HPr-C_rev	attcgagctcggtacccgggAACGAGGTTAAGGGAATTA	-
ptsH'_fwd	caagcttgcatgcctgcaggAAAGGACACTTTCCATGGC	-
ptsH'_rev	cggtgaacaggcttccTCCACCTCCCTCAGCGTC	-
'mVenus_fwd	gggaggtggaggaagcCTGTTCACCGGGGTGGTG	-
'mVenus_rev	acggccagtgaattcgagcttcaCTTGTACAGCTCGTCCA	-
eCFP_fwd	caagcttgcatgcctgcaggaggagagtatctATGGTGAGCA AGGGCGAGGAGCTG	-
eCFP_rev	agccactccgcttccACCCCCGGCGGCGGTCAC	-
'EI_fwd	cgccgggggtggaagcggaGTGGCTACTGTGGCTGAT	-
'EI_rev	acggccagtgaattcgagctTTAGACTGCTGCGTCGATC	-
YggB c-ter Sall fw	aaa<u>gtcgac</u>AAGAAACAGCAAAACCAGAT	Sall
YggB c-ter Xbal rev	aaa<u>tctaga</u>AGGGGTGGACGTCGG	Xbal
YggB dwn BamHI fw	aaa<u>ggatcc</u>GACGCTGATTACAGACG	BamHI
YggB dwn EcoRI rev	aaa<u>gaattc</u>GTAGCCGTCTTCTTGAACG	EcoRI

Table 2. Strains and plasmids used in this study

Strain or plasmid	Relevant characteristics	Source
E. coli strains		
DH5 α	F-Φ80lacZM15 (lacZYA-argF)U169 recA1 endA1 hsdR17(rk-,mk+) phoA supE44 thi-1 gyrA96 relA1 λ-	Invitrogen
C.glutamicum strains		
RES 167	Restriction-deficient derivative of strain ATCC 13032	(Tauch _et al._ 2002)
CGM001	RES167 derivative with _ptsF::mCherry-ptsF_	This work
CGM002	RES167 derivative with _ptsG::mNeonGreen-ptsG_	This work
CGM003	RES167 derivative with _ptsF::mCherry-ptsF_ and _ptsG::mNeonGreen-ptsG_	This work
CGM004	RES167 derivative with _ptsF::PAmCherry-ptsF_	This work
CGM005	RES167 derivative with _ptsG::PAmCherry-Linker-ptsG_	This work
CGM006	RES167 derivative with _sdhA::sdhA-mNeonGreen_	This work
CGM007	RES167 derivative with _hpr::hpr-mVenus_	Oliver Goldbeck
CGM008	ATCC13032 with chromosomal deletion of _ptsI_	(Kuhlmann _et al._ 2015)
CGM009	CGM008 derivative with pEKEx2_eCFP-EI for plasmid based expression of eCFP-EI	Oliver Goldbeck
CGM010	ATCC13032 derivative with _yggB::yggB-_	This work

	mNeonGreen	
CDC010	RES167 derivative with *DivIVA::DivIVA-mCherry*	(Donovan *et al.* 2012)
Plasmids		
pK19mobsacB	Kan^r; *E. coli/C. glutamicum* shuttle vector for construction of insertion and deletion mutants in *C. glutamicum*	(Schafer *et al.* 1994)
pK19msB-mNeonGreen-ptsG		This work
pK19msB-mCherry-ptsF		This work
pK19msB-PAmCherry-ptsF		This work
pK19msB-PAmCherry-ptsG		This work
pK19msB-sdhA-mNeonGreen		This work
pK19msb_Hpr-mVenus		Oliver Goldbeck
pEKEx2	*E. coli/C. glutmaicum* shuttle expression vector; Ptac, lacIq, Km	Eikmanns *et al.* (Eikmanns *et al.* 1991)
pEKEx2_eCFP-EI		Oliver Goldbeck

2.2   Media and growth conditions

For genetic manipulations, *E. coli* strain DH5α was grown at 37 °C in LB (Lysogeny Broth, 10 g/L tryptone, 5 g/L yeast extract, 10 g/L NaCl) medium supplemented, when appropriate, with kanamycin 25 µg/ml.

C. glutamicum cells were grown aerobically on rotatory shaker (200 RPM) at 30°C in brain heart infusion (BHI) medium (Becton Dickinson) for maintenance. For all microscopy and growth experiments, cells were grown in CGXII (Keilhauer, Eggeling, and Sahm 1993) composed of 20 g $(NH_4)_2SO_4$, 5 g urea, 2 g KH_2PO_4, 2 g K_2HPO_4, 0.25 g $MgSO_4$, 42 g MOPS (3-(N-morpholino)propanesulfonic acid) per liter of H_2O. The pH was adjusted to 7.0 with NaOH, and the medium was supplemented with 0.01 g $CaCl_2$, 200 µg biotin, 10 mg $FeSO_4$, 10 mg $MnSO_4$, 1 mg $ZnSO_4$, 0.2 mg $CuSO_4$, 0.02 mg $NiCl_2$ per liter. Glucose or alternative carbon sources were added to reach a concentration of 2% w/v. Acetate was used as a base carbon source, as it gives relatively good growth among non-PTS carbon sources in *C. glutamicum.* For our experiments with mixed carbon sources, each of the respective carbon source was added in a final concentration of 2% each. For our temperature experiments, cells were grown aerobically in CGXII on rotatory shaker (200 RPM) in incubator at 17°C. Microscopy was then performed at the same temperature in a heat controlled chamber.

For all the experiments, strains were cultivated during the day in 5 ml of LB medium and then diluted in 10 ml of LB/CGXII medium and grown overnight. The following day the cultures were diluted to an optical density (OD) of 1.0 in 10 ml CGXII. For microscopy, samples were taken in early exponential phase, when the OD_{600} reached 2.

2.3   Carbon consumption assays

The quantification of glucose, fructose and acetate in the supernatants of cultures was performed by high-performance liquid chromatography (HPLC) using a Dionex UltiMate 3000 (Thermo Scientific) HPLC system equipped with an Aminex HPX-87H column (300 by 7.8 mm; Bio-Rad). Isocratic elution was performed with 6 mM H_2SO_4 at 80°C for 20 min at a flow rate of 0.6 ml/min. Fructose and glucose were detected with a PDA-100 Photodiode Array Detector (Dionex) at 190 nm, and acetate was detected with a PDA-100 Photodiode Array Detector (Dionex) at 206 nm. Quantification was performed using calibration curves constructed by measurements of the sole carbon source in CGXII medium.

2.4   Generation of cell wall-deficient *C. glutamicum* cells

Unstable L-forms were generated by culturing the cells in MSM/NB osmo-protective medium, in presence of D-cycloserine (DCS). DCS is a cyclic analogue of D-alanine, acting against alanine racemase (Alr) and D-alanine:D-alanine ligase (Ddl), two crucial enzymes in the cytosolic stages of peptidoglycan synthesis, bypassing the need to block cell wall synthesis genetically.

First, the desired strain was plated from -80°C stock on a LB plate and grown over night at 30°C. On the next day, a colony was restreaked on a osmoprotective MSM/NB plate coated with 200 µl of 400 µg of DCS at 30°C until L-form colonies developed. These colonies were then used for flask experiments with MSM/CGXII with the desired sugar as sole carbon source. The MSM/CGXII medium is composed of 2× MSM medium, pH 7 (40 mM $MgCl_2$, 1 M xylose, and 40 mM maleic acid, pH 7 adjusted with NaOH), mixed 1:1 with 2x NB (Oxoid) or 2× CGXII supplemented with either glucose or fructose, depending on the sugar transported by the analyzed PTS protein. CWD cells for analysis of DivIVA dynamics and localization were grown in

standard CGXII with glucose. As RES167 does not utilizes xylose as carbon source, this sugar was used for osmotic protection instead of the original sucrose to avoid possible influences in the studied PTS complexes.

2.5   Fluorescence microscopy

For standard fluorescence microscopy, cells were grown to early exponential phase as described before (Sieger *et al.* 2013) and 1 µl of culture was spread on a 1% agarose gel pad. The setup used for fluorescent microscopy consisted of a Delta Vision Elite (GE Healthcare, Applied Precision) equipped with an Insight SSI™ illumination, an X4 laser module and a Cool Snap HQ2 CCD camera was used (100× oil PSF U-Plan S-Apo1.4 NA objective). Fluorescence microscopy images were analyzed using the Fiji Software (Schindelin *et al.* 2012) in combination with the MicrobeJ (Ducret, Quardokus, and Brun 2016). Cells were manually marked as regions of interest (ROI) in Fiji using the bright field channels, then exported to MicrobeJ. Then, binary masks from the fluorescent channels were made for detection of fluorescent foci using MicrobeJ. Finally, automated detection and measurements of area, number and fluorescence of foci inside of marked cells was performed. The data was then exported as a table and subsequently analyzed in RStudio. The corrected total fluorescence (CTF) was calculated according to following formula: CTF = Integrated Density - (Area of selected cell X Mean fluorescence of unspecific background readings) (Gavet and Pines 2010). Final image preparation was done in Inkscape 0.92.1.0. All imaging experiments were performed several times with biological replicates, and foci analysis was performed in >200 cells.

2.6   Fluorescence recovery after photobleaching (FRAP)

The setup used for our FRAP experiments consisted of a Delta Vision Elite (GE Healthcare, Applied Precision) equipped with an Insight SSI™ illumination, an X4 laser module and a Cool Snap HQ2 CCD camera was used (100× oil PSF U-Plan S-Apo1.4 NA objective). Bleaching of mCherry was performed using a 561 nm laser with 25% power and an illumination time of 0.02 s. Images were taken every 20 s on both DIC (0.01 s exposure time, 100% transmittance) and mCherry (0.25 s exposure time, 32% transmittance) channels. Images were analyzed with Fiji and values were normalized for both bleaching caused by imaging, and background fluorescence. Relative values were used in order to allow comparison between cells, where value 1 corresponds to the fluorescence intensity before the bleaching event and value 0 corresponds to the fluorescence intensity 20 s after the bleaching event. Time 20 s was chosen instead of time 0 s as a value 0 in order to exclude mCherry photoswitching.

2.7   Photoactivated Localization Microscopy (PALM)

After growing to early exponential phase in CGXII supplemented with the desired carbon source as described before, cultures were fixed through incubation for 30 minutes at 30°C in formaldehyde in a final concentration of 1% v/v. Cells were then harvested by centrifugation and washed 3 times with PBS + 10 mM glycin, to be finally resuspended to 2 ODunits (OD.mL) in 200 µL TSEMS (50 mM Tris, pH 7.4, 50 mM NaCl, 10 mM EDTA, 0.5 M sucrose, 1x Protease Inhibitor Cocktail (Sigma), 13.2 ml H_2O).

Imaging was performed using a Zeiss ELYRA P.1 equipped with the following laser lines: a HR diode 50 mW 405 nm laser and a HR DPSS 200 mW 561 nm laser and an Andor EM-CCD camera iXon DU 897 camera. Fluorescence was detected using a long pass 570nm filter (LP570), similar to a procedure described before (Bach, Giacomelli, and Bramkamp 2017).

An alpha Plan-Apochromat 100x/1,46 Oil DIC M27 objective was used for imaging. 100 nm TetraSpeck microsphere and the implemented drift correction tool were used to check for lateral drift and eventual drift correction. Calculation of the PALM image was performed via the 2D x/y Gaussian fit provided by the Zen2 software (Zeiss) with the following parameters: a peak mask size of 9 pixels (1 pixel = 100 nm) and a peak intensity to noise ratio of 6 (overlapping events were discarded). Z-axis was stabilized using the "Definite Focus" system.

The *C. glutamicum* strains *ptsF::pamCherry-ptsF* and *ptsG::PAmCherry-linker-ptsG* were imaged in the same way for each different condition: fructose, glucose and acetate. During the 10,000 frames that were collected during imaging, PAmCherry was activated using a linear gradient of the 405 nm laser ranging from 0.01 % to 10% (the 405 laser power was chosen in a way that minimized conversion of two separate PAmCherry molecules in close proximity at the same time). Converted PAmCherry was imaged using the 561 nm laser at 15 % (transfer mode) for 50 ms using an EMCCD gain of 200. The localization events recognized by the Gaussian fit were filtered for photon number (70-350 photons) and point spread function (PSF) width at 1/e maximum (70-170 nm) in order to exclude the localization events originated by background (i.e.: dust particles) and/or the co-occurrence of multiple PAmCherry molecules.

2.8 Western Blot and in-gel fluorescence

For western blot confirmation of the strains, cultures were grown in CGXII with 2% of the specific PTS sugars as carbon sources to an OD_{600} = 4, then harvested by centrifugation and resuspended in 1 mL of disruption buffer (100 mM NaCl, 100 mm KCl, DNAse, protease inhibitor). Cells were subsequently disrupted by 10 cycles of 30 s at 6 m/s in FastPrep 24 (MP Biomedicals). The lysate was then centrifuged (18894 *g*, 15 min) and the supernatant containing the membrane fraction was mixed with loading dye

and 15 µL was loaded on 0.1% SDS-containing 12% polyacrylamide gel, separated by electrophoresis and transferred to a PVDF membrane. Western blotting was carried out using standard methods: Blocking step was performed by incubation of the membrane in 10 ml TBS + 5% milk for 1h at RT, the primary antibody anti-mCherry was added in a 1:2000 dilution, followed by incubation for 1 hour. After washing the membrane 3 times with TBS, the secondary anti-rabbit antibody was added diluted 1:10000 to 10 ml TBS-T + 5% milk and incubated membrane for 1hr at RT. After another washing step, 5-bromo-4chloro-3-indolylphosphate and nitroblue tetrazolium solution (NBD/BCIP) was added and the membrane was incubated in the dark until the colors on the membrane were developed.

For in-gel fluorescence of strains containing mNeonGreen fusions, SDS gels were analyzed with a Typhoon Trio 9410 (Amersham Biosciences, GE) with 488nm laser excitation of mNeonGreen and fluorescence was detected using a 520nm filter.

2.9   Statistical analysis

All statistical analysis and plotting were performed in RStudio. The data were first submitted to the shapiro-wilk (SW) test to test if the values were normally distributed. As our data generally does not follow a Gaussian distribution according to SW test, we employed the non-parametric Kruskal-Wallis (KW) test to compare the different treatments by ranks. Once KW test showed at least one significant difference among the treatments, the data went through a Multiple comparison test after Kruskal-Wallis (kruskalmc in R), where each protein (e.g. PtsF, PtsG) in each treatment (e.g. fructose, glucose, acetate, L-forms) was compared among each other. The group pairs which have observed differences higher than a pre-established critical value were considered statistically different at a significance level of 0.05. The relevant comparisons were taken in account, and the differences found in kruskalmc are expressed as letters next to the average values or plots.

3 Results

3.1 Construction of functional fusion proteins

In this study, we were interested in investigating the subcellular localization and membrane occupancy of PTS EII permeases, which is not optimal with plasmid-based fusions, as a varied number of plasmids per cell might result in varied levels of expression of our desired genes and consequently protein localization, number, occupancy and dynamics, causing overexpression artifacts. Therefore, a crucial step in this direction was the construction of strains containing allelic replacements where the function of PtsF/G was not affected by the attachment of the desired fluorophore.

To this end, we constructed *C. glutamicum* strains with fluorescent fusions PtsF and PtsG, resulting in strains CGM001 and CGM002 expressing mCherry-PtsF and mNeonGreen-PtsG, respectively (Table 2). To investigate a possible influence of the general PTS components in the dynamics of PtsF/G, we constructed the strains CGM007 and CGM009 expressing HPr-mVenus and eCFP-EI respectively (Table 2). Despite multiple attempts, the construction of an allelic replacement fluorescent fusion of EI was not possible, therefore we utilized a fully functional plasmid-based eCFP-EI. We have not included the sucrose specific PTS, since sucrose is a disaccharide composed of fructose and glucose and we wanted to first test for the specific influence of glucose and fructose. *C. glutamicum* imports and phosphorylates sucrose via the sucrose-specific PtsS. The phosphorylated sucrose is cleaved intracellularly and the resulting fructose molecule is exported and taken up by the fructose specific PtsF. Hence, a clean separation between sucrose and fructose effects is not easily possible.

To check for potential co-localization of the glucose and fructose specific EII permeases a double labelled strain was constructed. To this end, CGM001 was used as a background for incorporation of *mNeonGreen-linker-ptsG* via allelic replacement, resulting in the double-labelled strain *ptsF::mCherry-*

ptsF, ptsG::*mNeonGreen-linker-ptsG* (CGM003) (Fig. 4A). In order to gain quantitative single molecule resolution data of PTS localization and clustering patterns, strains containing PtsF (CGM004) and PtsG (CGM005) tagged with photoactivatable mCherry (PAmCherry) were constructed for PALM microscopy. To avoid overexpression and artificial expression heterogeneity, the fusion constructs were all inserted as allelic replacement in the genome of wild type *C. glutamicum* (RES 167) cells. To test the functionality of constructed fusion proteins, growth experiments and sugar consumption assays via HPLC were performed. Strains CGM001, expressing mCherry-PtsF (Fig. 4B), CGM002 expressing mNeonGreen-PtsG (Fig. 4C) and the double labelled strain CGM003 displayed wild type like growth behavior (Figs. 4D and 4E). The growth rates of wild type did not differ from the constructed strains and ranged from 0.28 to 0.29 h^{-1} (Table 3), showing that the tagged PTS were functioning wild type-like. We also measured sugar consumption rates in CGXII supplemented with 2% fructose or 2% glucose. The specific sugar consumption rates q_s were highly similar for wild type and mutant strains (Table 3). The measured q_s values for the wild type of around 0.23 g g^{-1} h^{-1} for glucose and 0.14 g g^{-1} h^{-1} for fructose are very well within the expected range for the observed growth rate (Kawaguchi *et al.* 2018). The strain carrying the fluorescently labelled PtsG had consumption rates of 0.23 g g^{-1} h^{-1} for glucose and the strain with the PtsF fusion construct displayed consumption rates of 0.17 g g^{-1} h^{-1} for fructose. In summary, we conclude that the constructed fusions are fully functional. It should be noted here, that in a process to gain functional translational fusions, several constructs were made that were all not further analyzed when they turned out to be non-functional, as cells were not able to grow wild type-like when in minimal medium with the specific PTS sugar as sole carbon source.

Protein localization studies using translational fusions can be hampered by protein degradation and subsequent imaging of free fluorophore. Therefore, we investigated protein degradation by western blotting with anti-mCherry for mCherry and PAmCherry fusions, and in-gel fluorescence for mNeonGreen, eCFP and mVenus fusions. For each strain, it was possible to identify a band

corresponding to their full length fusion protein and when present, oligomers, revealing that no major degradation was present (Fig. 5). We therefore conclude that localization studies with these strains should reveal the native localization of the full length PTS EII permeases.
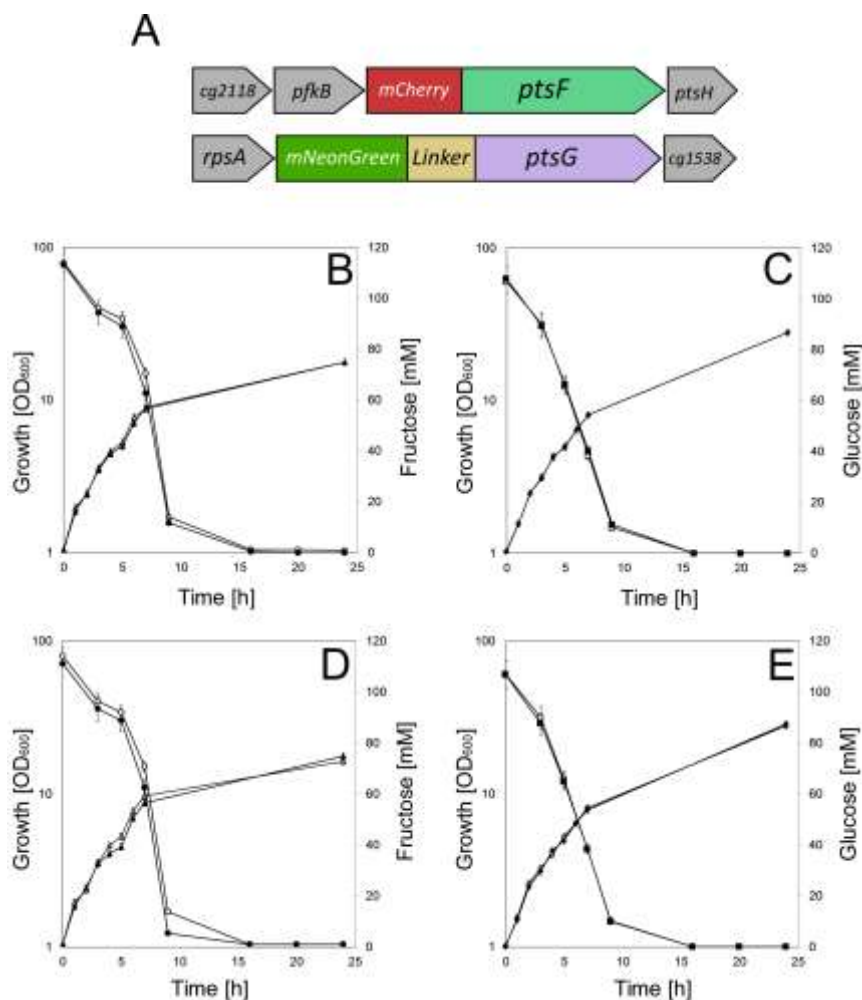

Figure 4. Fluorescent fusions of PtsF and PtsG are fully functional. (A) Genetic arrangement of fluorescent fusions constructed via allelic replacement of *ptsF::mCherry-ptsF* and *ptsG::mNeonGreen-linker-ptsG*. Growth and sugar consumption of *C. glutamicum* strains CGM001 (B), CGM002 (C) and CGM003 (D, E) (filled symbols) versus wild type RES 167 (open symbols) on CGXII containing (B, D) 100 mM fructose and (C, E) 100 mM glucose. Fructose consumption (circles), glucose consumption (squares), growth on fructose (triangles), and growth on glucose (diamonds) are indicated. Each point represents biological triplicates and standard deviation is indicated.

Table 3. Growth rates and sugar consumption rates. Growth rate [h^{-1}] and substrate uptake [g g-1 h-1] of RES 167 WT and strains CGM001, CGM002, CGM003 and CGM005 in CGXII supplemented with glucose and fructose.

|	Glucose		Fructose	
	growth rate [h^{-1}]	uptake (qs) [g g^{-1} h^{-1}]	growth rate [h^{-1}]	uptake (qs) [g g^{-1} h^{-1}]
WT	0.28	0.23 ± 0.003	0.289	0.14 ± 0.005
CGM001	-	-	0.286	0.17 ± 0.004
CGM002	0.28	0.23 ± 0.001	-	-
CGM003	0.29	0.23 ± 0.001	0.280	0.17 ± 0.004
CGM005	0.28	0.23 ± 0.001	-	-
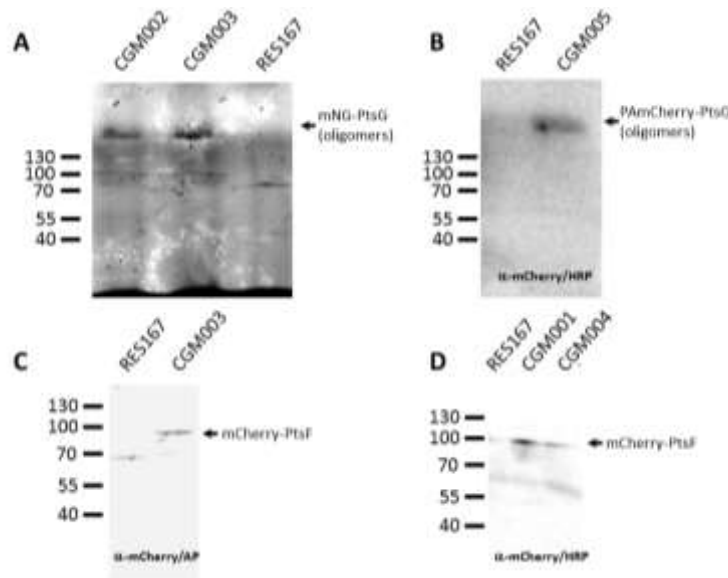
Figure 5. Control for full-length fusion proteins. In gel-fluorescence (A) and western blot analysis (B-D) with cell lysates of strains CGM001-006. (A) In gel fluorescence of cell lysates of CGM002 (mNeonGreen-PtsG) and CGM003 (mNeonGreen-PtsG in double labelled strain background) reveal the existence of oligomeric mNeonGreen-PtsG. (B) Western blot of cell lysate of CGM005 (PA-mCherry-PtsG) developed with α-mCherry antibodies and HRP-coupled secondary antibodies. PA-mCherry-PtsG is detected as oligomeric band with no apparent degradation products. (C) Western blot of cell lysate of CGM003 (mCherry-PtsF) developed with α-mCherry and AP-coupled secondary antibodies. (D) Western blot of cell lysate of CGM001 (mCherry-PtsF) and CGM004 (PA-mCherry-PtsF) developed with α-mCherry and HRP-coupled secondary antibodies. Note that little degradation is observed for all fusion constructs. PtsF = 70.51 kDa, PtsG = 72.57 kDa, mCherry = 28.8 kDa, mNeonGreen = 26.6 kDa.

3.2   Localization of the general PTS components HPr and EI

Previous work has shown that also the general components EI and HPr might be localized in a substrate dependant manner in *E. coli* (Lopian *et al.* 2010). Therefore, we wanted to address the localization of the general PTS components in *C. glutamicum*. Similar to the strategy employed for the EII components, we wanted to construct functional allelic replacements of EI and HPr. We succeeded in the generation of a HPr-mVenus fusion (h*pr::hpr-mVenus,* CGM007), and despite several attempts, we were not able to construct an allelic replacement-based EI fusion, therefore we utilized a plasmid-based eCFP-EI fusion in a *ΔptsI* background (CGM009). The strains had wild-type growth in CGXII with glucose as sole carbon source (Fig. 6A and B), confirming the functionality of HPr and EI. In-gel fluorescence revealed the expected size of HPr fused to mVenus, as well as monomers, dimers and trimers of EI, with no signs of protein degradation (Fig. 6C).

Widefield microscopy of cells grown in CGXII for 5 hours with different carbon sources revealed that both HPr and EI localize dispersly in the cytoplasm regardless of the presence or absence of PTS sugars. We noticed that EI seems to localize more densely over the nucleoid when cells were grown in glucose or fructose (Fig. 6D and E). The corrected total fluorescence (CTF) was calculated with ImageJ based on the obtained fluorescence microscopy images and corrected for the cell area, and the values for cells expressing eCFP-EI and HPr-mVenus grown in different carbon sources are: glucose EI = 5665.92 ± 2212.942, HPr = 2117.72 ± 619.75, fructose EI = 5152.70 ± 1600.91, HPr = 1940.18 ± 440.30 and sodium acetate EI = 4983.00 ± 1918.99, HPr = 1807.13 ± 311.95. This suggests an inverse correlation between cell size and CTF readings, as cells grown in glucose (3.48 ±0.42 µm²) tend to be smaller than cells grown in fructose (3.24 ±0.36 µm²) and acetate (4.06 ±0.72 µm²). HPr and EI expressions are therefore constitutive. Overall, our data with eCFP-EI and HPr-mVenus show that in *C. glutamicum*, the general PTS components EI and HPr do not form clusters.
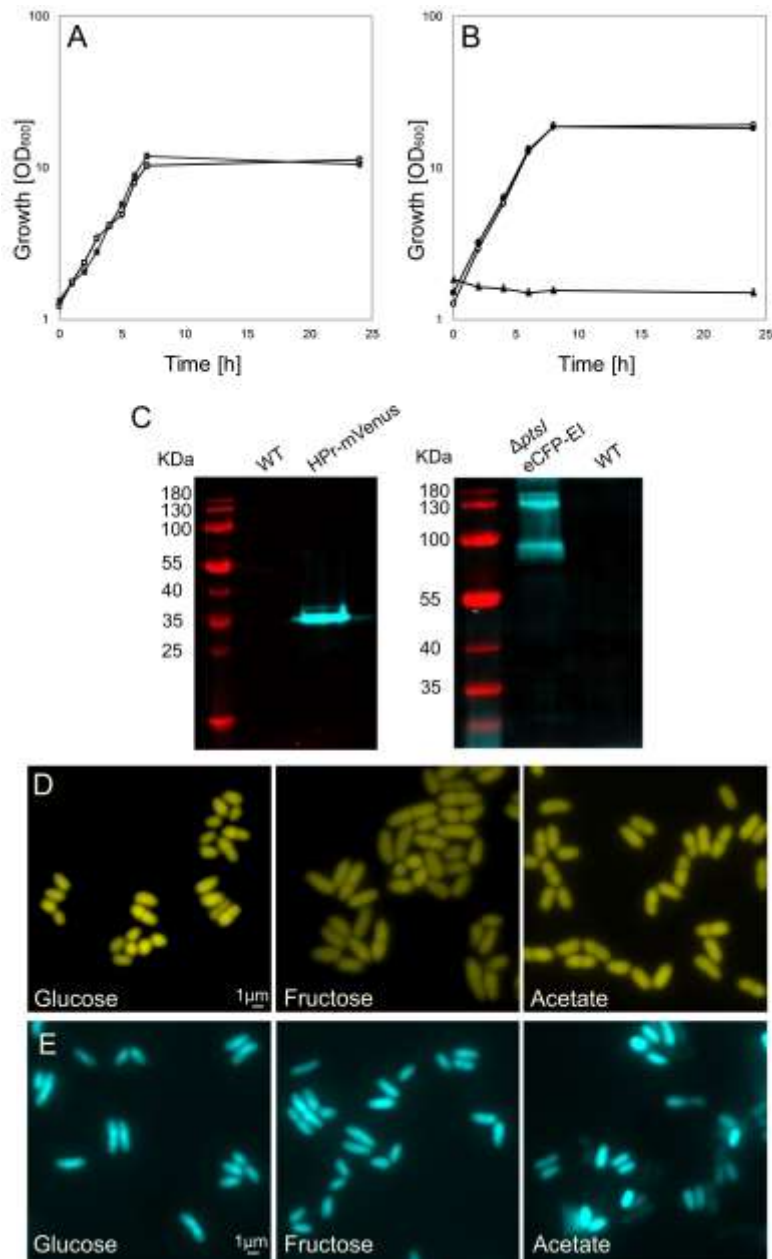
Figure 6. HPr and EI localize dispersely in the cytoplasm. (A) Growth of *C. glutamicum* strain CGM007 (*hpr::hpr-mVenus*) (filled squares) versus wild type RES 167 (open squares) in CGXII containing 100 mM glucose (B) Growth of *C. glutamicum* strain CGM009 (*ΔptsI* with pEKEx2_eCFP-EI) (filled circles) versus wild type RES 167 (open circles) and CGM008 (*ΔptsI*) (filled triangles) in CGXII containing 100 mM glucose (C) In-gel fluorescence of crude extract of RES 167, CGM007 and CGM009. The expected size of the HPr-mVenus fusion protein is 35,5 kDa and eCFP-EI is 85,61 kDa (D) Epifluorescence microscopy images of *C. glutamicum* expressing HPr-mVenus grown for 5 hours in indicated carbon sources (E) Epifluorescence microscopy images of *C. glutamicum* expressing eCFP-EI grown for 5 hours in indicated carbon sources.

38

3.3 Subcellular localization of EII^{fru} EII^{glc} permeases in *C. glutamicum*

Next we wanted to investigate whether PTS EII proteins distribute uniformly or in clusters along the cytoplasmic membrane under aerobic conditions in presence of the transported sugars. To this end, fluorescence microscopy was performed on *C. glutamicum* strains expressing mNeonGreen-PtsG and mCherry-PtsF grown in CGXII supplemented with the transported sugars as sole carbon sources. Analysis of fluorescence images showed that both proteins form membrane embedded clusters that localize punctually within the cell membrane with no preferred positions (Fig. 7A-B). EII^{fru} and EII^{glc} foci of varying intensity were observed, suggesting complexes with different amounts of proteins. Most cells contained few bright and intense foci that were randomly distributed. However, bright foci seemed to be present with higher frequency close to cell poles (Fig. 7A-B).
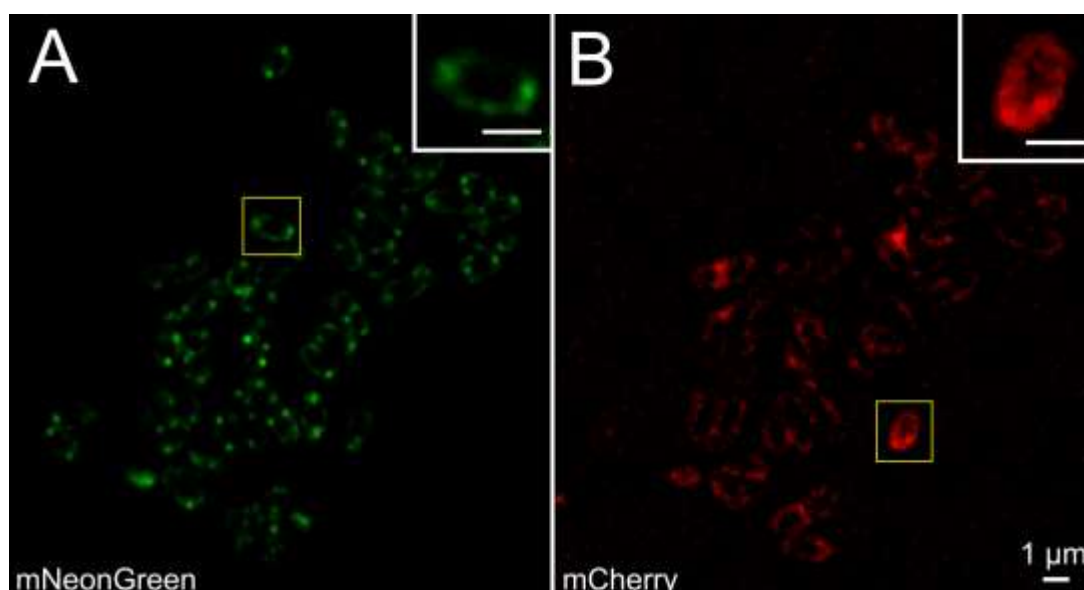
Figure 7. PtsF and PtsG localize as clusters distributed along the cytoplasmic membrane. Epifluorescence microscopy images of *C. glutamicum* expressing mCherry-PtsF and mNeonGreen-PtsG under different growth conditions: Cells grown in CGXII with (A) glucose and (B) fructose as sole carbon sources.

3.4   Cell wall-deficient *C. glutamicum*

We next wanted to test whether cell shape and the surface/volume ratio might have an influence on the PTS EII permeases. Therefore, we analyzed PTS localization in L-form bacteria, generated out of the corresponding strains. Cells expressing mNeonGreen-PtsG and mCherry-PtsF were grown in MSM/CGXII medium supplemented with the transported sugars in presence of D-cycloserine (DCS). DCS is a cyclic analogue of D-alanine that competitively inhibits alanine racemase (Alr) and D-alanine:D-alanine ligase (Ddl), stopping the synthesis of peptidoglycan precursors, effectively stopping cell wall synthesis when present in medium, and as DCS was previously used in *Mycobacterium tuberculosis* (Prosser and de Carvalho 2013), which shares the characteristic cell wall common to all *Corynebacterineae*, it was chosen for L-form formation with *C. glutamicum*. L-form bacteria require an osmotically stabilized medium. Usually, the osmoprotective environment would be achieved by adding sucrose to the media, but since this sugar is taken up by the sucrose specific PtsS, we complemented the L-form medium with xylose, a carbohydrate that does not support growth of *C. glutamicum* (Fig. 8) (Kawaguchi *et al.* 2006).

Unlike most rod-shaped bacteria, *C. glutamicum* grows apically. In our experiments with L-forms, cells from a pre-culture were grown in presence of DCS in osmoprotective medium, where the expected growth from the poles with no new synthesis of peptidoglycan was observed. This resulted in early cells with vestigial cell wall from before addition of DCS in medium (Fig. 9A). The polar growth continued until spherical cells, deficient of cell wall, would detach from the mother cell (Fig. 9B). Further propagation of cell wall-deficient cells (L-forms) was disorganized, seeming to follow the classical FtsZ-independent, extrusion-resolution mechanism (Leaver *et al.* 2009) and happened when cells grew past a certain threshold, which gave rise to a variety of cell sizes, from tiny to very big (Fig. 9C). This method of division was previously observed in L-forms of other bacteria, such as *B. subtilis* (Mercier, Kawai, and Errington 2014; Leaver *et al.* 2009), *K. viridifaciens*

(Ramijan *et al.* 2018), and *E. coli* (Mercier, Kawai, and Errington 2014). Importantly, to maintain L-form cultures, new DCS was added every 24h, and our DCS-induced L-forms were able to generate rod-shaped cells until the culture was fully composed of normal cells if no new DCS was added in medium.

Fluorescence microscopy with L-forms revealed the same PtsF and PtsG clustering that was observed in rod-shaped cells (Fig. 10A, B). We conclude from this, that cluster formation of PTS EII permeases may be an intrinsic property of these complexes and not dependent only on cell shape or surface/volume ratios.
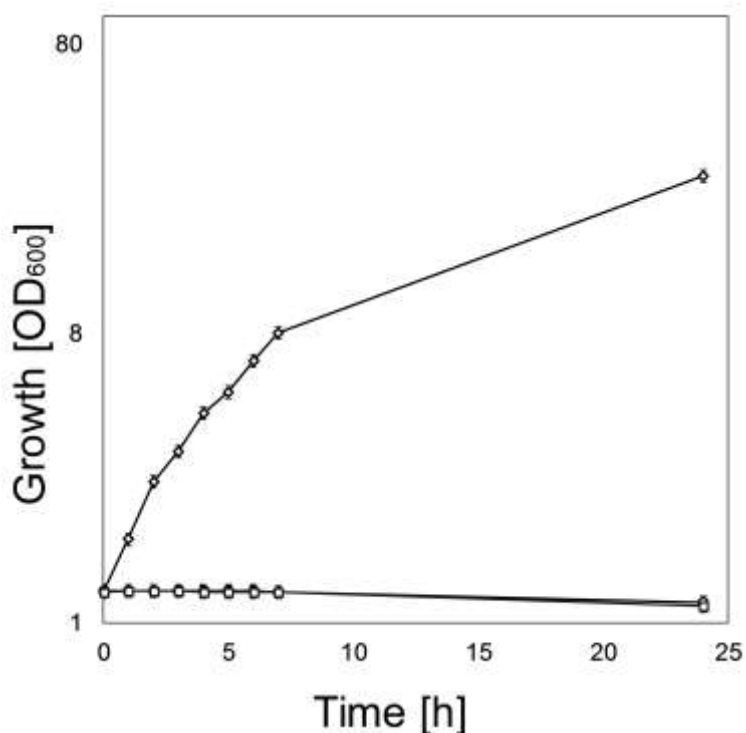
Figure 8. Growth of *C. glutamicum* wild type RES 167 in CGXII containing 100 mM glucose (diamonds), xylose (squares) and no carbon source (circles). Each point represents biological triplicates and standard deviation is indicated.
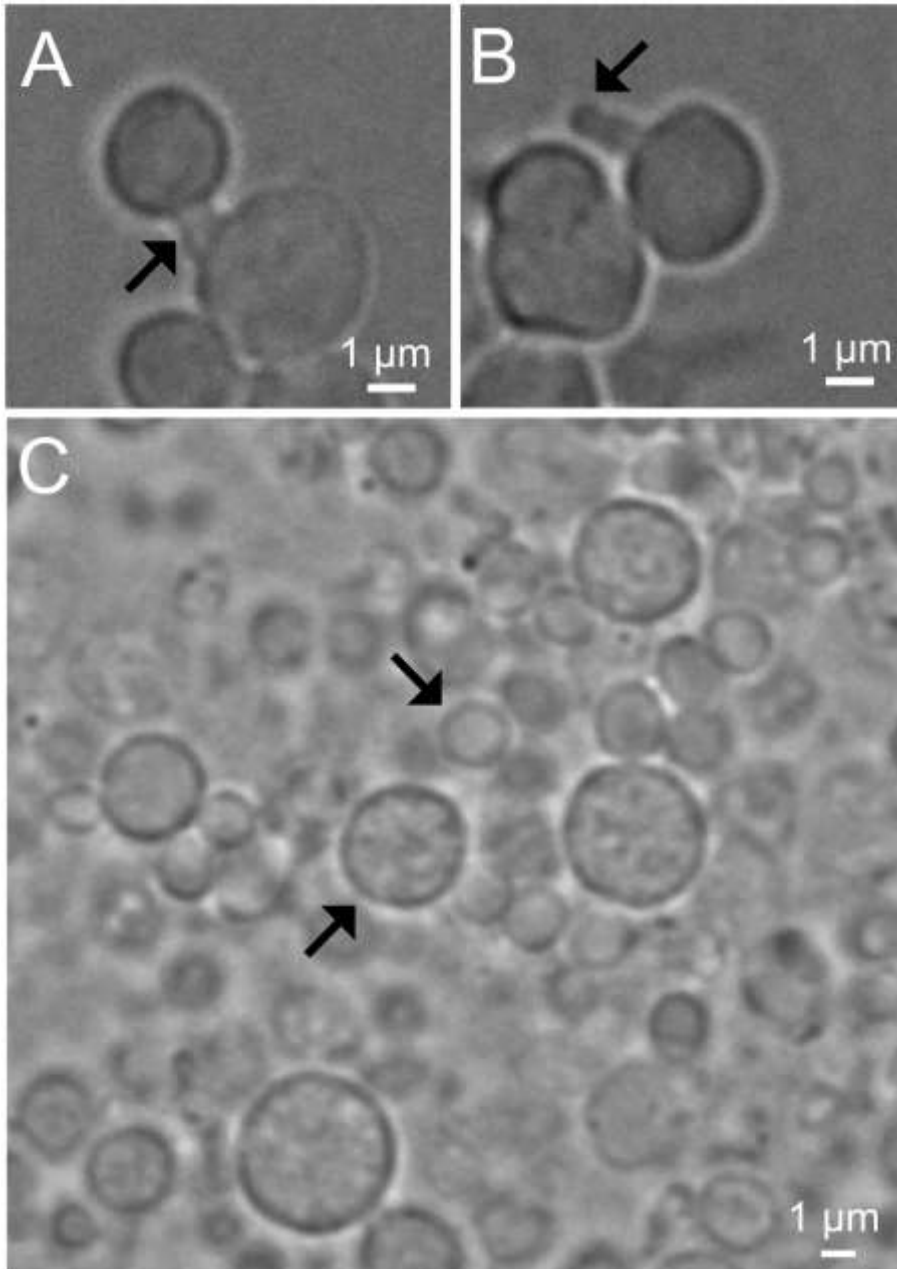
Figure 9. *C. glutamicum* **in presence of DCS is able to grow as L-forms.** Arrows indicate (A) vestigial cell wall with growth from the poles, (B) pole with no growth, (C) L-forms of varied sizes. L-form cells grown in MSM/CGXII with glucose as sole carbon source in presence of 200 µg/ml of DCS.
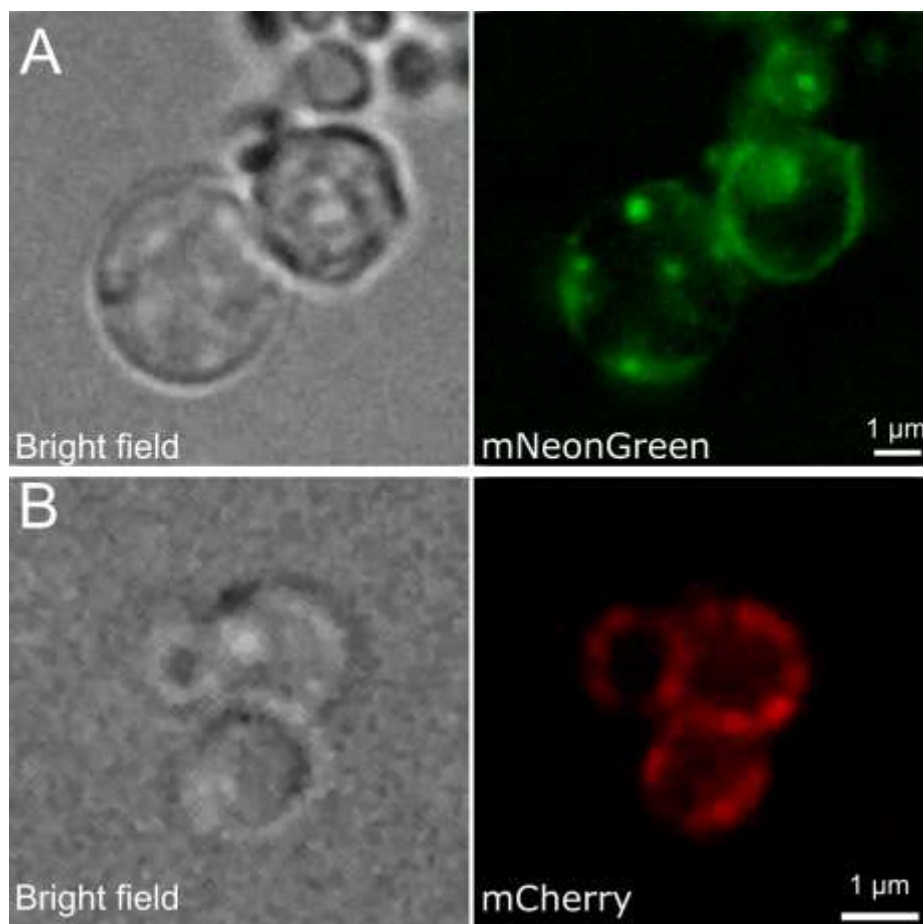
Figure 10. PTS clusters in cell wall deficient *C. glutamicum* cells. L-form cells expressing (A) mNeonGreen-PtsG and (B) mCherry-PtsF. L-form cells grown in MSM/CGXII with (A) glucose and (B) fructose as sole carbon sources in presence of 200 µg/ml of DCS.

3.5 *C. glutamicum* EII^{fru} EII^{glc} spatial dynamics upon presence or absence of the transported sugars

We next wanted to investigate whether presence or absence of the specific PTS carbohydrates influence the PTS EII permeases localization and expression. To this end, the strains containing fluorescent reporters linked to the EII complexes were grown in CGXII minimal medium with 2% glucose, fructose or acetate as sole carbon sources to early exponential phase, and fluorescent microscopy was subsequently performed. Acetate is taken up by

diffusion and/or via MctC, a secondary transporter that belongs to the class of sodium solute symporters (Jolkver *et al.* 2009). Importantly, both proteins are expressed in the absence of their specific transported sugars (Fig. 11A-C), and no differences among early, mid and late log phases were observed (data not shown). We also observed EII clustering when cells were grown in acetate (Fig. 11C). Observed PtsG/F foci did not show evident co-localization (Fig. 11D), suggesting that phosphotransferase systems localize independently within the membrane. This is an important observation, because the general PTS components EI and HPr are required for activation of both EII complexes.

As a control we analyzed localization of the EII[fru] complexes with a protein from the respiratory chain. Here, we have chosen the succinate dehydrogenase subunit A (SdhA) in combination with PTS EII[Fru]. SdhA is part of the complex II of the respiratory chain, and previous work suggested that the PTS and respiratory chain proteins form separate complexes that compete against each other for membrane space. In this scenario, bacteria regulate their membrane occupancy according to its necessity, where an increase in respiration would cause an increase in RC proteins and a decrease in PTS proteins. At the same time, an increase in sugar uptake causes an increase in PTS permeases and concomitant decrease in RC proteins (Zhuang *et al.* 2011). We did observe a large degree of co-localization between PtsF and SdhA (Fig. 11E). SdhA localizes in a similar fashion as PtsF and PtsG, forming membrane embedded clusters of varied sizes and shapes with a slightly higher concentration on cell poles (Fig. 11E). On a scale that can be analyzed in diffraction limited microscopy, our data rule out that in *C. glutamicum,* components of the respiratory chain and the PTS would always occupy specific and different membrane domains.
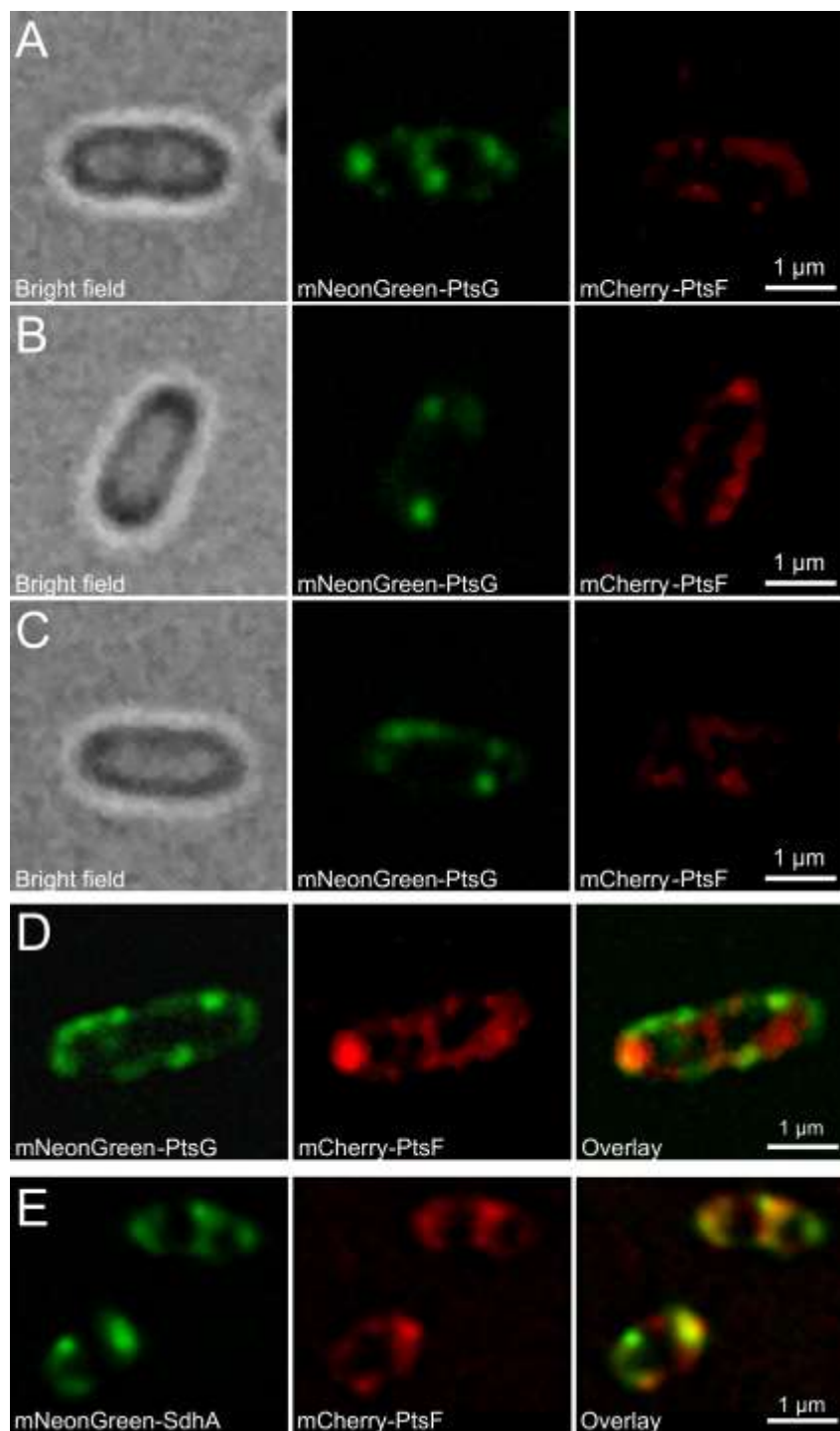
Figure 11. PtsF and PtsG clustering changes upon presence or absence of transported substrate. Epifluorescence microscopy images of *C. glutamicum* expressing mCherry-PtsF and mNeonGreen-PtsG under different growth conditions. Cells grown in CGXII with 2% (A) glucose, (B) fructose or (C) acetate as sole carbon sources. (D) mNeonGreen-PtsG and mCherry-PtsF in CGXII with 2% glucose and fructose. (E) mNeonGreen-SdhA and mCherry-PtsF in CGXII with 2% fructose.

45

After the observation that clustering and expression of PTS EII occurs even in absence of the transported substrate, we next wanted to determine the influence of different carbon sources on PTS foci number per cell, foci area, fluorescence, and how much of the membrane space is covered by PTS. Analysis of fluorescent images of the strain CGM003, expressing mCherry-ptsF and mNeonGreen-ptsG both in rod shaped cells and L-forms grown in minimal medium in presence of different carbon sources, revealed that the number of PtsF/G clusters per cell was significantly decreased in presence of the transported sugar in rod-shaped cells (Table 4 and Fig. 12). Statistically, the number of PtsF clusters per cell was equal in acetate and glucose treatments, and differed in rod-shaped and L-form cells grown in fructose. PtsG foci number per cell in rod-shaped cells grown in fructose or acetate did not differ statistically, whilst when grown in glucose, the values were significantly lower. L-form cells showed a tendency to have more foci, having higher averages (3.3 per cell for both PtsF/G), being statistically different from all the other treatments. The absence of a cell wall in L-forms results in significantly larger cells (mean values: rod-shaped 3.6 µm², L-forms 8.9 µm²), which leads to a drastic reduction in the cell surface/volume (S/V) ratio. Despite being grown in medium containing the same carbon source, the observed increase in number of PtsF/G clusters in L-forms suggests that PTS EII foci pattern can be changed in response to variations in cell area, volume or morphology, although these changes are proportional to the larger cell size of L-forms.

Table 4. Number of PTS EII foci per cell in various growth conditions. Mean values of foci number per cell of mCherry-PtsF and mNeonGreen-PtsG. "Fructose", "Glucose" and "Acetate" represent rod-shaped cells in CGXII medium with the respective carbon sources. "L-forms" represent L-form cells in MXM/CGXII supplemented with the transported substrate. Significant statistical differences according to multiple comparison test after Kruskal-Wallis are represented as letters next to each value.

	Fructose	Glucose	Acetate	L-forms
PtsF	2.4 (b)	2.6 (a)	2.9 (a)	3.3 (c)
PtsG	2.8 (a)	2.5 (b)	2.8 (a)	3.3 (c)
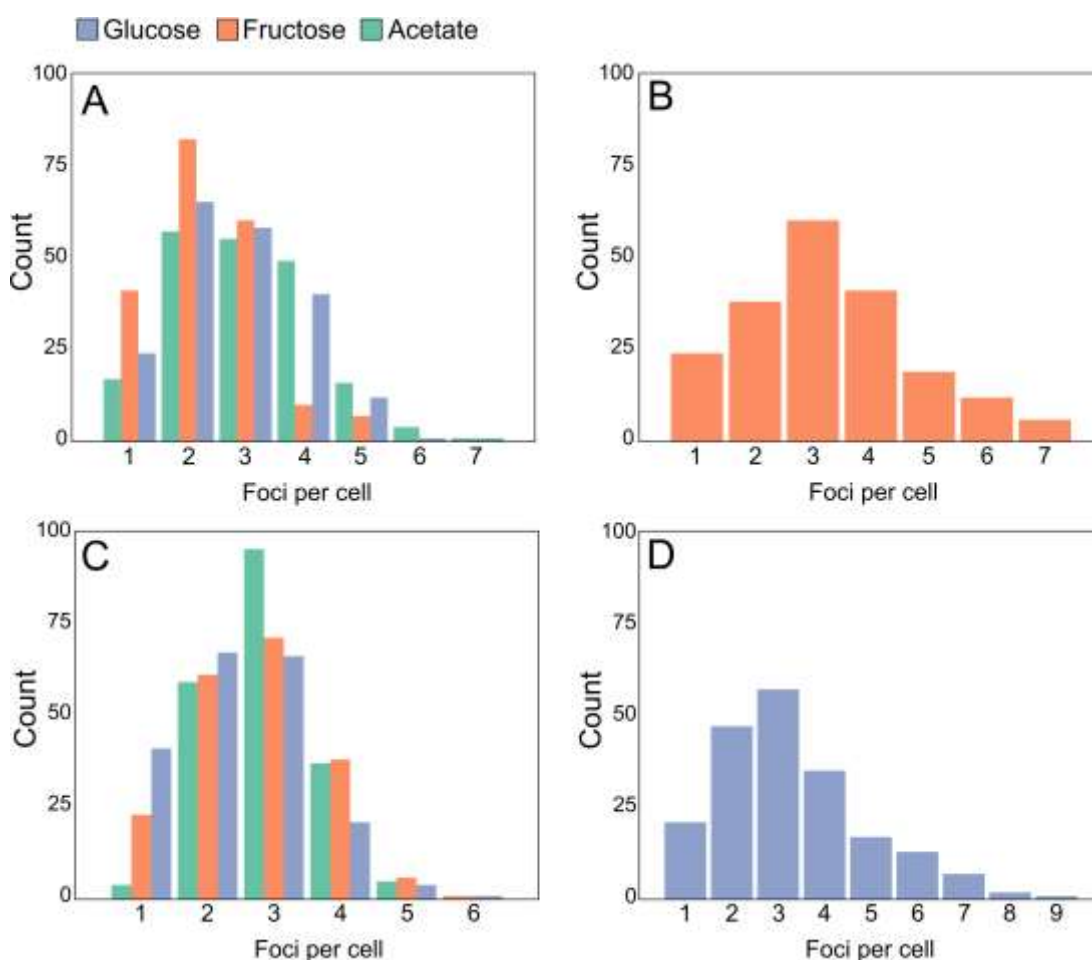
Figure 12. mCherry-PtsF and mNeonGreen-PtsG foci number decreases in presence of transported sugar. Frequency of the number of foci per cell of (A) mCherry-PtsF in rod shaped cells, (B) mCherry-PtsF in L-form cells. (C) mNeonGreen-PtsG in rod shaped cells, D) mNeonGreen-PtsG in L-form cells.

Previous studies have revealed that the expression of the *C. glutamicum* PTS is induced when cells are cultured in presence of the transported sugar (Parche *et al.* 2001; Engels and Wendisch 2007; Tanaka *et al.* 2008; Engels, Lindner, and Wendisch 2008). In order to test the influence of different carbon sources on PTS foci, PtsF/G Corrected Total Fluorescence (CTF) was calculated with ImageJ based on the obtained fluorescence microscopy images and corrected for the cell area (Fig. 13A-B). Analysis of CTF of tagged proteins served as a proxy to assess levels of protein expression and concentration, and both PtsF and PtsG were similar regarding the fluorescence readings in this work. Although all the treatments were statistically different from each other, CTF of both proteins increased in presence of the transported substrate and decreased in its absence. This indicates that indeed, *ptsF* and *ptsG* expression was induced in presence of the transported substrate as described before (Tanaka *et al.* 2008).

The areas of the individual PtsF/G foci of cells grown in different carbon sources are summarized in Figure 14A and Table 5. In rod-shaped cells, PtsF foci area values were statistically similar when cells were grown in glucose or acetate, and significantly higher in fructose. Likewise, PtsG foci area in glucose was 3 times higher than in fructose, and 4 times than in acetate. However, unlike PtsF, the PtsG cluster area values obtained for cells grown in fructose were higher than cells grown in acetate. L-form cells exhibited the highest PtsF/G foci areas compared to every other condition in rod-shaped cells, suggesting that a larger membrane area create more space to be occupied by transmembrane proteins.

In order to know how much of the cytoplasmic membrane is occupied by PTS, the ratio foci area/cell area (Fig. 14B) was calculated. For rod-shaped cells, the ratio of cells expressing mCherry-PtsF grown in fructose (0.10 ±0.04) was significantly higher than cells grown in glucose (0.05 ±0.04), which was in turn, statistically similar as cells grown in acetate (0.06 ±0.03). For mNeonGreen-PtsG, cells had a higher ratio in presence of glucose (0.20 ±0.15), followed by fructose (0.06 ±0.03), and finally acetate (0.04 ±0.02)

(Table 6). Therefore, rod-shaped cells had the highest ratios when in presence of the transported sugar, meaning that more membrane space is reallocated for PTS proteins in such conditions.

In general, L-forms exhibited larger PTS clusters, in a higher overall number, and fluorescence. This leads to the logical assumption that a larger cell area increases the area available for protein insertion, possibly resulting in more transmembrane PTS proteins. However, the foci area/cell area ratio of L-forms was not higher than other rod-shaped cells. In fact, despite PtsF L-form values (0.08 ±0.07) being higher than in rod-shaped cells grown in glucose (0.05 ±0.04) or acetate (0.06 ±0.03), they were lower than rod-shaped cells in fructose (0.10 ±0.04) (Table 6). Roughly the same was observed for PtsG: even though L-forms had a higher foci area/cell area ratio (0.09 ±0.10) than rod-shaped cells in general, there was no statistical difference between their values and rod-shaped cells grown in fructose (0.06 ±0.03), a condition where PtsG is hardly induced.
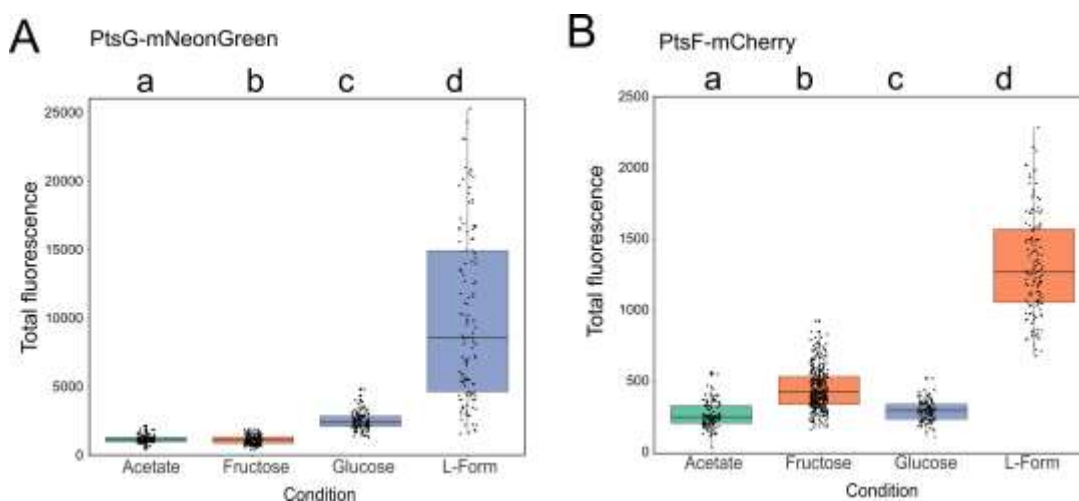

Figure 13. *C. glutamicum* PTS expression increases in presence of transported sugar. Corrected total fluorescence of (A) mNeonGreen-PtsG and (B) mCherry-PtsF. "Fructose", "Glucose" and "Acetate" represent rod-shaped cells in CGXII medium with the respective carbon sources. "L-form" represents L-form cells in MSM/CGXII supplemented with fructose for PtsF and glucose for PtsG. Significant statistical differences according to multiple comparison tests after Kruskal-Wallis are represented as letters above each graph.

Table 5. PtsF and PtsG cover different membrane surface areas. Mean values of foci area [µm²] of mCherry-PtsF and mNeonGreen-PtsG. "Fructose", "Glucose" and "Acetate" represent rod-shaped cells in CGXII medium with different carbon sources. "L-forms" represent L-form cells in MXM/CGXII supplemented with the transported substrate. Values are in µm². Significant statistical differences according to Multiple comparison tests after Kruskal-Wallis are represented as letters next to each value.

	Fructose	Glucose	Acetate	L-forms
PtsF	0.35 (b)	0.18 (a)	0.24 (a)	0.71 (c)
PtsG	0.22 (a)	0.70 (b)	0.17 (c)	1.00 (d)
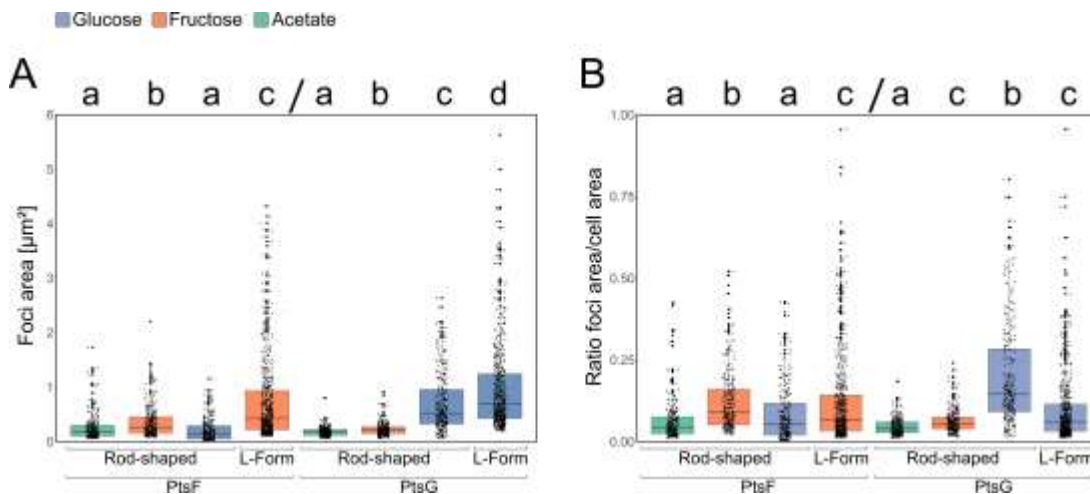
Figure 14. mCherry-PtsF and mNeonGreen-PtsG foci area increases upon presence of transported sugar. (A) mCherry-PtsF and mNeonGreen-PtsG fluorescent foci area in rod-shaped and L-form cells in CGXII supplemented with different carbon sources (B) Ratio foci area and cell area under different carbon sources and cell shapes. "L-form" represent L-form cells in MSM/CGXII supplemented with the transported sugar. Significant statistical differences according to multiple comparison tests after Kruskal-Wallis are represented as letters above each graph. Different letters indicate differences within the same PTS protein.

50

Table 6. PTS EII complex surface coverage. Foci area/cell area ratio of mCherry-PtsF and mNeonGreen-PtsG. "Fructose", "Glucose" and "Acetate" represent rod-shaped cells in CGXII medium with different carbon sources. "L-forms" represent L-form cells in MXM/CGXII supplemented with the transported substrate. Significant statistical differences according to multiple comparison tests after Kruskal-Wallis are represented as letters next to each value.

	Fructose	Glucose	Acetate	L-forms
PtsF	0.10±0.04 (b)	0.05 ±0.04 (a)	0.06 ±0.03 (a)	0.08 ±0.07 (c)
PtsG	0.06 ±0.03 (c)	0.20 ±0.15 (b)	0.04 ±0.02 (a)	0.09 ±0.10 (c)

3.6   PTS subcellular localization in mixed carbon sources

Next, we wanted to test the effects of mixed carbon sources on PTS foci. To this end, the strain CGM003 expressing mCherry-PtsF and mNeonGreen-PtsG was grown in CGXII minimal medium containing, as carbon source, 2% glucose + 2% sodium acetate (namely "GlcAce"), 2% glucose + 2% fructose (namely "GlcFru"), and 2% fructose + 2% sodium acetate (namely "FruAce") for the same widefield microscopy experiments and image analysis performed previously. We found that PtsF and PtsG once again had similar patterns: the PTS foci area, foci number and ratio foci area/ cell area of cells grown in the mixed treatments had generally values in between the ones found for cells grown in medium with only one carbon source.

The number of fluorescent foci observed in the treatments for both PtsF (glucose = 2.6, fructose = 2.4, acetate = 2.9, glucose + fructose = 2.3, glucose + acetate = 3.2, fructose + acetate = 2.8) and PtsG (glucose = 2.6, fructose = 2.8, acetate = 2.8, glucose + fructose = 2.4, glucose + acetate = 3.1, fructose + acetate = 2.6) followed the same pattern: In presence of the transported sugar in medium, cells tend to have less clusters (Table 7).

Values of mNeonGreen-PtsG foci area were statistically significantly higher in treatments where glucose was present in medium (glucose = 0.70 µm², fructose = 0.22 µm², acetate = 0.17 µm², glucose + fructose = 0.44 µm²,

glucose + acetate = 0.55 µm², fructose + acetate = 0.17 µm²), and the same was observed for mCherry-PtsF foci in presence of fructose (glucose = 0.18 µm², fructose = 0.35 µm², acetate = 0.24 µm², glucose + fructose = 0.27 µm², glucose + acetate = 0.22 µm², fructose + acetate = 0.38 µm²). The ratio foci area/ cell area represents the membrane surface covered by PTS foci, and the values observed for treatments where the transported sugar was present were significantly higher in both PtsG glucose = 0.20 ±0.15, fructose = 0.06 ±0.03, acetate = 0.04 ±0.02, glucose + fructose = 0.16 ±0.12, glucose + acetate = 0.14 ±0.13, fructose + acetate = 0.05 ±0.05 and PtsF (glucose = 0.05 ±0.04, fructose = 0.10 ±0.04, acetate = 0.06 ±0.03, glucose + fructose = 0.11 ±0.13, glucose + acetate = 0.06 ±0.05, fructose + acetate = 0.12 ±0.12) (Tables 8 and 9, Fig. 15).

Table 7. Number of PTS EII foci per cell in various growth conditions. Mean values of foci number per cell of mCherry-PtsF and mNeonGreen-PtsG. Headers represent cells in CGXII medium with 2% of different carbon sources, and mixtures were made with the final concentration of 2% of each carbon source. Significant statistical differences according to multiple comparison test after Kruskal-Wallis are represented as letters next to each value.

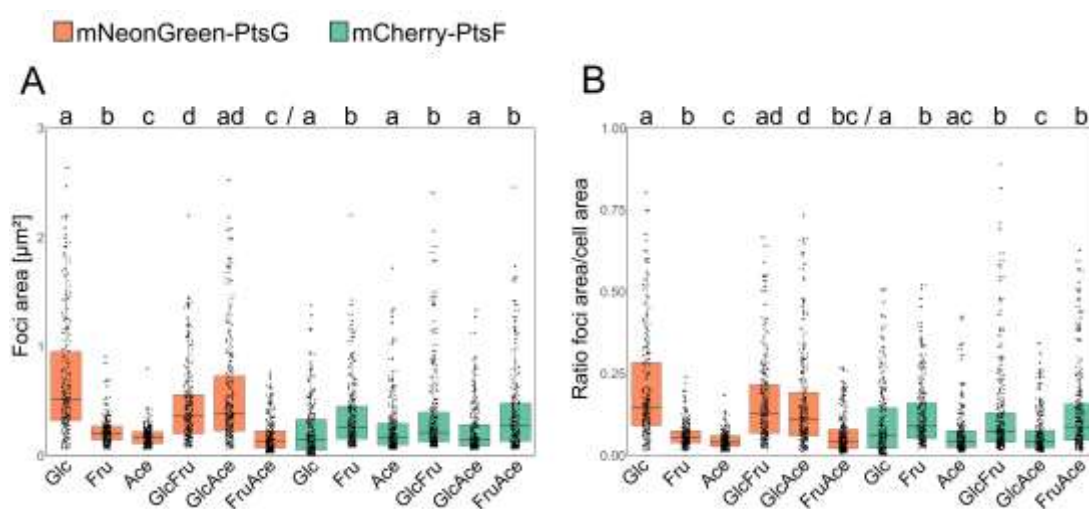|	Glucose	GlcFru	GlcAce	Fructose	FruAce	Acetate
PtsF	2.6 (a)	2.3 (c)	3.2 (a)	2.4 (b)	2.8 (b)	2.9 (a)
PtsG	2.5 (a)	2.4 (c)	3.1 (d)	2.8 (b)	2.6 (c)	2.8 (b)

Table 8. PtsF and PtsG cluster sizes based on carbon source. Mean values of foci area [µm²] of mCherry-PtsF and mNeonGreen-PtsG. Headers represent cells in CGXII medium with 2% of different carbon sources, and mixtures were made with the final concentration of 2% of each carbon source. Values are in µm². Significant statistical differences according to Multiple comparison tests after Kruskal-Wallis are represented as letters next to each value.

	Glucose	GlcFru	GlcAce	Fructose	FruAce	Acetate
PtsF	0.18 (a)	0.27 (b)	0.22 (a)	0.35 (b)	0.38 (b)	0.24 (a)
PtsG	0.70 (a)	0.44 (d)	0.55 (ad)	0.22 (b)	0.17 (c)	0.17 (c)

Table 9. PTS EII complex surface coverage. Foci area/cell area ratio of mCherry-PtsF and mNeonGreen-PtsG. Headers represent cells in CGXII medium with 2% of different carbon sources, and mixtures were made with the final concentration of 2% of each carbon source. Significant statistical differences according to multiple comparison tests after Kruskal-Wallis are represented as letters next to each value.

	Glucose	GlcFru	GlcAce	Fructose	FruAce	Acetate
PtsF	0.05 ±0.04	0.11 ±0.13	0.06 ±0.05	0.10±0.04	0.12 ±0.12	0.06 ±0.03
	(a)	(b)	(c)	(b)	(b)	(ac)
PtsG	0.20 ±0.15	0.16 ±0.12	0.14 ±0.13	0.06 ±0.03	0.05 ±0.05	0.04 ±0.02
	(a)	(ad)	(d)	(b)	(bc)	(c)

Figure 15. mCherry-PtsF and mNeonGreen-PtsG foci area increases upon presence of transported sugar. (A) mCherry-PtsF and mNeonGreen-PtsG fluorescent foci area on cells grown in CGXII supplemented with different carbon sources (B) Ratio foci area and cell area under different carbon sources. Glc = 2% glucose, Frc = 2% fructose, Ace = 2% sodium acetate, GlcAce = 2% glucose + 2% sodium acetate, GlcFrc = 2% glucose + 2% fructose, and FruAce = 2% fructose + 2% sodium acetate. Significant statistical differences according to multiple comparison tests after Kruskal-Wallis are represented as letters above each graph. Different letters indicate differences within the same PTS protein.

### 3.7 Effect of growth temperature on PTS occupancy

Many external factors such as nutrients, temperature, pressure, pH, water activity, ion concentration, and growth phase of the microbial culture affect physico-chemical properties of the cytoplasmic membrane and consequently their functioning. These changes include the balance between bilayer and nonbilayer lipids, stability and fluidity of membrane as well as altering lipid-protein interactions (A. Mrozik 2004). Most bacteria change the fatty acid composition of their membrane lipids in response to variations in environmental temperature (Russell N.J. 1980). Rising the growth temperature increases the proportion of long-chain and saturated fatty acids within the membrane. At the same time, a lowering of growth temperature results in an increase in unsaturation, a decrease in average chain length or an increase in branched-chain fatty acids (A. Mrozik 2004). Membrane fluidity can be regulated by changing the ratio of saturated to unsaturated fatty acids, branched to unbranched structures, type of branching, cis or trans unsaturated fatty acids, and acyl chain length (Quinn 1981; Russell 1984).

Based on this, we wanted to see if a drastic change in temperature and therefore membrane fluidity and lipid composition would affect subcellular localization of *C. glutamicum* PTS permeases. To this end, flask experiments where the strains CGM001 and CGM002 were grown in CGXII with the transported PTS sugar as sole carbon source at 17°C since inoculation, and fluorescence microscopy with cells on mid-exponential growth phase at the same temperature was performed.

Cells grown at 17°C grew significantly slower (Fig. 16) and were significantly larger, with averages: 4.76 µm² at 17°C and 3.57 µm² at 30°C in fructose, and 4.12 µm² at 17°C and 2.97 µm² at 30°C in glucose (Table 10 and Fig. 17A). The number of PtsF foci was significantly higher when cells were grown at 17°C, whereas PtsG foci number showed no significant difference in the same conditions (Fig. 17B).

PtsF foci were significantly larger on cells growing at 17°C (0.73 µm²) when compared to cells growing at 30°C (0.35 µm²). The same was observed for PtsG foci (0.86 µm² at 17°C, 0.69 µm² at 30°C) (Fig. 17C). However, the ratio

foci area/ cell area was not significantly increased under these conditions, and strongly correlates to the observed increase in cell area (0.64 on PtsG, and 0.61 on PtsF) (Fig. 17D). This suggests that although the absolute foci area of PTS permeases increased in cells grown in lower temperatures, this increase is an effect of the proportional larger cell size and consequent larger membrane area observed in such conditions. Moreover, clustering of PTS is unaffected by the growth rate, as cells grown at 17°C grew significantly slower (0.17 h^{-1}) than cells grown at 30°C (0.28 h^{-1}).
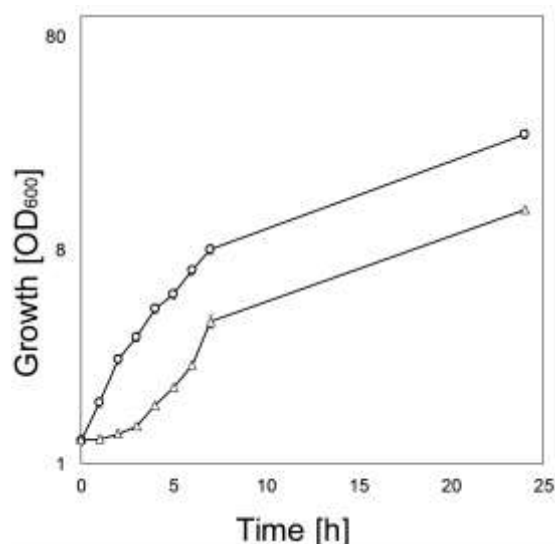

Figure 16. Growth of *C. glutamicum* wild type RES 167 in CGXII containing 100 mM glucose at 17°C (triangles) and 30°C (circles). Each point represents biological triplicates and standard deviation is indicated.

Table 10. Lower growth temperature increases cell size and therefore absolute PTS clusters area. Significant statistical differences according to multiple comparison tests after Kruskal-Wallis are represented as letters next to each value. Different letters indicate statistical differences within the same PTS protein.

	Cell area (µm²)		Foci/cell		Foci area		Ratio	
	17 °C	30 °C	17 °C	30 °C	17 °C	30 °C	17 °C	30 °C
PtsF	4.22 (a)	2.97 (b)	3.03 (a)	2.73 (b)	0.73 (a)	0.35 (b)	0.14 (a)	0.12 (a)
PtsG	4.76 (a)	3.57 (b)	2.79 (a)	2.72 (a)	0.86 (a)	0.69 (b)	0.18 (a)	0.20 (a)
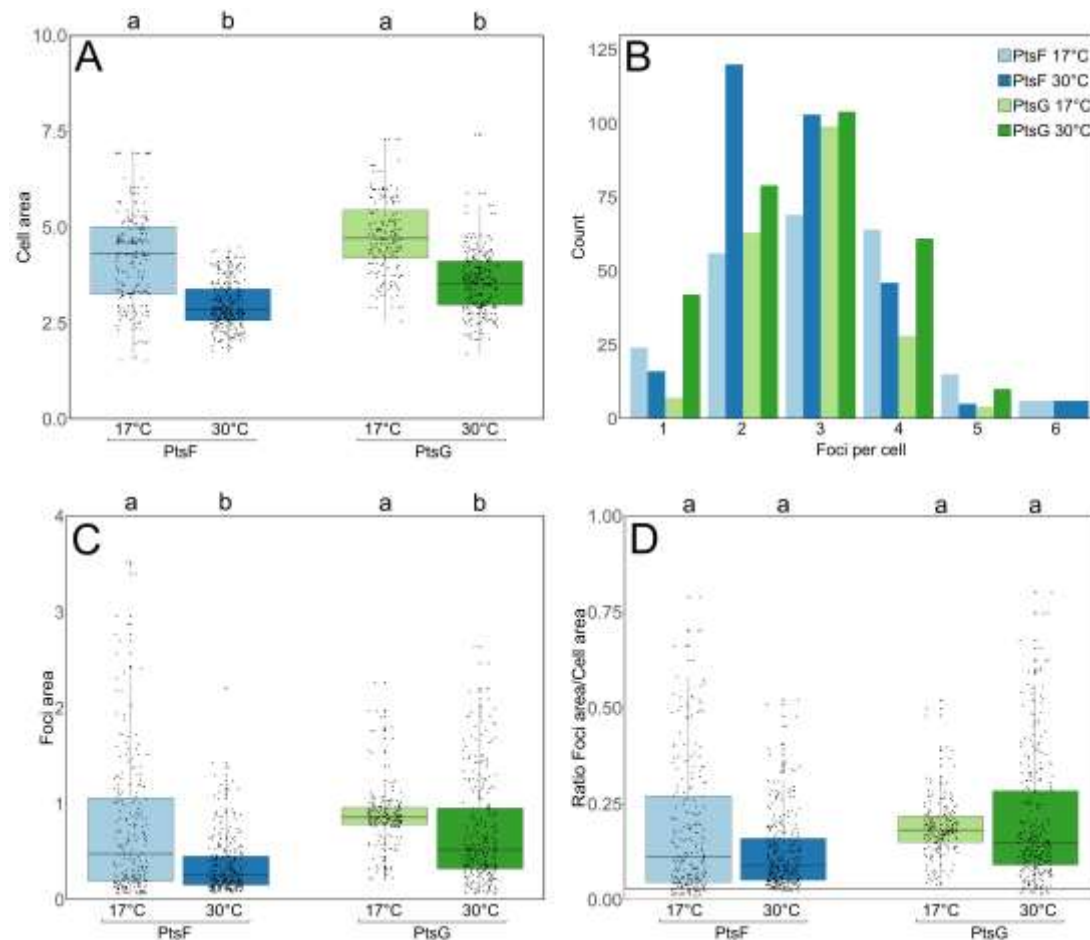
Figure 17. PTS foci changes in lower growth temperatures. Microscopy-based data of strains CGM001 and CGM011 grown and imaged at 17 and 30°C. (A) Cell area, (B) PTS foci per cell, (C) PTS foci area, (D) Ratio foci area/cell area. Cells were grown in CGXII minimal medium with the respective PTS sugar as sole carbon source. Significant statistical differences according to multiple comparison tests after Kruskal-Wallis are represented as letters above each graph. Different letters indicate statistical differences within the same PTS protein.

3.8 Single molecule localization and spatial rearrangement of PtsG in presence of glucose

The data obtained with widefield microscopy suggested that PTS EII cluster rearrange when their specific transport substrate is present. However, epifluorescence microscopy is limited by the diffraction limit of light, and detailed information about PTS EII clusters such as density or number of

molecules cannot be obtained. Therefore, the next step we took towards a deeper and more quantitative understanding of PTS EII complex dynamics was to use single molecule photo-activated localization microscopy (PALM) data. To this end, we constructed strains tagged with photoactivatable mCherry (PAmCherry) *ptsG::PAmCherry-Linker-ptsG* and *ptsF::PAmCherry-ptsF* and showed that they are fully functional as judged by sugar uptake and growth rates (Fig. 18). The observed clustering pattern in epifluorescence was confirmed by PALM data of cells expressing PAmCherry-PtsG (strain CGM005) (Fig. 19A, B).

For analysis of PALM data, we first needed to precisely define what a valid cluster is. Clusters are defined as regions of high density separated by regions of lower density, and the distribution our data suggests is that there are three populations separated by the amount of fluorescence events composing each cluster: (A) $X<10$, (B) $10 \leq X \leq 24$, and (C) $X \geq 25$ events (Fig. 20). The first population could in theory still be composed of PTS complexes close to each other by mere coincidence. Although this randomness effect is never fully absent, it decreases with increasing cluster size. Therefore, clusters composed of ≥ 10 and ≥ 25 events were analyzed regarding their maximum span, density, number of events per µm², and number of clusters per µm². The stretched exponential distribution of PTS cluster size is reminiscent to that observed with chemotaxis receptors (Greenfield *et al.* 2009) and therefore suggests a stochastic self-assembly process. We detected around 177.65 ±92.48 PtsG events per µm² cell area in glucose, 111.22 ±49.51 events per µm² in fructose, and 114.69 ±60.28 events per µm² in acetate.

The increase in foci area observed in epifluorescence brought up the question whether the cluster area increases due to an increase in number of PTS complexes present in each cluster, or to a rearrangement of the same number of EII permeases per cluster. At single molecule resolution, foci area can be estimated by the cluster maximum span (Fig. 21), which is the maximum distance between two events belonging to the same cluster.

PAmCherry-PtsG clusters from population C exhibited significantly higher max span in the presence of glucose when compared to fructose or acetate, which exhibited no statistical difference among each other, corroborating our findings with epifluorescence, where in presence of the transported sugars, PtsG/F covered a larger membrane area. The analysis of these same populations of clusters revealed that cells in presence of glucose exhibited significantly higher number of PtsG clusters per µm² when compared to fructose and acetate, which exhibited no differences among each other (Fig. 22).

Likewise, PAmCherry-PtsF formed membrane embedded clusters localizing with no preferred positions (Fig.23). However, a low number of events was detected per cell, which made it impossible to obtain significant statistical analysis that would show cluster density changes. However, the averages for cluster max span in glucose (33.41 µm), fructose (34.99 µm), acetate (32.83 µm), clusters/µm² and events/µm² show a tendency that is in accord with the data obtained for PtsG (Fig. 24)
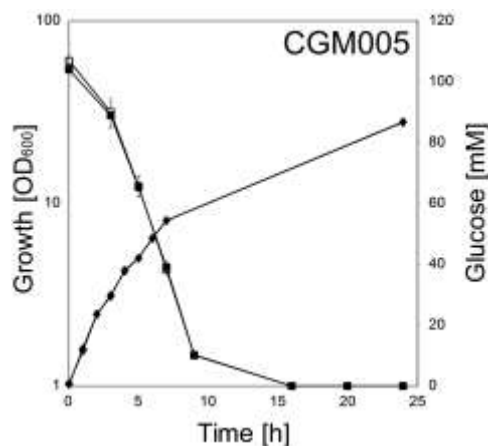
**Figure 18. Strain CGM005 expressing *PAmCherry-ptsG* is fully functional.** Growth and sugar consumption of *C. glutamicum* strain CGM005 (*PAmCherry-ptsG* filled symbols) versus wild type RES 167 (open symbols) in CGXII containing 100 mM glucose. Glucose consumption (squares) and growth (diamonds) are indicated. Each point represents biological triplicates and standard deviation is indicated.
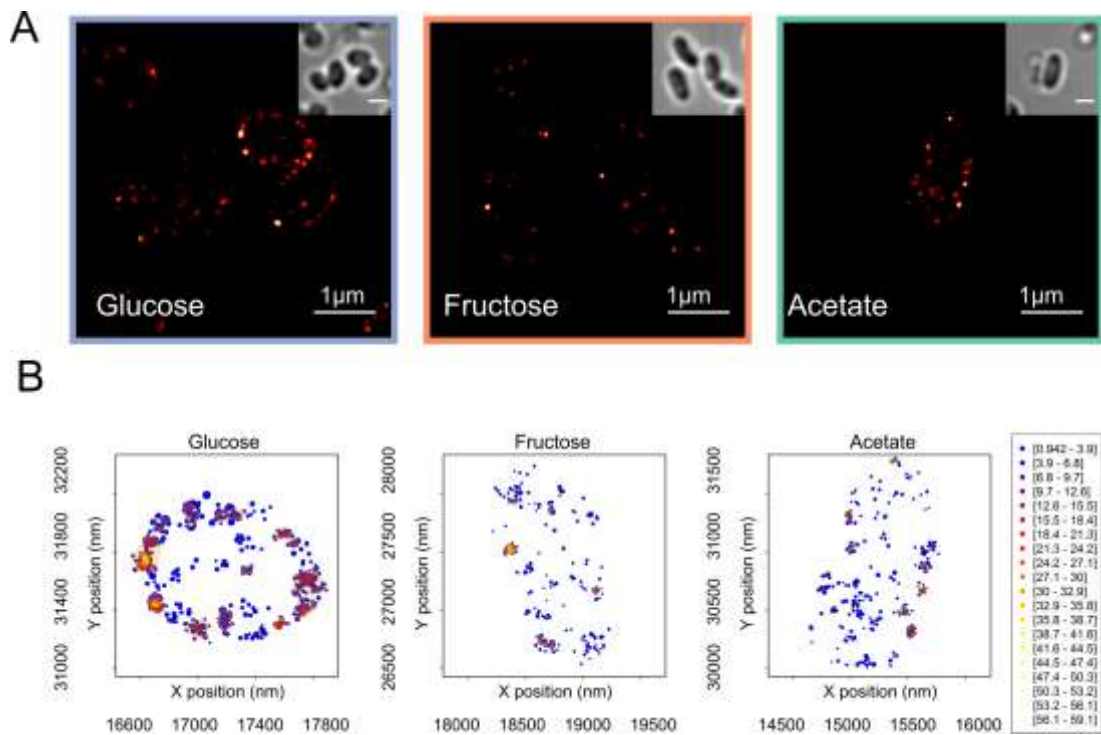
Figure 19. Single molecule localization microscopy reveals dynamic PAmCherry-PtsG clustering. (A) Super resolution images of *C. glutamicum* strain CGM005 expressing PAmCherry-PtsG under different growth conditions. Cells were grown in CGXII minimal medium with 2% of indicated carbon source. Insets show transmitted light images to see cell outlines. (B) Plot of detected single molecule localization, events localization and clusters identification for a representative cell for each tested condition. Localizations are color coded according to the local event density while the plotted radius is indicating localization precision. The identified clusters are highlighted by orange contours.
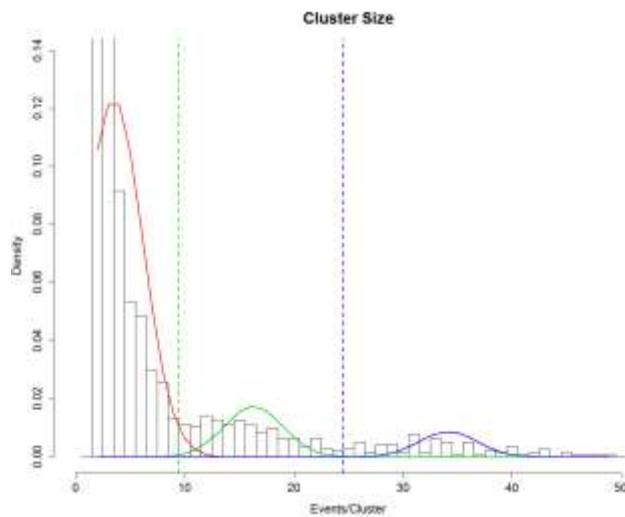
Figure 20. PAmCherry-PtsG clusters size distribution. Three different populations were identified by univariate normal mixture analysis: clusters composed of 2-9, 10-24, 25+ events. Lines of different colors represent Gaussian fits for each different population.
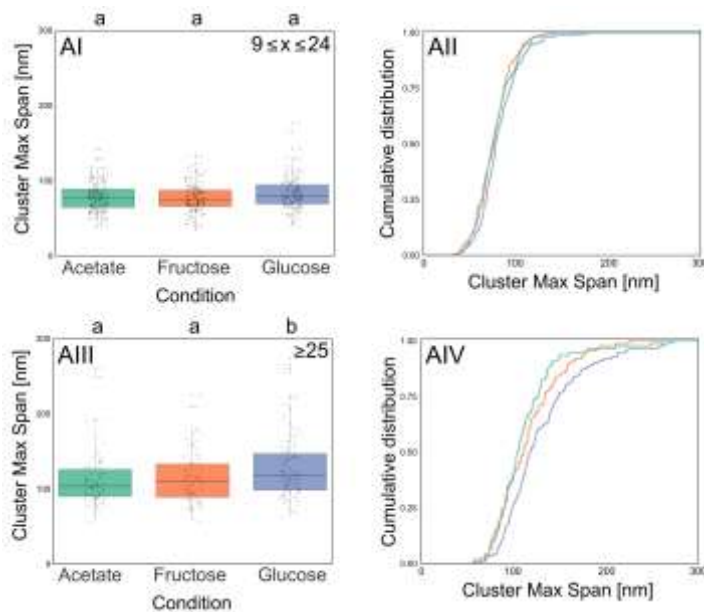
Figure 21. PtsG clusters maximum span increase in presence of glucose. Each parameter is analyzed via boxplot (AI, AIII) and cumulative distribution function (AII, AIV). Clusters composed of $9 \leq x \leq 24$ events (AI, AII) and >25 events (AIII, AIV) were analyzed. Significant statistical differences according to multiple comparison tests after Kruskal-Wallis are represented as letters above each graph. Different letters indicate statistical differences within the same PTS protein.

60
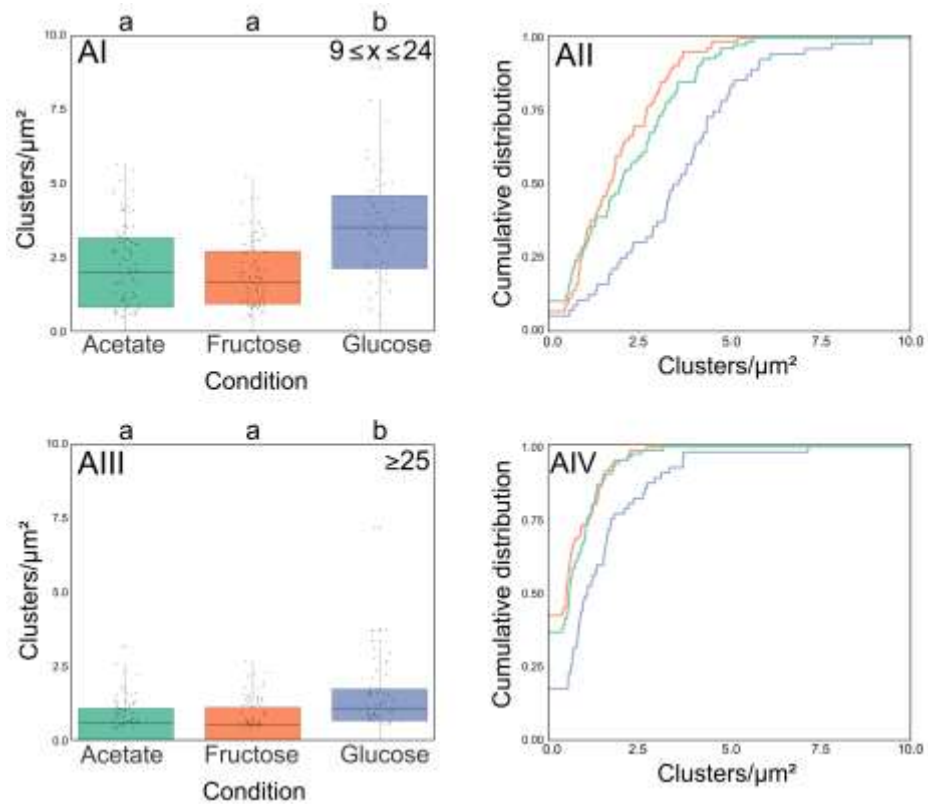
**Figure 22. PtsG clusters are more abundant in presence of glucose.** Each parameter is analyzed via boxplot (AI, AIII) and cumulative distribution function (AII, AIV). Clusters composed of $9 \leq x \leq 24$ events (AI, AII), and >25 events (AIII, AIV) were analyzed. Data based on super resolution images of *C. glutamicum* strain CGM006 expressing PAmCherry-PtsF under different growth conditions. Cells were grown in CGXII minimal medium with 2% of indicated carbon source. Significant statistical differences according to multiple comparison tests after Kruskal-Wallis are represented as letters above each graph. Different letters indicate statistical differences within the same PTS protein.
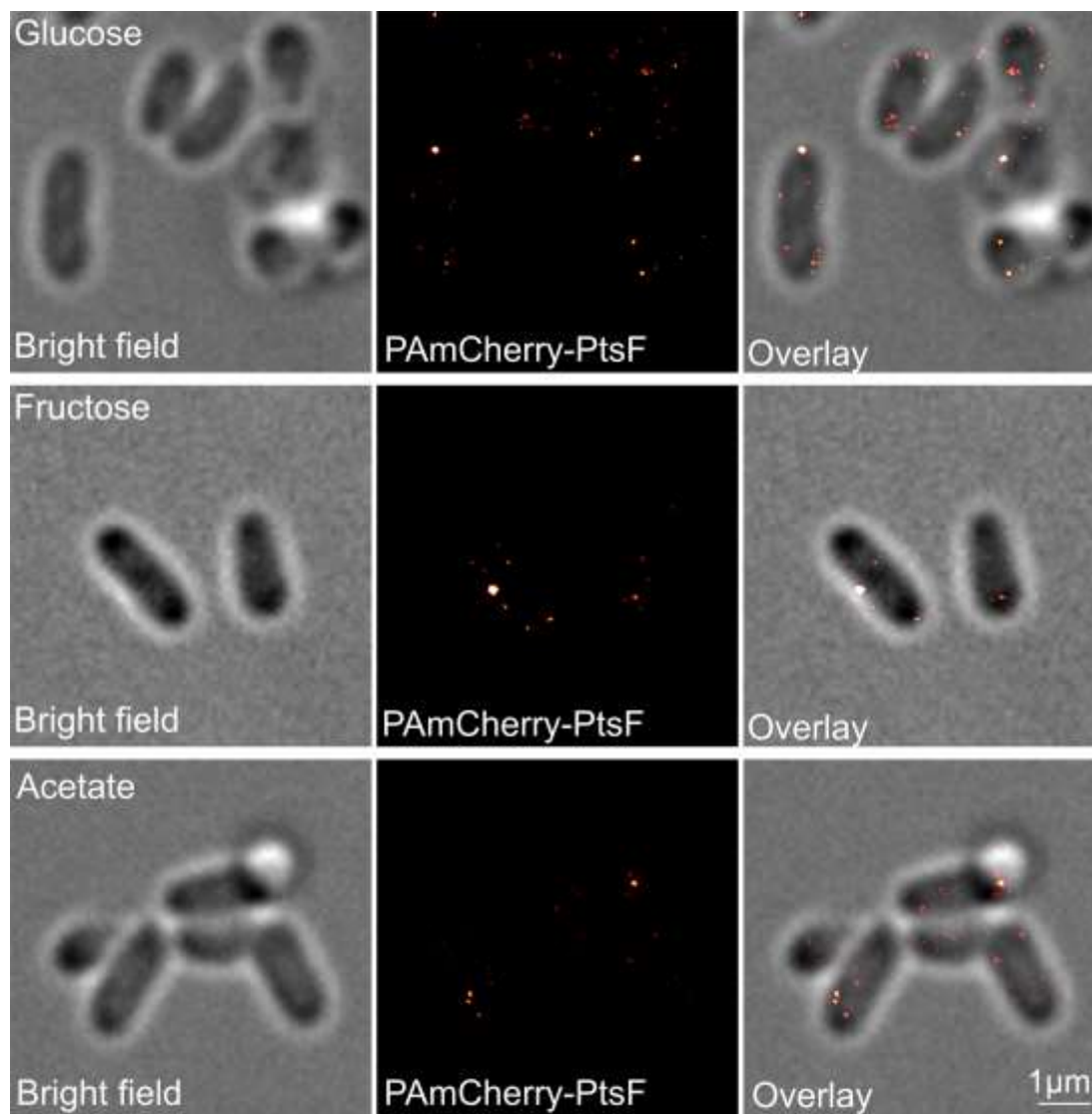
Figure 23. Single molecule localization microscopy reveals subtle carbon source-based changes in PAmCherry-PtsF clustering. Super resolution images of *C. glutamicum* strain CGM004 expressing PAmCherry-PtsF under different growth conditions. Cells were grown in CGXII minimal medium with 2% of indicated carbon source. Insets show transmitted light images to see cell outlines.
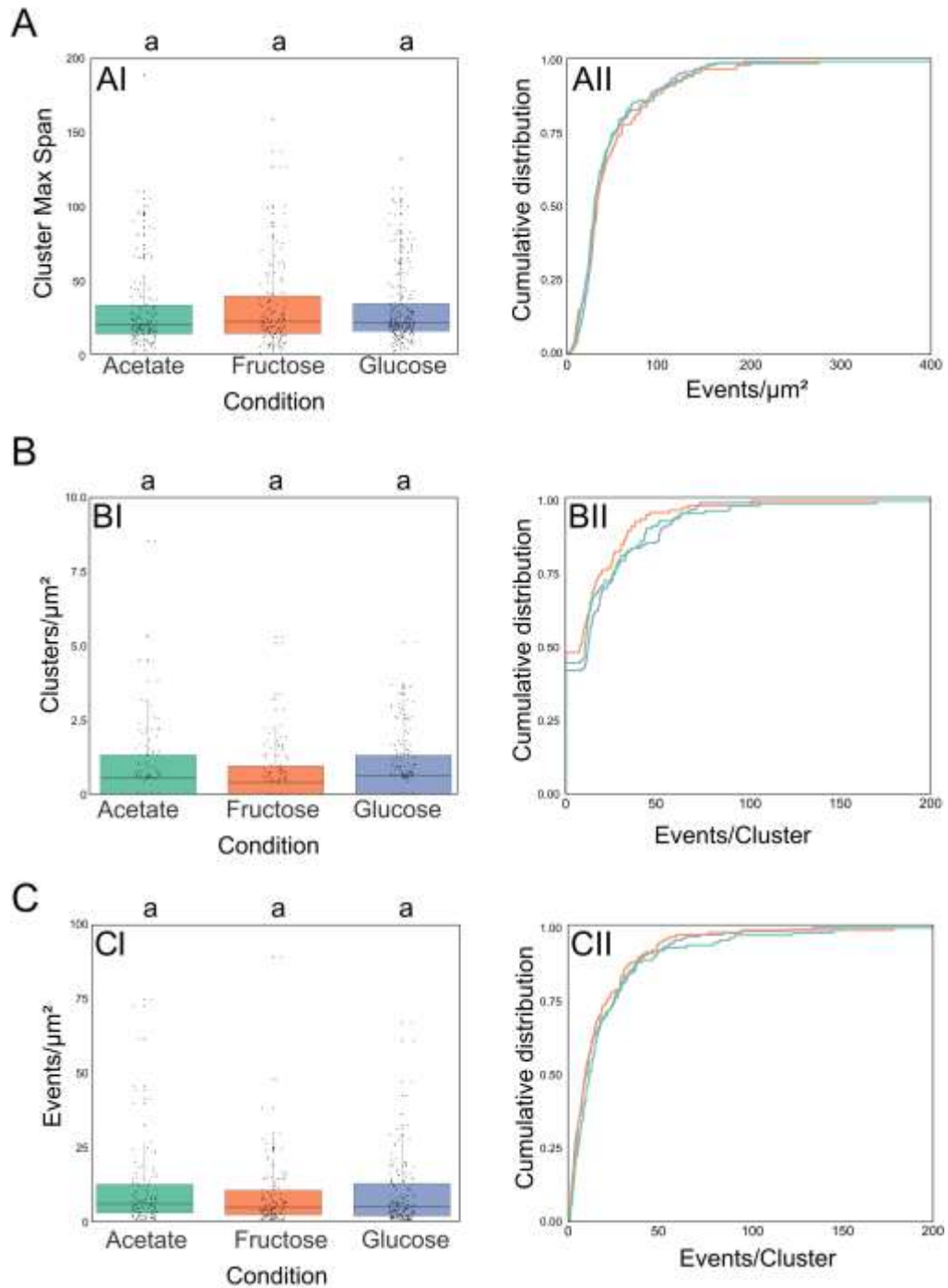
Figure 24. PtsF clusters exhibit subtle changes in response to different carbon sources. Data based on super resolution images of *C. glutamicum* strain CGM004 expressing PAmCherry-PtsF under different growth conditions. Each parameter is analyzed via boxplot (AI, BI, CI) and cumulative distribution function (AII, BII, CII). Cells were grown in CGXII minimal medium with 2% of indicated carbon source. Significant statistical differences according to multiple comparison tests after Kruskal-Wallis are represented as letters above each graph. Different letters indicate statistical differences within the same PTS protein.

63

CTF readings of epifluorescence images showed increased values when cells expressing mCherry-PtsF and mNeonGreen-PtsG were grown in presence of the transported sugars, suggesting increased expression of PTS complexes under these conditions. This data correlates with our PALM data for PamCherry-PtsG (Fig. 25A). In presence of glucose, a significantly higher number of events per µm² was observed, meaning that the number of PtsG in the cytoplasmic membrane increases with the addition of glucose in the medium, again confirming induction of *ptsG* in presence of glucose as expected. Our epifluorescence data suggested that in presence of the transported sugar, PtsF/G assemble in larger complexes, while the overall number of clusters per cell decreases. However, our PALM analysis of cells expressing PAmCherry-PtsG in glucose showed an increase in the number of clusters and events per µm². Single molecule detection allowed visualization of clusters with fewer proteins, thereby explaining the apparent discrepancy to the widefield microscopy data. While in widefield the number of bright, visible foci decreased (while their area increased) when the transport substrate was present, in PALM we observed more clusters with lower protein numbers that likely account from substrate induced gene expression.

Although the CTF of cells increases in presence of glucose, PALM data showed that the number of PAmCherry-PtsG events per cluster remain the same independently of the carbon source, suggesting that the carbon source does not affect the number of PTS events present in each cluster (Fig. 25B). This is an important finding since larger cluster size could have been the trivial consequence of more protein in the cell. Since we have found that the number of PTS EII molecules in a cluster remained similar in presence or absence of the transported substrate, we wanted to analyze the protein density in individual clusters. The local density is defined as the number of events present in a squared area of side 50 nm centered on the event. The average density of events is defined as the arithmetic average of local density of the events composing the cluster. PAmCherry-PtsG clusters of population C exhibited significant lower average density values in presence

of glucose (Fig. 26), meaning that PtsG complexes belonging to the same cluster localize further apart from each other when in presence of glucose, thereby occupying a larger membrane area.
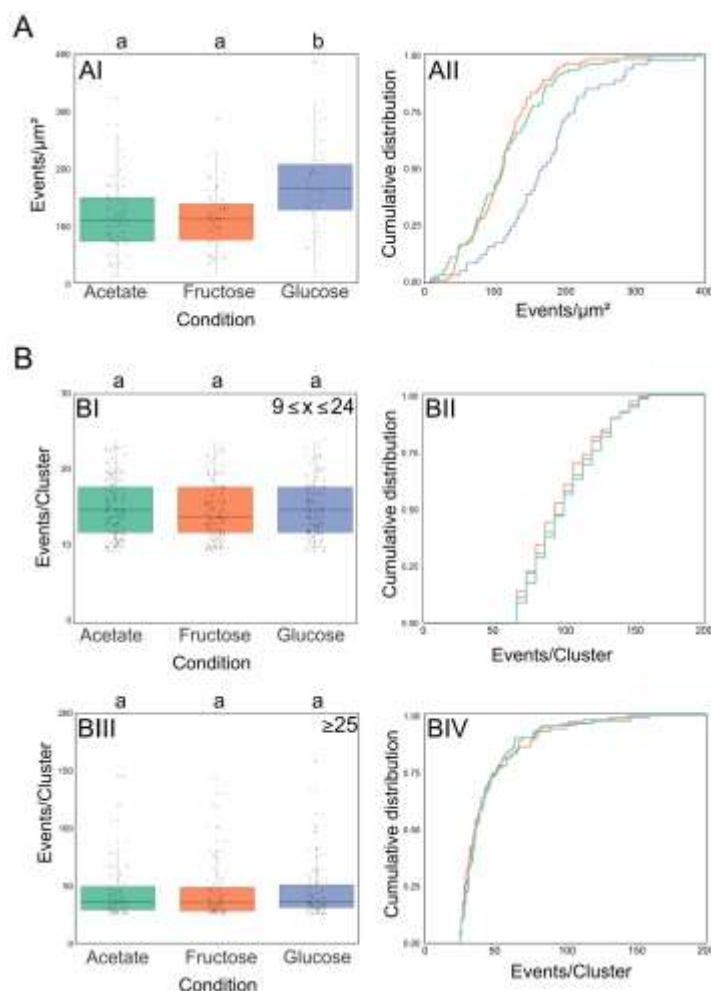
Figure 25. PtsG clusters maintain protein number in presence of the transport substrate. Super resolution PALM data of CGM005 strain (*ptsG::PAmCherry-ptsG*) grown in CGXII supplemented with 2% of the indicated carbon sources (A) PtsG number of events per µm² increases in presence of glucose, (B) PtsG clusters are composed by the same amount of molecules regardless of the carbon source. Each parameter is analyzed via boxplot (AI, BI, BIIII) and cumulative distribution function (AII, BII, BIV). Clusters composed of $9 \leq x \leq 24$ events (BI, BII), and ≥ 25 events (BIII, BIV) were analyzed. Significant statistical differences according to multiple comparison tests after Kruskal-Wallis are represented as letters above each graph. Different letters indicate statistical differences within the same PTS protein.
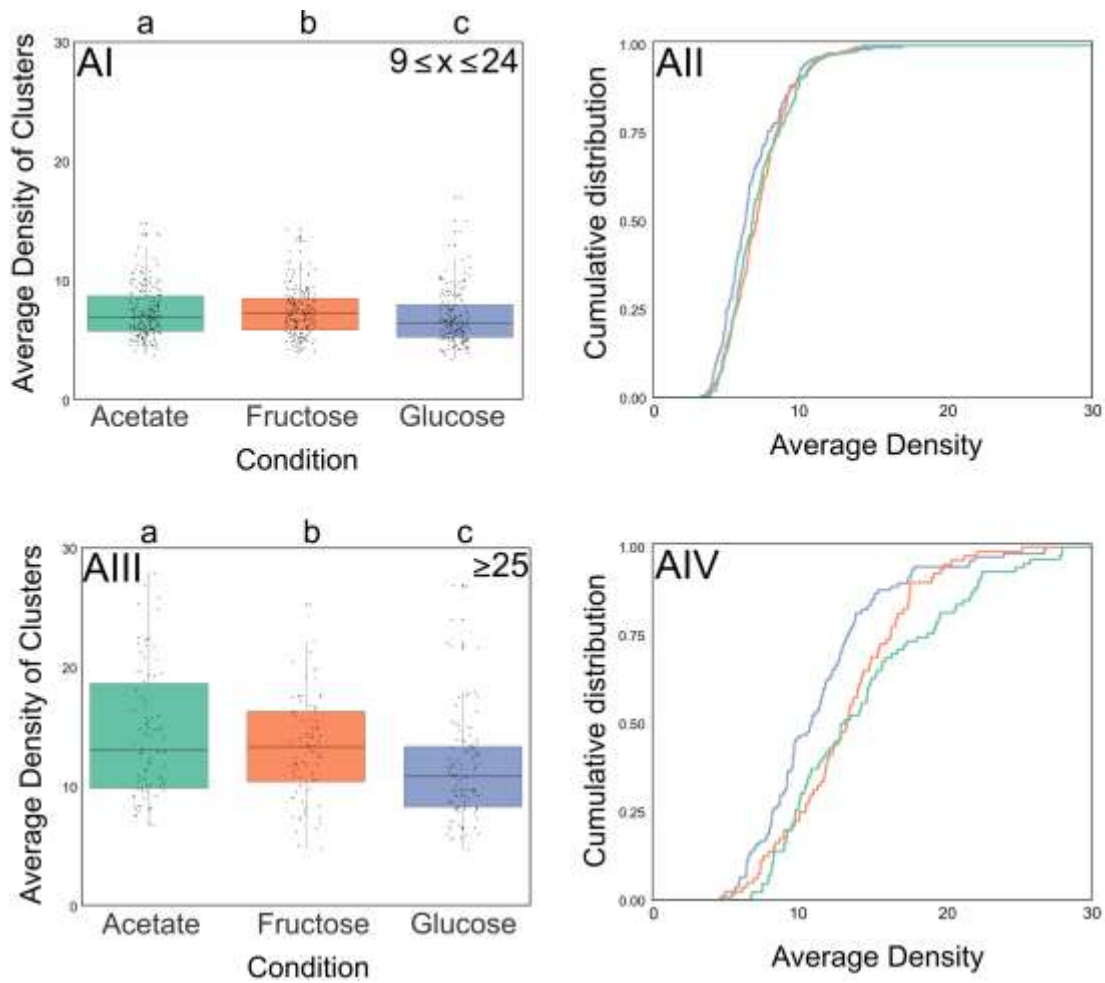
Figure 26. PtsG clusters decrease protein density in presence of the transport substrate. Average density of PtsG clusters in cells grown in different carbon sources. Each parameter is analyzed via boxplot (AI, AIII) and cumulative distribution function (AII, AIV). Clusters composed of $9 \leq x \leq 24$ events (AI, AII) and ≥ 25 events (AIII, AIV) were analyzed. Significant statistical differences according to multiple comparison tests after Kruskal-Wallis are represented as letters above each graph. Different letters indicate statistical differences within the same PTS protein.

3.9   YggB localizes as foci embedded in the cytoplasmic membrane

Mechanosensitive channels play an important role in the cytoplasmic membrane in osmolarity regulation on cells under hypo and hyperosmotic stress, and the small conductance MS channel YggB was previously found to partially regulate glutamate excretion (Borngen *et al.* 2010; Nakamura *et al.* 2007). In this work we wanted to investigate the membrane occupancy by YggB in *C. glutamicum*. To this end, the strain *yggB::yggB-mNeonGreen* (CG010) was constructed using the wild-type ATCC 13032 as background. As the strain is an allelic replacement fusion, *yggB* is expressed from its native promoter and therefore, the results reflect the natural expression levels of this protein. In-gel fluorescence revealed the expected size of YggB fused to mNeonGreen, with no signs of degradation (Fig. 27).
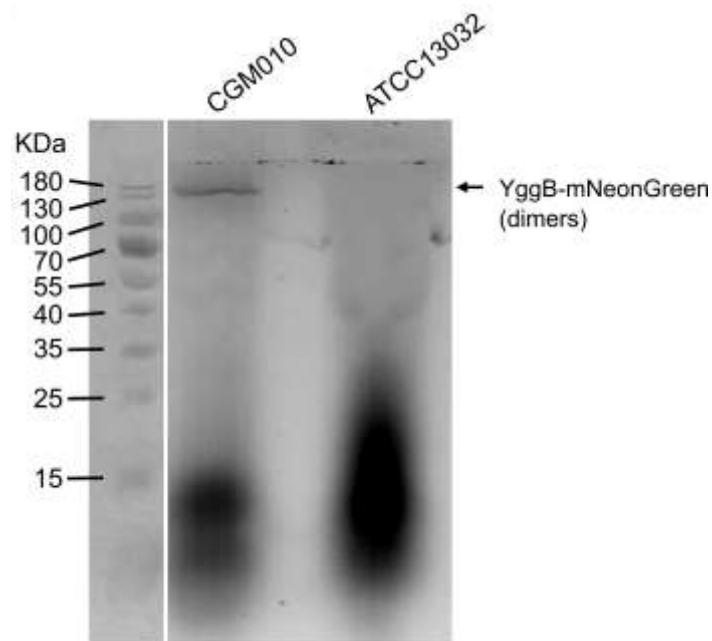
Figure 27. Control for full-length fusion YggB-mNeonGreen. In gel-fluorescence with cell lysates of strains CGM010 and WT ATCC13032 reveal the existence of dimeric YggB-mNeonGreen (YggB = 57,33 kDa, mNeonGreen = 26,65 kDa).

In order to assess YggB subcellular localization, epifluorescence microscopy was performed with cells grown to early exponential phase in flask experiments with LB medium. Based on fluorescence images of cells expressing YggB-mNeonGreen, we found that most cells contained few bright and intense foci that were randomly distributed along the cytoplasmic membrane (Fig. 28), in an average of 3.15 ± 0.92 clusters per cell. Foci of various intensities were observed, suggesting clusters with different amounts of proteins. Image-based fluorescence measurements of the aforementioned foci revealed an average of 26.56 ± 4.35 relative fluorescence units (RFU) per foci. Overall, our data suggests that YggB localizes as punctual clusters distributed along the cytoplasmic membrane of *C. glutamicum*.
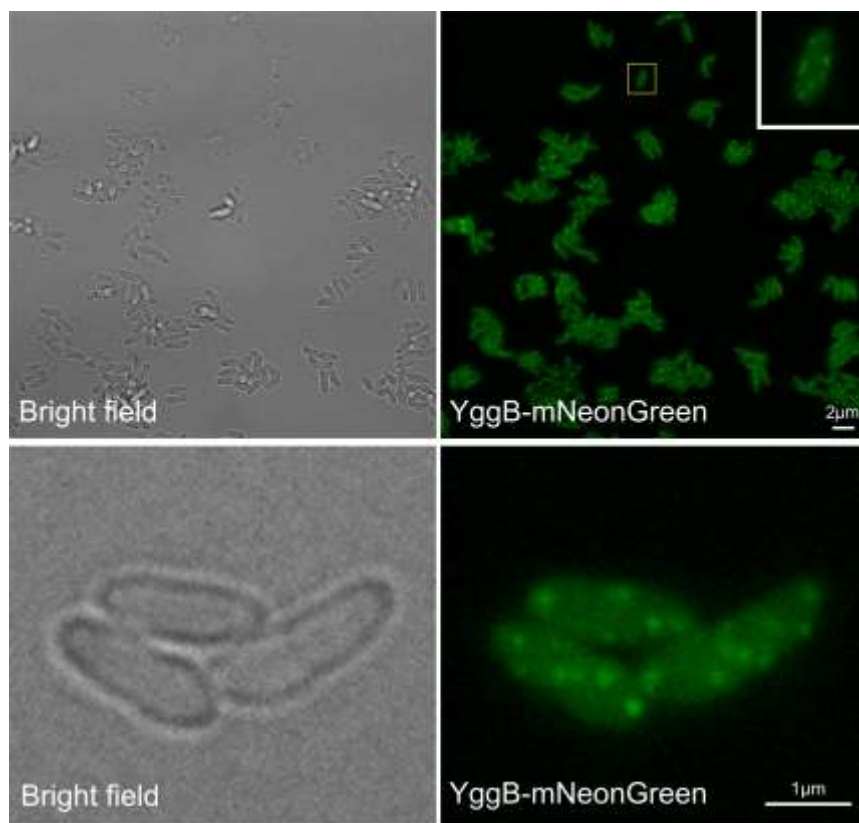
Figure 28. YggB localize as punctate foci. Epifluorescence microscopy images of *C. glutamicum* expressing YggB-mNeonGreen. Flask experiments, cells grown for 2 hours in LB medium.

3.10 YggB subcellular localization under different NaCl concentrations

As YggB is activated in both hypo and hyperosmotic stress (Borngen *et al.* 2010), we wanted to test if different osmolarity conditions ranging from hypoosmotic to low hyperosmotic would affect YggB levels and foci count over a long period of time. Cells were then grown in flas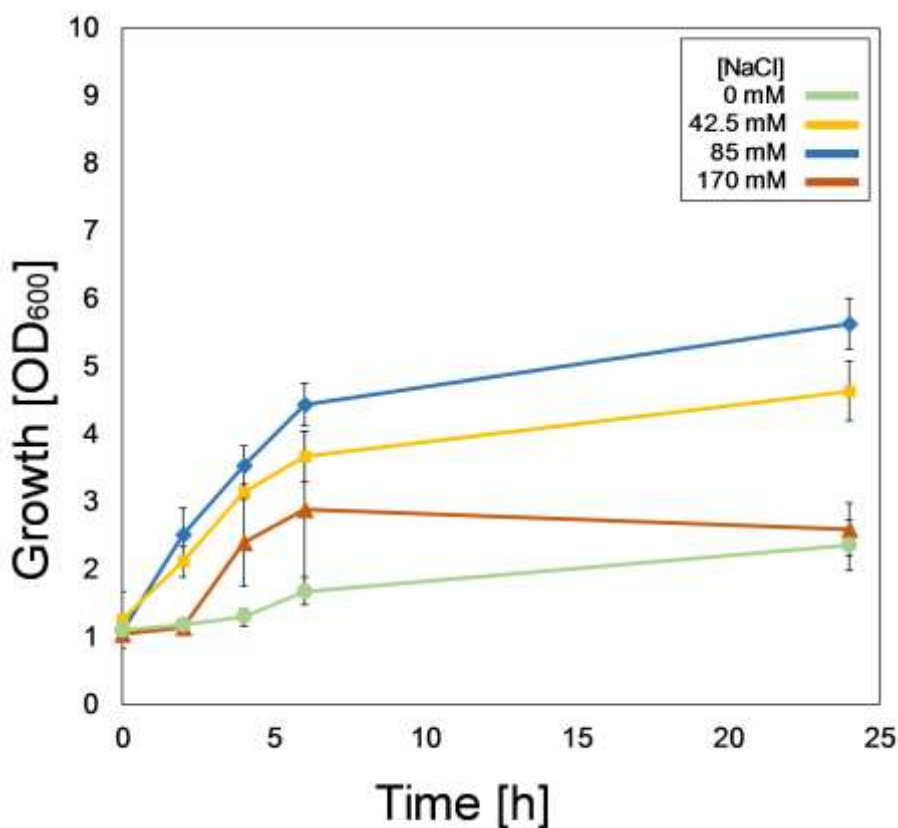ks containing LB medium with varied NaCl concentrations: 5g (85mM), 10g (170 mM), 2.5g (42.5 mM), and 0g of NaCl per 500 ml of final medium, and widefield microscopy was performed, followed by fluorescence measurements of individual foci through the acquired images.

The growth of cells in LB medium with different NaCl concentrations in medium is expressed in Figure 29. Cells grown in 0 mM of added NaCl ($0.06h^{-1}$) had the lowest growth rates compared to the other treatments, followed by 42.5 mM NaCl (0.18 h^{-1}), 170 mM NaCl (0.18 h^{-1}) and finally 85 mM NaCl (0.22 h^{-1}). However, the final OD_{600} reached in each treatment differed significantly: 0% = 2.35 ±0.36, 200% = 2.58 ±0.39, 50% = 4.63 ±0.44, 100% = 5.64 ±0.37.

A tendency for higher values of RFU in YggB clusters was observed when cells were grown in 200% of standard NaCl concentration (30.54 ± 3.63), when compared to cells grown in standard LB (26.56 ± 4.35) although this difference was found to be not statistically significant according to Kruskal-Wallis test. The foci count per cell remained the same across the different treatments: 3.15 ± 0.92 in standard LB, 3.38 ± 0.97 in LB 200% NaCl, 3.26 ± 1.16 in 50% NaCl, 3.34 ± 1.04 in 0% NaCl (Fig. 30A, Table 11). Cells grown in 50% NaCl (26.34 ± 4.59) had similar RFU values to cells grown in medium with no NaCl (26.55 ± 3.11) and standard LB (Fig. 30B). In overall, although the tested conditions had a drastic effect on cell growth, no effects on RFU values or count of YggB-mNG foci were observed. When cells were grown under hyperosmotic conditions (200% NaCl), RFU values of slightly increased. Our results suggest that changing the ion concentration in

medium for prolonged times does not result in a higher number of MS channels per cell.

Figure 29. Growth of *C. glutamicum* ATCC 13032 in LB medium with different concentrations of NaCl. Cells were grown in LB flasks containing 5g (85mM), 10g (170 mM), 2.5g (42.5 mM), and 0 mM of NaCl. Corresponding growth rates are: 0% NaCl = 0.06h^{-1}, 50% NaCl = 0.18 h^{-1}, 100% NaCl = 0.22 h^{-1}, and 200% NaCl = 0.18 h^{-1}.

Table 11. *C. glutamicum* growth and YggB foci in cells grown under different NaCl concentrations. Foci count and relative fluorescence (RF) of cells expressing YggB-mNeonGreen in different NaCl concentrations. Cells grown in LB flasks containing 5g (100%, 85mM), 10g (200%, 170 mM), 2.5g (50%, 42.5 mM), and 0g of NaCl.

	0 mM NaCl	42.5 mM NaCl	85 mM NaCl	170 mM NaCl
Final OD$_{600}$	2.35 ±0.36	4.63 ±0.44	5.64 ±0.37	2.58 ±0.39
Growth rate [h^{-1}]	0.06	0.18	0.22	0.18
Foci count	3.34 ±1.04	3.26 ±1.16	3.15 ±0.92	3.38 ±0.97
Foci RF	26.55 ±3.11	26.34 ±4.59	26.56 ±4.35	30.54 ±3.63
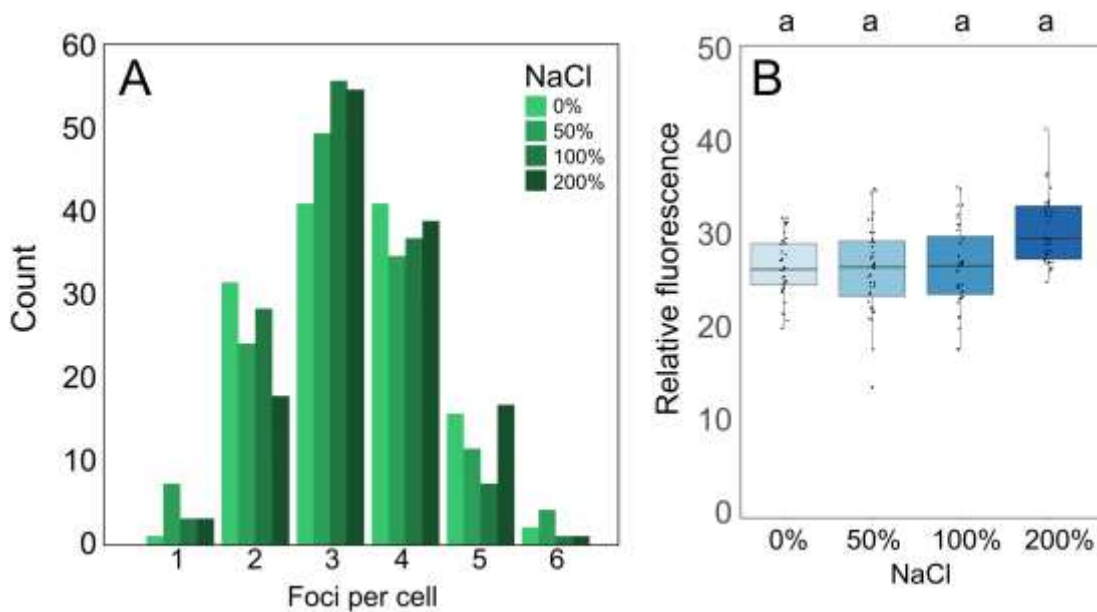
Figure 30. YggB foci expression is slightly increased in cells grown in higher osmolarity medium. (A) Number of YggB-mNG foci per cell in different NaCl concentrations in medium, (B) Fluorescence of YggB-mNG based on epifluorescence images in different NaCl concentrations in medium. Cells grown in LB flasks containing 10g (200%, 170 mM), 5g (100%, 85mM), 2.5g (50%, 42.5 mM), and 0g of NaCl. Significant statistical differences according to multiple comparison tests after Kruskal-Wallis are represented as letters above each graph.

3.11 DivIVA localization and dynamics in L-forms

After analysis of membrane integral proteins, we wanted to address the localization and dynamics of a membrane associated protein. DivIVA is a cytoplasmic protein that works as a polar scaffold in processes related to cell growth and cell division. Its oligomers have the ability to sense membrane curvature and as a result, it normally localizes in the poles and septa (Fig. 31A). Changes in cell shape lead to changes in the cell S/V ratio and cytoplasmic membrane. With our findings studying membrane proteins in L-forms, we wanted to verify the consequences of cell shape change in proteins that are sensitive to it, as DivIVA. Moreover, we wanted to address the question whether the kinetics of DivIVA molecules throughout the cell

would be affected by the cells shape. To this end, we used the strain CDC010 (Donovan *et al.* 2012), a RES 167 derivative where *divIVA* was replaced by *divIVA-mCherry,* and is thus, chromosomally expressed as a single copy from its native promoter. Importantly, CDC010 contains fully functional allele of DivIVA-mCherry strain. Therefore, we are confident that the data presented here reflect the localization and dynamics of DivIVA.

In our microscopy experiments using synthetic L-forms, we were able to observe DivIVA in fully spherical cells, where portions of the cell with different shapes and angles were absent. In these cells, DivIVA localized as foci that spread through larger areas (Fig. 31B-C). L-forms were generated by the addition of DCS in osmoprotective medium as described before, and because DCS acts against two crucial enzymes in the cytosolic stages of peptidoglycan synthesis (alanine racemase and D-alanine:D-alanine ligase), some cells still presented vestigial cell wall material from before the addition of DCS in medium and consequent L-form escape. In these cases, bumps on the cell surfaces were observed, where DivIVA preferentially localized due to its curvature sensitivity (Fig. 31D). Therefore, although the overall cell shape was drastically modified in L-forms, the ability of DivIVA to sense negative curvature was unaltered.

The two different localizations of DivIVA in regions with or without bumps in the cell membrane brought up the question whether the kinetics of diffusion of DivIVA would be affected by such morphology. Therefore, the exchange of DivIVA-mCherry monomers and/or oligomers between DivIVA-mCherry clusters and the rest of the environment were measured by Fluorescence Recovery After Photobleaching (FRAP). Bleaching of mCherry was performed using a 561 nm laser with 20% power and an illumination time of 0.02 s. Images were taken every 20 s on both DIC (100 ms exposure time, 100% transmittance) and mCherry (250 ms exposure time, 32% transmittance) channels. Preliminary FRAP experiments in our lab (Giacomelli 2014) with the strain CDC010 demonstrated that DivIVA has a

diffusion rate of 2.7×10^{-3} µm²/s and half-time recovery of 161.88 ±42.86 s at the poles of rod-shaped cells (Table 12).

FRAP of DivIVA-mCherry clusters in regions with bumps or without bumps, showed significant different results. In regions with no bumps, DivIVA occupied larger areas, had higher diffusion rates (4.4×10^{-3} µm²/s) and lower half-time recovery (98.78 ±75.64 s), whereas in regions with bumps, DivIVA had a lower diffusion rate (2.1×10^{-3} µm²/s) and a significant higher half-time recovery of (197.47 ±108.88 s) when compared to regions without bumps or poles of rod-shaped cells (Fig. 32, Table 12).
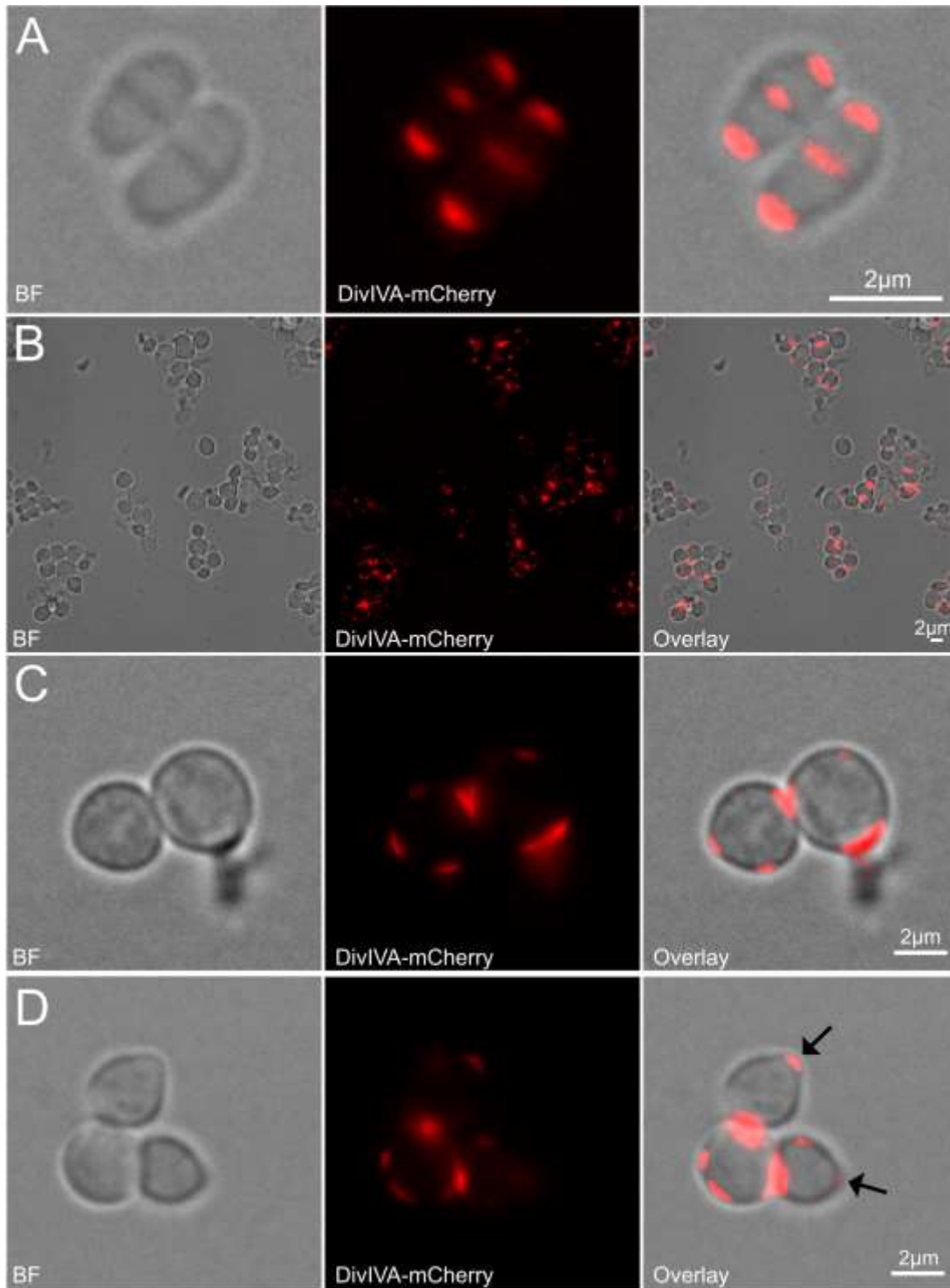
Figure 31. DivIVA localizes in regions of negative curvature regardless of the cell shape. Epifluorescence images of strain CDC010 expressing DivIVA-mCherry in (A) Rod shaped cells, (B) L-forms, (C) L-forms with no protrusions (D) L-forms with protrusions. Protrusions are indicated with arrows.
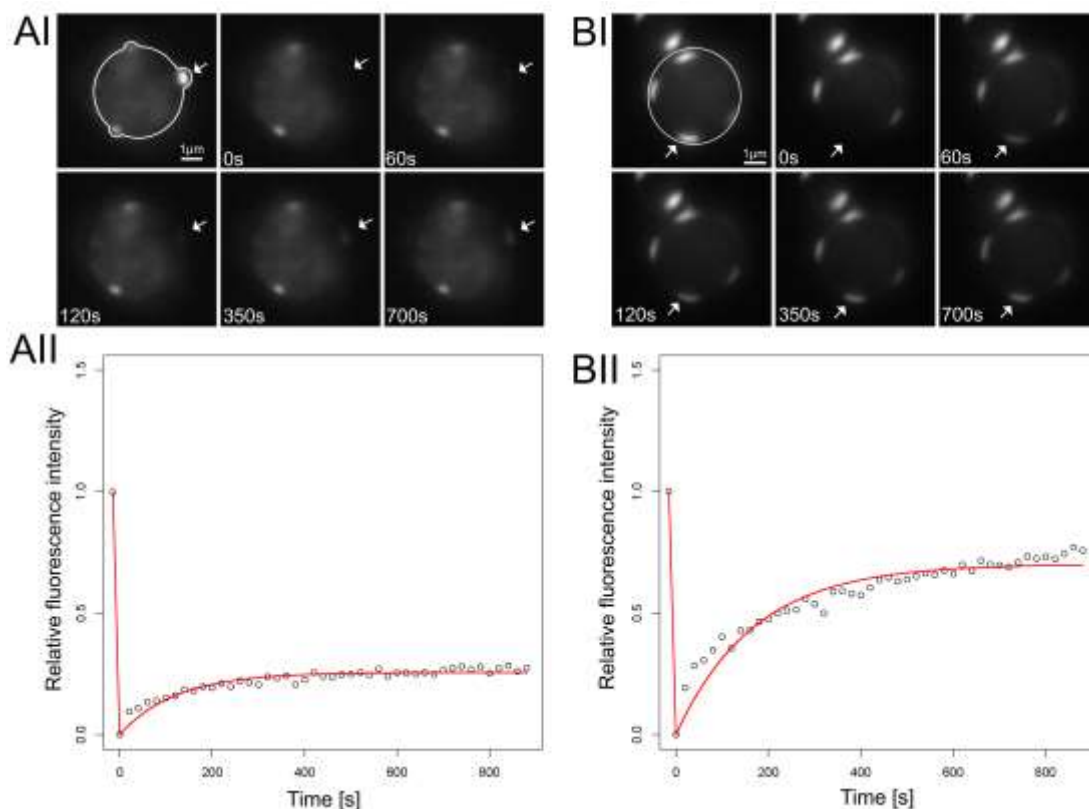
Figure 32. DivIVA diffuses slower in regions with bumps. *divIVA::divIVA_mCherry* L-forms fluorescence recovery after photobleaching. (AI, AII) Data of cells with bumps, (BI, BII) data of cells without bumps. (AI, BI) Snapshot of a cell during data acquisition. First frame with the cell before photobleaching, and elapsed time after the photobleaching pulse is indicated. (AII, BII) Change of fluorescence intensity in the course of the recovery at the bleached area of the cell. Black circles show the normalized data points and red line the corresponding fit.

Table 12. DivIVA is more mobile in fully spherical cells. FRAP data of DivIVA-mCherry. Diffusion rate and half-time recovery of poles in rod-shaped cells, regions with protrusions (bumps) and smooth (no bumps) of the cytoplasmic membrane of L-forms. Bleaching of mCherry was performed using a 561 nm laser with 20% power and an illumination time of 0.02 s. Images were taken every 20 s.

	Diffusion rate (µm²/s)	Half-time recovery (s)
Rod-shaped	2.7×10^{-3} (a)	161.88 ±42.86 (a)
Bumps	2.1×10^{-3} (b)	197.47 ±108.88 (b)
No bumps	4.4×10^{-3} (c)	98.78 ±75.64 (c)

4   Discussion

4.1   Phosphotransferase systems membrane occupancy in *C. glutamicum*

Most bacteria transport various carbohydrates via a phosphotransferase system. The tremendous advantage of using a PTS coupled transport is that the substrate is phosphorylated in the process of import (hence the term group translocation), thereby effectively being removed from the chemical equilibrium of outside and inside concentrations. This allows the highly effective transport even under low external carbohydrate concentrations. Yet, a second, similarly important feature of PTS transport is that the complex PTS is composed of a sensory part and a regulatory part (Lengeler 2000; Lengeler and Jahreis 2009). In enteric bacteria the EIIA[crr] protein is a central component in the complex regulation cascade and a main part in the observed catabolite repression. EIIA[crr] binds and inhibits the lactose permease as well as the GlpK protein in *E. coli*, while the phophsphorylated P~EIIA[crr] activates the adenylate cycles (Gorke and Stulke 2008). It is therefore not surprising that the EIIA component in *E. coli* is therefore a soluble protein that can dissociate from the membrane bound EIIBC complex. In line with this function subcellular localization of EIIA[Crr] was shown to be dispersed in the cytoplasm (Lopian *et al.* 2010). Also the general PTS components HPr is involved in regulation in *E. coli* and phosphorylates the transcriptional regulator BglG. For HPr a polar localization was described in *E. coli* that is alleviated when transport substrates are present (Lopian *et al.* 2010). These data were in line with early suggestions that the PTS complex should act in multi-protein complexes (Rohwer *et al.* 1998), thereby improving its function (Norris *et al.* 1999). A major unsolved question is still the unclear localization and assembly of the membrane embedded permease part of the PTS. Up to date there are only few reports about the localization of an EII complex, the BglF in *E. coli* (Lopian *et al.* 2010) and the BglP in *B. subtilis* (Rothe *et al.* 2013). However, BglF localization studies were

performed with a plasmid borne expression system, potentially causing overexpression and therefore masking the possible clustering behavior of this PTS protein. While the general setup of proteins making a functional PTS is conserved in most bacteria, their genetic arrangement and regulatory role differs greatly among bacteria. In the high GC, gram positive *C. glutamicum*, four specific PTS were described (Ikeda 2012). *C. glutamicum* differs greatly from organisms in which the PTS is well studied by the fact that it prefers utilization of several carbon sources simultaneously (Wendisch *et al.* 2000; Frunzke *et al.* 2008). Hence, for most carbon sources *C. glutamicum* does not show diauxic growth behavior (except under conditions with ethanol or glutamate plus glucose). It is therefore not surprising that the permease subunits are fusion proteins composed of EIIABC and that they do not have a diffusible EIIA subunit. Our data using an N-terminal fluorescent fusion for the fructose specific EIIABC confirms clear membrane localization of the entire complex. It was generally assumed that the EII parts of the PTS are uniformly distributed in the cytoplasmic membrane, similar to other transport proteins, such as the Hxt hexose transporter in yeast (Nijland *et al.* 2016), and the mentioned BglF (Lopian *et al.* 2010). However, data on subcellular localization of transport proteins is rather scarce. This may in part be based on the relatively low copy number of many transport proteins that renders microscopy localization studies difficult. We have succeeded here in the subcellular localization of the EIIC permease parts of the fructose and glucose specific PTS. Both membrane integral transporters show a clustered membrane distribution. Importantly, both fusion constructs are fully functional based on their growth rates and the respective carbon sources consumption rates. Since the constructs replaced the native allele, we confidently assume also a wild type like copy number. Wide field microscopy not only revealed the heterogeneous, clustered localization of the two PTS components, but also showed that they hardly co-localize. Rather PtsG and PtsF seem to exclude each other. Interestingly, we could show that PtsF does co-localize with the succinate dehydrogenase, a protein of the TCA cycle and the respiratory chain. This finding indicates that in *C. glutamicum* proteins of the

respiratory chain and transport proteins can co-occur in the same membrane region. The membrane economy model proposed (Zhuang *et al. 2011)* suggests that bacteria regulate their membrane composition based on efficient usage of the limited membrane space and idealized a model in which a clear membrane separation of proteins involved in transport and respiration might occupy distinct membrane areas. For *C. glutamicum* we can exclude such a strict spatial distribution on a scale larger than 250 nm.

C. glutamicum PTS EII expression is known to be induced by the presence of the transported sugars, and regulation of the PTS gene expression is mainly controlled at the stage of transcription initiation or at transcription elongation (Cramer *et al.* 2007; Auchter *et al.* 2011; Patek and Nesvera 2011; Shah *et al.* 2018). It has been shown before that in presence of PTS sugars, the expression of *ptsF/G/S* as well as *ptsI* and *ptsH* was induced (Tanaka *et al.* 2008). The mRNA levels of *ptsG*, *ptsH* and *ptsI* increased in presence of glucose, whereas sucrose and fructose induced the expression of all pts genes *ptsF/G/S/I/H* (Tanaka *et al.* 2008). Our epifluorescence data support the induction of *ptsF* and *ptsG* in presence of the transported sugars by the increase in total fluorescence readings of cells under these conditions expressing mNeonGreen-PtsG and mCherry-PtsF. Moreover, PtsF/G clusters increase in both size and foci area/cell area ratio, occupying more membrane space upon presence of transported sugars, while the overall number of large complexes, visible in widefield microscopy, decreases. We observed an increase in membrane area occupation by PtsG in presence of fructose (0.06 ±0.03) when compared to acetate (0.04 ±0.02) (Table 4). PtsG is known to contribute to fructose uptake (Kiefer *et al.* 2004), and these data are in agreement with the induction of *ptsG* by fructose observed by Tanaka *et al.* (Tanaka *et al.* 2008) when measuring *ptsG* mRNA levels. PtsF membrane area occupation in cells grown in presence of glucose (0.05 ±0.04) was statistically similar as in acetate (0.06 ±0.03), suggesting that glucose does not play a role in PtsF clusters dynamics. Likewise, Tanaka *et al.* (2008) did not observe an increase in *ptsF* mRNA levels in presence of glucose.

The observed influence of the transported substrates in PTS clustering is corroborated by our experiments with mixed carbon sources. The foci area of PTS complexes largely increased when the specific PTS sugar was in medium. At the same time, the foci count decreased and the membrane area occupied by PTS increased. These effects are more noticeable in PtsG clusters but are clearly present in PtsF, being also statistically significant. More pronounced values in foci number, area and ratio were observed in cells grown in minimal medium with the specific PTS sugars alone, when compared to mixes containing another carbon source. Studies concerning *C. glutamicum* growth in mixtures of carbon sources were performed before (Cocaign, Monnet, and Lindley 1993; Dominguez, Cocaign-Bousquet, and Lindley 1997). When growing in a mixture of glucose and fructose, the growth and the uptake capacity of PtsG is significantly lower than the one measured on cells growing on glucose only (Dominguez, Cocaign-Bousquet, and Lindley 1997). The same pattern was observed for the cell growth and the uptake rates of PtsF and fructose. Therefore, it is not surprising that the clustering of PtsG and PtsF were more dramatically stimulated when cells were grown in presence of the transported sugar as sole carbon source, rather than in mixtures.

Patchy distribution of membrane proteins has been described for many signaling and scaffold proteins. Prime examples of membrane receptor clustering are the chemotactic receptors. A seminal publication describing the self-organization of the *E. coli* chemotaxis receptors using localization microscopy reveled that polar chemotaxis clusters mature by a stochastic assembly of smaller clusters and single receptor proteins (Greenfield *et al.* 2009). Other membrane proteins, such as flotillins (Donovan and Bramkamp 2009; Lopez and Kolter 2010), the OXPHOS components Nuo, CydAB, CyoABCD, SdhABC (Erhardt *et al.* 2014; Llorente-Garcia *et al.* 2014) (and own results, see Fig, 7E) have also been shown to localize in clusters of various size in the membrane. It is reasonable to assume that the clustering in these cases is based on stochastic self-assembly and that cluster formation is important for function. In contrast to scaffolding proteins such as

flotillins (Lopez and Kolter 2010; Bach and Bramkamp 2013), it is not immediately apparent why a transport protein should cluster for an improved function. The PTS is, however, as we described above, not only a transport system, but also a signaling device. Hence, clustering may be advantageous for signaling. In this context, it is interesting to note that a direct link between the PTS and the chemotaxis system has been described in *E. coli* (Lux *et al.* 1995; Lux *et al.* 1999).

Here, we could show with single molecule localization microscopy, that the observed PTS cluster dynamically change their cluster density based on presence or absence of substrate. PAmCherry-PtsG PALM data showed that the presence of glucose in the medium induces expression and leads to cells exhibiting a higher number of larger clusters composed of 10<x<25 and 25<x events. These clusters showed a higher Cluster Max Span, but lower Average Density of Clusters values, meaning that the number of PtsG EII proteins around another decreases in presence of the transported sugar. At the same time, the distribution of number of events per cluster remained the same independently of the carbon source. These data strongly suggest a spatial rearrangement of PTS complexes, which might be a strategy to increase efficiency of membrane space utilization, or a form of regulation employed by cells (Fig. 33). Furthermore, a similarity between the function of chemotaxis receptors and the membrane bound EII complexes of the PTS is the crucial involvement of phosphorylation reactions. For the chemotaxis receptors, it has been described that clustering improves phosphorylation reactions. Strikingly, it has also been described that different chemoreceptor densities lead to different kinase activity based on the local concentration of the receptors (Besschetnova *et al.* 2008). In widefield microscopy these clusters are polar localized, but when cells treated with an excess of attractant, polar clusters disperse and proteins distribute over a large area of the membrane. It has been proposed that signal amplification under conditions of high attractant concentration is not needed (Lamanna *et al.* 2005). In a similar concept one might speculate that the PTS EII complexes in *C. glutamicum* increase their cluster density in absence or at very low

concentration of the transport substrate. Under such conditions a positive cooperative effect might be useful. At higher concentrations of the transport substrate, this cooperativity may not be advantageous and hence the PTS spreads over a larger membrane area. We observed a change in cluster size with PtsF and PtsG. Statistically solid data in super resolution microscopy were only achieved for PtsG due to the higher natural expression level. However, our widefield microscopy data further support this observation.

Another approach for interpretation of the observed dynamism of PTS clusters is from the phosphorylation point of view. For phosphorylation of oncoming sugars, the phospshoryl group needs to be translocated from EI to HPr, then finally to EII. EI and HPr are distributed in the cytoplasm, not following EII localization. Here, we show that EI localizes dispersed in the cytoplasm, with enrichment where the nucleoid is expected to be, and HPr localizes uniformly diffused in the cytoplasm. Assuming that uniformly distributed EII complexes would be more easily encountered by HPr than small and densely packed foci sparsely localized, the larger spread of EII clusters along the cytoplasmic membrane in presence of the transported sugar might then be a strategy employed by cells to increase the probability of EII to be phosphorylated by HPr.

This is the first time that a dynamic change in cluster density has been observed in cells and reveals an unexpected spatial regulation of the PTS. Several groups report data that suggest dimer formation of EII permeases (Chen & Amster-Choder 1998; Veldhuis *et al.* 2006; Cao *et al.* 2011). Although the nature of our experimental design in single molecule localization does not allow to distinguish between monomers and dimers in the membrane of *C. glutamicum* reliably, it is possible to study these complexes in their minimal oligomerization state.
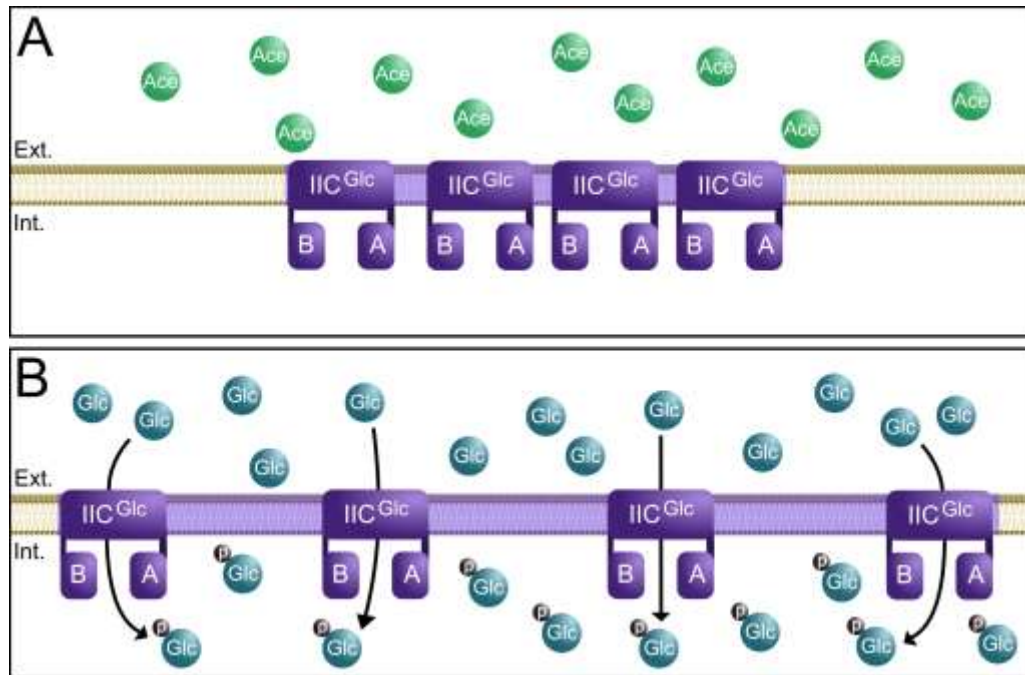
Figure 33. Membrane integral PtsG cluster undergo spatial rearrangement in presence of glucose. Schematic view of PtsG membrane occupancy in *C. glutamicum*. (A) In absence of the PTS sugar, in this case glucose, PtsG cluster are densely packed with proteins. These clusters occupy only a minimal membrane area. (B) In presence of the correct PTS substrate PtsG clusters rearrange, reducing the overall cluster density and occupying larger membrane areas.

Using artificial, induced CWD cells, we could show that PTS cluster formation is not due to the rod-shape of the cells and the limited membrane surface. Although L-form cells show a grossly altered number of PTS clusters at the same time as the cluster size was larger, the same foci area/cell area ratio was retained, supporting the notion that membrane space is indeed a constraint that limits membrane occupancy by PTS proteins. However, clustering is an intrinsic function of the PTS EII.

Membrane-associated proteins are expected to be likely candidates for sensing environmental conditions, such as temperature (Ray *et al.* 1994). Changes in the growth temperature might impact the functioning of membrane proteins due to changes in the lipid composition of the plasma

membrane. A notable example is the activation of BetP by both osmotic stress and chill stress in *C. glutamicum* cells grown at and adapted to low temperatures, where BetP from cold-adapted cells was shown to be less sensitive to osmotic stress (Ozcan *et al.* 2007). Furthermore, BetP is activated at low temperatures without noticeable perturbation of the cytoplasmic solute concentration (Ozcan *et al.* 2007). Our experiments with PTS clusters of cells grown at 17°C showed that although there was an increase in PTS foci area, it was proportional to the increase in cell area observed under such conditions, suggesting that the PTS are insensitive to lower growth temperatures and therefore lower growth rates. Moreover, at lower temperatures, an increase in unsaturation, branched-chain fatty acids, or a decrease in average chain length in the cytoplasmic membrane are expected (Mrozik 2004). Our data hints that the observed PTS dynamics remain unaffected by changes in lipid composition. This is in accord with our observations that there were no differences in PTS foci among exponential and stationary phases, as the membrane lipid composition commonly changes during growth phases: In *E. coli* and *B. stearothermophilus*, cardiolipin amount rises as cells enter the stationary phase (Card 1973; Hiraoka *et al.* 1993), and *S. aureus* suffers changes in the proportion of vitamin K_2 isoprenologues present in the membrane (Hammond & White 1969; Joyce *et al.* 1970). The cytoplasmic membrane of *B. subtilis* remains relatively the same along different growth phases, but the phosphatidylglycerols reportedly decreased while the amount of phosphatidylethanolamines increased during stationary growth (Gidden *et al.* 2009).

Understanding the precise membrane coverage and spatio-temporal distribution of the PTS systems will help to model and scale up growth specific sugar uptake in industrial processes such as amino acid production in *C. glutamicum*. A kinetic model for glucose PTS in *E. coli* has been constructed (Rohwer *et al.* 2000; Francke *et al.* 2003) and converted spatio-temporally to address the possible effects of diffusion in the PTS systems. Based on the model, it was concluded that the soluble *E. coli* EIIA^{glc} remains

with up to 20% close to the membrane (Francke *et al.* 2002; Francke *et al.* 2003). Thus in larger cells such as eukaryotic cells (or as shown here with L-forms) diffusion may disrupt efficient signaling due to diffusion limitation and subsequent gradient formation. However, these data were made under the assumption that membrane complexes as well as general PTS proteins are uniformly distributed either in the membrane (permeases) or cytosol (general PTS components). In the light of the data provided in this work, kinetic flux models might be adapted.

4.2   YggB subcellular localization

Mechanosensitive channels are crucial membrane integral proteins that aid in the survival of bacteria in different environments. These channels work as valves that participate in the regulation of osmotic balance in the cells and are divided into MscL (large), MscS (small), MscM (medium) according to their conductance. Different channels open in different thresholds and are characterized by short bursts of activity that last a few seconds (Cui, Smith, and Adler 1995; Levina *et al.* 1999). YggB is the MscS homolog in *C. glutamicum* and participates in the excretion of compatible solutes (e.g. glutamate) upon osmotic downshift. Considering that *C. glutamicum* is the most important organism for the industrial production of glutamate and that yggB mutants have been shown to have a drastic reduction of glutamate excretion (Nakamura *et al.* 2007) studies concerning YggB localization are relevant for a better understanding of MS channels and glutamate excretion.

Here, we analyzed the subcellular localization of YggB and its response to prolonged growth under different NaCl concentrations in medium. Through epifluorescence microscopy of cells expressing YggB-mNeonGreen, we found that YggB localizes as punctate foci of same size along the membrane. By varying the NaCl concentration in flask experiments, we were able to analyze cells under different osmolarity conditions. The foci number did not change in response to different NaCl concentrations. A previous study

stressing *C. glutamicum* cells by varying the NaCl concentration in medium was performed before (Nottebrock *et al.* 2003). However, the analyzed cells were investigated under osmotic shock for short periods of time regarding their betaine flux through YggB and MscL, and no microscopy with YggB was performed. The used NaCl concentration was of 750 mM, which leads to an osmolality of 1.9 osmol kg^{-1} (Nottebrock *et al.* 2003). Here, fluorescence microscopy was performed with cells expressing YggB-mNeonGreen after hours of growth under different NaCl concentrations, ranging from 0 mM to 170 mM. In WT cells, efflux of compatible solutes in low osmolarity conditions is complete within 60 seconds (Ruffert *et al.* 1997), whereas the efflux in *ΔyggB* takes 5 minutes to be complete (Nottebrock *et al.* 2003). Moreover, *ΔyggB* strain has a reduced ability to excrete betaine compared to the WT, meaning that the other efflux systems were not able to fully substitute the loss of YggB (Nottebrock *et al.* 2003). In our studies, the lack of a response in terms of YggB-mNeonGreen fluorescence (i.e. protein levels) under conditions where YggB is known to be recruited, suggests that *yggB* expression is constitutive. However, the measured fluorescence of YggB-mNG foci slightly increased when cells were grown in LB with 170 mM of NaCl, two times the standard concentration, which resulted in significant lower growth rates. Abrupt changes in osmolarity require fast counter responses, hence the short time previously observed for efflux of compatible solutes by MS channels (Ruffert *et al.* 1997). Therefore, despite the slight increase in YggB fluorescence in a condition where YggB is active, we discard the possibility of new protein biosynthesis driven by changes in osmolarity in the conditions tested here.

So far it is not clear why YggB localize as clusters and not equally dispersed within the cytoplasmic membrane. *C. glutamicum* harbors the osmosensory system MtrAB, consisting of a membrane-bound MtrB and a soluble response regulator MtrA (Moker *et al.* 2004). Noteworthy, YggB is not only employed in the excretion of compatible solutes; it also works as a sensor of deforming forces within the cytoplasmic membrane (Börngen 2009). However, the mechanism by which MS channels respond to mechanical

forces is not completely understood. In a similar concept to DivIVA, that oligomerizes in large multimers in order to be able to sense negative curvatures, the observed clustering of YggB might indicate an advantageous behavior for sensing of membrane deformation and/or signaling.

Moreover, cellular membrane components are not uniformly distributed along the cell envelope, and the organization of the cytoplasmic membrane in domains of different lipid species is a concept that has been gaining strength throughout the years (Mueller, Wedlich-Soldner, and Spira 2012; Bagatolli *et al.* 2010). A notable example of such domains are lipid rafts, a subdomain of the plasma membrane that contains high concentrations of cholesterol and glycosphingolipids, resulting in distinctive protein and lipid composition (Pike 2003). In this sense, in addition to a potential cooperative behavior, clustering of membrane proteins can be arguably based on protein-lipid interactions, where protein clusters are generated by specific and higher-affinity molecular interactions between lipids, proteins and carbohydrates of the cytoplasmic membrane, and the specificity in domain formation is provided by general properties of the interaction partners, such as size, rigidity and charge (Mueller *et al.* 2012; Lucena *et al.* 2018).

4.3 DivIVA dynamics in *C. glutamicum* L-forms

Division in bacterial cells in their normal walled state is carried out by a dedicated cell division machinery, occurring with relative precision at midcell. In *C. glutamicum*, as in other bacteria, replication of the DNA starts at the origin of replication (oriC) (Donovan *et al.* 2013). The ParB protein interacts with centromere-like DNA sequences: the *parS* sites, which are located in the proximity of oriC. DivIVA binds to ParB, and the direct physical interaction between the DNA sequence and the DivIVA-ParB complex tethers the chromosome origin to the cell pole DNA replication and the movement of the segments as it is being copied occurs simultaneously and independently of the growth of the cells (Ben-Yehuda *et al.* 2005; Donovan *et al.* 2013). The

hydrolytic activity of ParA oligomers is believed to drive the active segregation process, and its replication initiation is regulated so that the overall rate of DNA synthesis is controlled and coordinated with cell growth, chromosome segregation as well as cell division. In contrast, L-forms proliferate randomly, with the extension of protrusions from the cell's surface and these protrusions then pinching off to form new cells. Division is also aided by simple shape perturbations, including tabulation, blebbing and vesiculation. This disorganized cell division, gives rise to a variety of cell sizes, from tiny to very big, and it is not uncommon for L-form cells to have multiple chromosomes (Mercier, Kawai, and Errington 2014). Localization of DivIVA clusters is usually confined to regions of the cells characterized by strong negative curvatures, such as the cell poles. These clusters, when not present in such regions, either move across the cell until they meet a region characterized by strong curvatures (cell poles/septum) or stably localize in correspondence of little protuberances along the cell membrane. This pattern was still observed in L-forms, despite the disorganized cell division present in cells in this state. We did not observe cells with DivIVA uniformly distributed, or regions of bumps without DivIVA, suggesting that it still accumulates in areas of negative curvaure that are formed randomly and do not necessarily correlate with a vestigial cell pole.

Analyzing L-forms and regions of cells without bumps, we were able to study the dynamics of DivIVA in spherical cells with no regions of higher negative curvature, where DivIVA localizes. In these smooth surfaces, DivIVA accumulates in larger foci, and our FRAP data shows that the diffusion rate on smooth surfaces was more than double than the one observed in bumps, and concomitantly, the half-time recovery less half as the one measured in bumps, suggesting that DivIVA is significantly more mobile in these larger regions, when compared to poles in rod-shaped or bumps in L-forms. The mobility of membrane-associated proteins within the cell is normally determined by three behaviors: reversible plasma membrane association, lateral diffusion in the membrane-associated state, and free, rapid diffusion in the cytoplasm (Goehring *et al.* 2010). We hypothesize that the higher mobility

found in regions/cells without bumps corroborates the idea that in such locations, where a larger area is occupied by DivIVA foci, a higher number or proteins is able to diffuse to the cytoplasm unimpeded by the membrane. Accordingly, in regions of higher negative curvature such as bumps or poles (in rod-shaped cells), proteins not only have their movement obstructed by other molecules, but are also confined by the membrane morphology, needing more energy to diffuse to the cytoplasm and as consequence, are less mobile (Fig. 34).
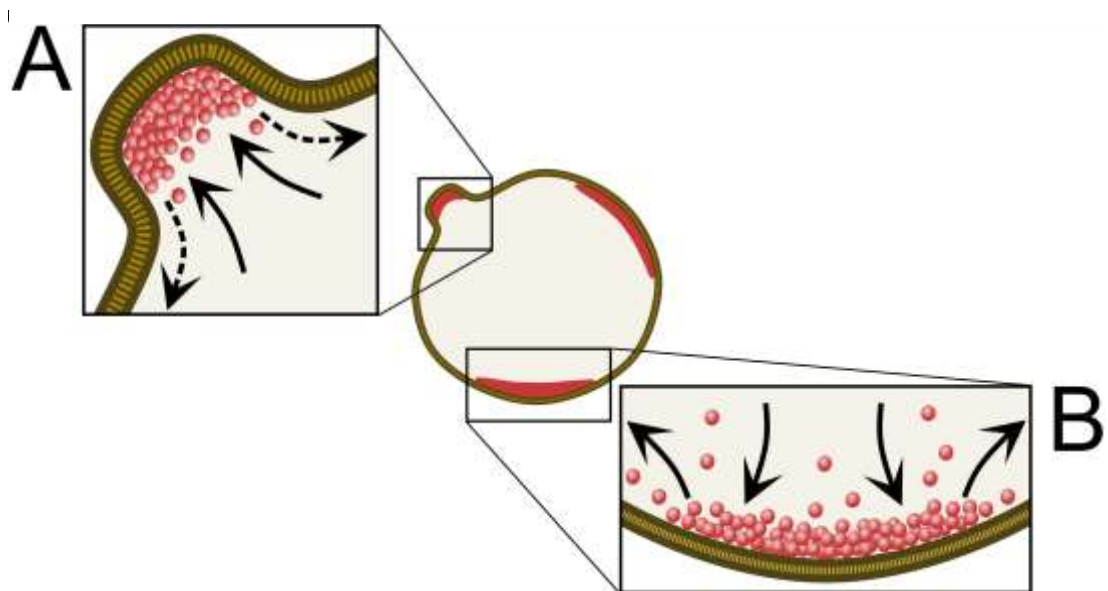
Figure 34. DivIVA dynamics is dependent on membrane morphology. Model based on our FRAP data with *C. glutamicum* L-forms expressing DivIVA-mCherry. Red areas and circles correspond to DivIVA and arrows indicate the direction of molecule diffusion. (A) Bumps in the cytoplasmic membrane supports the preference of DivIVA for negative curvature areas. In such areas, DivIVA is confined and has shown to be less mobile, suggesting that less molecules diffuse away from these regions. (B) In the absence of bumps, DivIVA localizes as larger foci with more molecule exchange with the cytoplasm.

5   Conclusions and outlook

The study of the subcellular localization of proteins is of prime importance for two reasons: first in the further elucidation of their role inside bacterial cells, and secondly in the refinement of knowledge of cellular processes, as proteins must be present at their correct subcellular location in order to fulfill their function. *C. glutamicum* has been used as a producer or glutamate and other aminoacids in industry for over 60 years, and knowledge about proteins linked to its sugar metabolism, physiology, and cell growth and division, might prove useful for future improvements of production processes in industry.

Here, we have discovered that the fructose-specific and glucose-specific phosphotransferase systems of *C. glutamicum* localize as membrane-integral clusters that are highly affected by the transported substrate, undergoing spatial rearrangements in presence or absence of their corresponding sugars in medium. Currently, it remains unclear what triggers this remarkable change in cluster conformation. Future works need to discriminate whether substrate binding or the transport (e.g. phosphorylation) of the carbohydrates is required. This question can be addressed by placing mutations within the phosphotransfer reaction site of EIIAB or by using carbohydrate mimetics that bind to EIIAB, but do not get transported. Furthermore, it remains to be tested whether the observed dynamic cluster response to substrates is a peculiar finding in *C. glutamicum* or whether this could be a general mechanism found in other bacteria such as firmicutes or enteric bacteria.

The small-conductance mechanosensitive channel YggB was found in our experiments to localize as foci in the cytoplasmic membrane, with no response to prolonged changes in NaCl concentration in medium. Future works might explore the reason behind the observed clustering, and possible responses to abrupt osmotic changes in medium by microfluidic chamber experiments. Other facets to be explored are the effects of overexpression of *yggB*, and deletion of other MS channels in YggB subcellular localization.

The membrane-associated protein DivIVA normally localizes in regions of negative curvature, where it works as a scaffold for different proteins related to cell growth and cell division. *In vivo* characterization of the mobility and kinetics of cellular components are essential to fully understand the biochemical processes occurring within bacterial cells. Our microscopy experiments with DivIVA-mCherry shed a light on how the kinetics of this important protein are affected by different shapes on the cytoplasmic membrane. However, FRAP studies are not able to resolve spatial scales below the diffraction limit of light microscopy, being useful for examining diffusive properties on the bacterial cell dimension scale. An interesting field for future research lies on single particle tracking, where the kinetics of DivIVA in regions of different degrees of negative curvature in L-form cells can be further and precisely analyzed in a short time scale.

Taken together, by the use of novel microscopy techniques, this work provides new insights into the subcellular localization and dynamics of membrane proteins of varied functions. The results presented here serve as starting points for several possible studies in different areas of the membrane proteome of *Corynebacterium glutamicum*.

6   Acknowledgements

7   References

A. Mrozik, Z. Piotrowska-Seget, S. Łabużek. 2004. 'Cytoplasmatic Bacterial Membrane Responses to Environmental Perturbations', *Polish Journal of Environmental Studies*, 13: 487-94.

Arndt, A., M. Auchter, T. Ishige, V. F. Wendisch, and B. J. Eikmanns. 2008. 'Ethanol catabolism in *Corynebacterium glutamicum*', *J Mol Microbiol Biotechnol*, 15: 222-33.

Arora, D., Y. Chawla, B. Malakar, A. Singh, and V. K. Nandicoori. 2018. 'The transpeptidase PbpA and noncanonical transglycosylase RodA of Mycobacterium tuberculosis play important roles in regulating bacterial cell lengths', *J Biol Chem*, 293: 6497-516.

Auchter, M., A. Cramer, A. Huser, C. Ruckert, D. Emer, P. Schwarz, A. Arndt, C. Lange, J. Kalinowski, V. F. Wendisch, and B. J. Eikmanns. 2011. 'RamA and RamB are global transcriptional regulators in *Corynebacterium glutamicum* and control genes for enzymes of the central metabolism', *J Biotechnol*, 154: 126-39.

Bach, J. N., and M. Bramkamp. 2013. 'Flotillins functionally organize the bacterial membrane', *Mol Microbiol*, 88: 1205-17.

Bach, J. N., G. Giacomelli, and M. Bramkamp. 2017. 'Sample Preparation and Choice of Fluorophores for Single and Dual Color Photo-Activated Localization Microscopy (PALM) with Bacterial Cells', *Methods Mol Biol*, 1563: 129-41.

Bagatolli, L. A., J. H. Ipsen, A. C. Simonsen, and O. G. Mouritsen. 2010. 'An outlook on organization of lipids in membranes: searching for a realistic connection with the organization of biological membranes', *Prog Lipid Res*, 49: 378-89.

Baumchen, C., E. Krings, S. Bringer, L. Eggeling, and H. Sahm. 2009. 'Myo-inositol facilitators IolT1 and IolT2 enhance D-mannitol formation from D-fructose in *Corynebacterium glutamicum*', *FEMS Microbiol Lett*, 290: 227-35.

Ben-Yehuda, Sigal, Masya Fujita, Xiaole Shirley Liu, Boris Gorbatyuk, Dunja Skoko, Jie Yan, John F. Marko, Jun S. Liu, Patrick Eichenberger, David Z. Rudner, and Richard Losick. 2005. 'Defining a Centromere-like Element in Bacillus subtilis by Identifying the Binding Sites for the Chromosome-Anchoring Protein RacA', *Molecular Cell*, 17: 773-82.

Berrier, C., M. Besnard, B. Ajouz, A. Coulombe, and A. Ghazi. 1996. 'Multiple mechanosensitive ion channels from Escherichia coli, activated at different thresholds of applied pressure', *J Membr Biol*, 151: 175-87.

Bertram, R., M. Schlicht, K. Mahr, H. Nothaft, M. H. Saier, Jr., and F. Titgemeyer. 2004. 'In silico and transcriptional analysis of carbohydrate uptake systems of Streptomyces coelicolor A3(2)', *J Bacteriol*, 186: 1362-73.

Besschetnova, T. Y., D. J. Montefusco, A. E. Asinas, A. L. Shrout, F. M. Antommattei, and R. M. Weis. 2008. 'Receptor density balances signal stimulation and attenuation in membrane-assembled complexes of bacterial chemotaxis signaling proteins', *Proc Natl Acad Sci U S A*, 105: 12289-94.

Blencke, H. M., G. Homuth, H. Ludwig, U. Mader, M. Hecker, and J. Stulke. 2003. 'Transcriptional profiling of gene expression in response to glucose in Bacillus subtilis: regulation of the central metabolic pathways', *Metab Eng*, 5: 133-49.

Bohm, K., F. Meyer, A. Rhomberg, J. Kalinowski, C. Donovan, and M. Bramkamp. 2017. 'Novel Chromosome Organization Pattern in Actinomycetales-Overlapping Replication Cycles Combined with Diploidy', *MBio*, 8.

Borngen, K., A. R. Battle, N. Moker, S. Morbach, K. Marin, B. Martinac, and R. Kramer. 2010. 'The properties and contribution of the *Corynebacterium glutamicum* MscS variant to fine-tuning of osmotic adaptation', *Biochim Biophys Acta*, 1798: 2141-9.

Börngen, Kirsten. 2009. *YggB of Corynebacterium glutamicum - Dual function in osmotic stress response and glutamate production*.

Bussmann, M., D. Emer, S. Hasenbein, S. Degraf, B. J. Eikmanns, and M. Bott. 2009. 'Transcriptional control of the succinate dehydrogenase operon sdhCAB of *Corynebacterium glutamicum* by the cAMP-dependent regulator GlxR and the LuxR-type regulator RamA', *J Biotechnol*, 143: 173-82.

Cai, M., D. C. Williams, Jr., G. Wang, B. R. Lee, A. Peterkofsky, and G. M. Clore. 2003. 'Solution structure of the phosphoryl transfer complex between the signal-transducing protein IIAGlucose and the cytoplasmic domain of the glucose transporter IICBGlucose of the Escherichia coli glucose phosphotransferase system', *J Biol Chem*, 278: 25191-206.

Cao, Y., X. Jin, E. J. Levin, H. Huang, Y. Zong, M. Quick, J. Weng, Y. Pan, J. Love, M. Punta, B. Rost, W. A. Hendrickson, J. A. Javitch, K. R. Rajashankar, and M. Zhou. 2011. 'Crystal structure of a phosphorylation-coupled saccharide transporter', *Nature*, 473: 50-4.

Card, G. L. 1973. 'Metabolism of phosphatidylglycerol, phosphatidylethanolamine, and cardiolipin of Bacillus stearothermophilus', *J Bacteriol*, 114: 1125-37.

Chavarría, Max, Gonzalo Durante-Rodríguez, Tino Krell, César Santiago, Jan Brezovsky, Jiri Damborsky, and Víctor de Lorenzo. 2014. 'Fructose 1-phosphate is the one and only physiological effector of the Cra (FruR) regulator of Pseudomonas putida', *FEBS Open Bio*, 4: 377-86.

Chen, Q., and O. Amster-Choder. 1998. 'BglF, the sensor of the bgl system and the beta-glucosides permease of Escherichia coli: evidence for dimerization and intersubunit phosphotransfer', *Biochemistry*, 37: 8714-23.

Claypool, S. M. 2009. 'Cardiolipin, a critical determinant of mitochondrial carrier protein assembly and function', *Biochim Biophys Acta*, 1788: 2059-68.

Clore, G. M., and V. Venditti. 2013. 'Structure, dynamics and biophysics of the cytoplasmic protein-protein complexes of the bacterial phosphoenolpyruvate: sugar phosphotransferase system', *Trends Biochem Sci*, 38: 515-30.

Cocaign, Muriel, Christophe Monnet, and Nic Lindley. 1993. *Batch kinetics of Corynebacterium glutamicum during growth on various carbon substrates: use of substrate mixtures to localise metabolic bottlenecks*.

Cramer, A., M. Auchter, J. Frunzke, M. Bott, and B. J. Eikmanns. 2007. 'RamB, the transcriptional regulator of acetate metabolism in *Corynebacterium glutamicum*, is subject to regulation by RamA and RamB', *J Bacteriol*, 189: 1145-9.

Cramer, A., R. Gerstmeir, S. Schaffer, M. Bott, and B. J. Eikmanns. 2006. 'Identification of RamA, a novel LuxR-type transcriptional regulator of genes involved in acetate metabolism of *Corynebacterium glutamicum*', *J Bacteriol*, 188: 2554-67.

Cui, C., D. O. Smith, and J. Adler. 1995. 'Characterization of mechanosensitive channels in Escherichia coli cytoplasmic membrane by whole-cell patch clamp recording', *J Membr Biol*, 144: 31-42.

Deutscher, J. 2008. 'The mechanisms of carbon catabolite repression in bacteria', *Curr Opin Microbiol*, 11: 87-93.

Deutscher, J., F. M. Ake, M. Derkaoui, A. C. Zebre, T. N. Cao, H. Bouraoui, T. Kentache, A. Mokhtari, E. Milohanic, and P. Joyet. 2014. 'The bacterial phosphoenolpyruvate:carbohydrate phosphotransferase system: regulation by protein phosphorylation and phosphorylation-

dependent protein-protein interactions', *Microbiol Mol Biol Rev*, 78: 231-56.

Deutscher, J., C. Francke, and P. W. Postma. 2006. 'How phosphotransferase system-related protein phosphorylation regulates carbohydrate metabolism in bacteria', *Microbiol Mol Biol Rev*, 70: 939-1031.

Dominguez, H., M. Cocaign-Bousquet, and Nic Lindley. 1997. *Simultaneous consumption of glucose and fructose from sugar mixtures during batch growth of Corynebacterium glutamicum*.

Dominguez, H., and N. D. Lindley. 1996. 'Complete Sucrose Metabolism Requires Fructose Phosphotransferase Activity in *Corynebacterium glutamicum* To Ensure Phosphorylation of Liberated Fructose', *Appl Environ Microbiol*, 62: 3878-80.

Donovan, C., and M. Bramkamp. 2009. 'Characterization and subcellular localization of a bacterial flotillin homologue', *Microbiology*, 155: 1786-99.

Donovan, C., A. Schauss, R. Kramer, and M. Bramkamp. 2013. 'Chromosome segregation impacts on cell growth and division site selection in *Corynebacterium glutamicum*', *PLoS One*, 8: e55078.

Donovan, C., B. Sieger, R. Kramer, and M. Bramkamp. 2012. 'A synthetic Escherichia coli system identifies a conserved origin tethering factor in Actinobacteria', *Mol Microbiol*, 84: 105-16.

Ducret, A., E. M. Quardokus, and Y. V. Brun. 2016. 'MicrobeJ, a tool for high throughput bacterial cell detection and quantitative analysis', *Nat Microbiol*, 1: 16077.

Edwards, D. H., and J. Errington. 1997. 'The Bacillus subtilis DivIVA protein targets to the division septum and controls the site specificity of cell division', *Mol Microbiol*, 24: 905-15.

Eikmanns, B. J. 1992. 'Identification, sequence analysis, and expression of a *Corynebacterium glutamicum* gene cluster encoding the three glycolytic enzymes glyceraldehyde-3-phosphate dehydrogenase, 3-phosphoglycerate kinase, and triosephosphate isomerase', *J Bacteriol*, 174: 6076-86.

Eikmanns, B. J., E. Kleinertz, W. Liebl, and H. Sahm. 1991. 'A family of *Corynebacterium glutamicum*/Escherichia coli shuttle vectors for cloning, controlled gene expression, and promoter probing', *Gene*, 102: 93-8.

References

Engels, V., S. N. Lindner, and V. F. Wendisch. 2008. 'The global repressor SugR controls expression of genes of glycolysis and of the L-lactate dehydrogenase LdhA in *Corynebacterium glutamicum*', *J Bacteriol*, 190: 8033-44.

Engels, V., and V. F. Wendisch. 2007. 'The DeoR-type regulator SugR represses expression of ptsG in *Corynebacterium glutamicum*', *J Bacteriol*, 189: 2955-66.

Epand, R. M., and R. F. Epand. 2009. 'Lipid domains in bacterial membranes and the action of antimicrobial agents', *Biochim Biophys Acta*, 1788: 289-94.

Erhardt, H., F. Dempwolff, M. Pfreundschuh, M. Riehle, C. Schafer, T. Pohl, P. Graumann, and T. Friedrich. 2014. 'Organization of the Escherichia coli aerobic enzyme complexes of oxidative phosphorylation in dynamic domains within the cytoplasmic membrane', *Microbiologyopen*, 3: 316-26.

Erni, B., and B. Zanolari. 1985. 'The mannose-permease of the bacterial phosphotransferase system. Gene cloning and purification of the enzyme IIMan/IIIMan complex of Escherichia coli', *J Biol Chem*, 260: 15495-503.

Erni, B., B. Zanolari, and H. P. Kocher. 1987. 'The mannose permease of Escherichia coli consists of three different proteins. Amino acid sequence and function in sugar transport, sugar phosphorylation, and penetration of phage lambda DNA', *J Biol Chem*, 262: 5238-47.

Evans, Glen A. 1990. 'Molecular cloning: A laboratory manual. Second edition. Volumes 1, 2, and 3. Current protocols in molecular biology. Volumes 1 and 2', *Cell*, 61: 17-18.

Farwick, M., R. M. Siewe, and R. Kramer. 1995. 'Glycine betaine uptake after hyperosmotic shift in *Corynebacterium glutamicum*', *J Bacteriol*, 177: 4690-5.

Francke, C., P. W. Postma, H. V. Westerhoff, J. G. Blom, and M. A. Peletier. 2003. 'Why the phosphotransferase system of Escherichia coli escapes diffusion limitation', *Biophys J*, 85: 612-22.

Francke, C., H. V. Westerhoff, J. G. Blom, and M. A. Peletier. 2002. 'Flux control of the bacterial phosphoenolpyruvate:glucose phosphotransferase system and the effect of diffusion', *Mol Biol Rep*, 29: 21-6.

Frunzke, J., V. Engels, S. Hasenbein, C. Gatgens, and M. Bott. 2008. 'Co-ordinated regulation of gluconate catabolism and glucose uptake in *Corynebacterium glutamicum* by two functionally equivalent

transcriptional regulators, GntR1 and GntR2', *Mol Microbiol*, 67: 305-22.

Gaigalat, L., J. P. Schluter, M. Hartmann, S. Mormann, A. Tauch, A. Puhler, and J. Kalinowski. 2007. 'The DeoR-type transcriptional regulator SugR acts as a repressor for genes encoding the phosphoenolpyruvate:sugar phosphotransferase system (PTS) in *Corynebacterium glutamicum*', *BMC Mol Biol*, 8: 104.

Galinier, A., and J. Deutscher. 2017. 'Sophisticated Regulation of Transcriptional Factors by the Bacterial Phosphoenolpyruvate: Sugar Phosphotransferase System', *J Mol Biol*, 429: 773-89.

Gavet, O., and J. Pines. 2010. 'Progressive activation of CyclinB1-Cdk1 coordinates entry to mitosis', *Dev Cell*, 18: 533-43.

Gerstmeir, R., A. Cramer, P. Dangel, S. Schaffer, and B. J. Eikmanns. 2004. 'RamB, a novel transcriptional regulator of genes involved in acetate metabolism of *Corynebacterium glutamicum*', *J Bacteriol*, 186: 2798-809.

Giacomelli, G. 2014. 'In vivo and in vitro characterization of *Corynebacterium glutamicum* DivIVA', *(Unpublished master thesis), Ludwig-Maximilians Universität München*.

Gidden, J., J. Denson, R. Liyanage, D. M. Ivey, and J. O. Lay. 2009. 'Lipid Compositions in Escherichia coli and Bacillus subtilis During Growth as Determined by MALDI-TOF and TOF/TOF Mass Spectrometry', *Int J Mass Spectrom*, 283: 178-84.

Goehring, N. W., D. Chowdhury, A. A. Hyman, and S. W. Grill. 2010. 'FRAP analysis of membrane-associated proteins: lateral diffusion and membrane-cytoplasmic exchange', *Biophys J*, 99: 2443-52.

Gorke, B., and J. Stulke. 2008. 'Carbon catabolite repression in bacteria: many ways to make the most out of nutrients', *Nat Rev Microbiol*, 6: 613-24.

Gourdon, P., and N. D. Lindley. 1999. 'Metabolic analysis of glutamate production by *Corynebacterium glutamicum*', *Metab Eng*, 1: 224-31.

Greenfield, D., A. L. McEvoy, H. Shroff, G. E. Crooks, N. S. Wingreen, E. Betzig, and J. Liphardt. 2009. 'Self-organization of the Escherichia coli chemotaxis network imaged with super-resolution light microscopy', *PLoS Biol*, 7: e1000137.

Hammond, R. K., and D. C. White. 1969. 'Formation of vitamin K2 isoprenologues by Staphylococcus aureus', *J Bacteriol*, 100: 573-8.

References

Heider, Sabine A. E., Natalie Wolf, Arne Hofemeier, Petra Peters-Wendisch, and Volker F. Wendisch. 2014. 'Optimization of the IPP Precursor Supply for the Production of Lycopene, Decaprenoxanthin and Astaxanthin by *Corynebacterium glutamicum*', *Frontiers in Bioengineering and Biotechnology*, 2.

Hiraoka, S., H. Matsuzaki, and I. Shibuya. 1993. 'Active increase in cardiolipin synthesis in the stationary growth phase and its physiological significance in Escherichia coli', *FEBS Lett*, 336: 221-4.

Huang, K. C., and K. S. Ramamurthi. 2010. 'Macromolecules that prefer their membranes curvy', *Mol Microbiol*, 76: 822-32.

Huber, F., and B. Erni. 1996. 'Membrane topology of the mannose transporter of Escherichia coli K12', *Eur J Biochem*, 239: 810-7.

Hvorup, R., A. B. Chang, and M. H. Saier, Jr. 2003. 'Bioinformatic analyses of the bacterial L-ascorbate phosphotransferase system permease family', *J Mol Microbiol Biotechnol*, 6: 191-205.

Ikeda, M. 2012. 'Sugar transport systems in *Corynebacterium glutamicum*: features and applications to strain development', *Appl Microbiol Biotechnol*, 96: 1191-200.

Ikeda, M., Y. Mizuno, S. Awane, M. Hayashi, S. Mitsuhashi, and S. Takeno. 2011. 'Identification and application of a different glucose uptake system that functions as an alternative to the phosphotransferase system in *Corynebacterium glutamicum*', *Appl Microbiol Biotechnol*, 90: 1443-51.

Ikeda, M., N. Noguchi, M. Ohshita, A. Senoo, S. Mitsuhashi, and S. Takeno. 2015. 'A third glucose uptake bypass in *Corynebacterium glutamicum* ATCC 31833', *Appl Microbiol Biotechnol*, 99: 2741-50.

Jolkver, E., D. Emer, S. Ballan, R. Kramer, B. J. Eikmanns, and K. Marin. 2009. 'Identification and characterization of a bacterial transport system for the uptake of pyruvate, propionate, and acetate in *Corynebacterium glutamicum*', *J Bacteriol*, 191: 940-8.

Joyce, G. H., R. K. Hammond, and D. C. White. 1970. 'Changes in membrane lipid composition in exponentially growing Staphylococcus aureus during the shift from 37 to 25 C', *J Bacteriol*, 104: 323-30.

Kalinowski, J., B. Bathe, D. Bartels, N. Bischoff, M. Bott, A. Burkovski, N. Dusch, L. Eggeling, B. J. Eikmanns, L. Gaigalat, A. Goesmann, M. Hartmann, K. Huthmacher, R. Kramer, B. Linke, A. C. McHardy, F. Meyer, B. Mockel, W. Pfefferle, A. Puhler, D. A. Rey, C. Ruckert, O. Rupp, H. Sahm, V. F. Wendisch, I. Wiegrabe, and A. Tauch. 2003. 'The complete *Corynebacterium glutamicum* ATCC 13032 genome

sequence and its impact on the production of L-aspartate-derived amino acids and vitamins', *J Biotechnol*, 104: 5-25.

Kawaguchi, H., A. A. Vertes, S. Okino, M. Inui, and H. Yukawa. 2006. 'Engineering of a xylose metabolic pathway in *Corynebacterium glutamicum*', *Appl Environ Microbiol*, 72: 3418-28.

Kawaguchi, H., K. Yoshihara, K. Y. Hara, T. Hasunuma, C. Ogino, and A. Kondo. 2018. 'Metabolome analysis-based design and engineering of a metabolic pathway in *Corynebacterium glutamicum* to match rates of simultaneous utilization of D-glucose and L-arabinose', *Microb Cell Fact*, 17: 76.

Kawamoto, H., T. Morita, A. Shimizu, T. Inada, and H. Aiba. 2005. 'Implication of membrane localization of target mRNA in the action of a small RNA: mechanism of post-transcriptional regulation of glucose transporter in Escherichia coli', *Genes Dev*, 19: 328-38.

Keilhauer, C., L. Eggeling, and H. Sahm. 1993. 'Isoleucine synthesis in *Corynebacterium glutamicum*: molecular analysis of the ilvB-ilvN-ilvC operon', *J Bacteriol*, 175: 5595-603.

Kiefer, P., E. Heinzle, O. Zelder, and C. Wittmann. 2004. 'Comparative metabolic flux analysis of lysine-producing *Corynebacterium glutamicum* cultured on glucose or fructose', *Appl Environ Microbiol*, 70: 229-39.

Koch-Koerfges, A., A. Kabus, I. Ochrombel, K. Marin, and M. Bott. 2012. 'Physiology and global gene expression of a *Corynebacterium glutamicum* DeltaF(1)F(O)-ATP synthase mutant devoid of oxidative phosphorylation', *Biochim Biophys Acta*, 1817: 370-80.

Kohl, T. A., and A. Tauch. 2009. 'The GlxR regulon of the amino acid producer *Corynebacterium glutamicum*: Detection of the corynebacterial core regulon and integration into the transcriptional regulatory network model', *J Biotechnol*, 143: 239-46.

Kotrba, P., M. Inui, and H. Yukawa. 2001. 'The ptsI gene encoding enzyme I of the phosphotransferase system of *Corynebacterium glutamicum*', *Biochem Biophys Res Commun*, 289: 1307-13.

Kramer, R., and C. Lambert. 1990. 'Uptake of glutamate in *Corynebacterium glutamicum*. 2. Evidence for a primary active transport system', *Eur J Biochem*, 194: 937-44.

Kramer, R., C. Lambert, C. Hoischen, and H. Ebbighausen. 1990. 'Uptake of glutamate in *Corynebacterium glutamicum*. 1. Kinetic properties and regulation by internal pH and potassium', *Eur J Biochem*, 194: 929-35.

Kramer, R., and S. Morbach. 2004. 'BetP of *Corynebacterium glutamicum*, a transporter with three different functions: betaine transport, osmosensing, and osmoregulation', *Biochim Biophys Acta*, 1658: 31-6.

Kuhlmann, N., D. P. Petrov, A. W. Henrich, S. N. Lindner, V. F. Wendisch, and G. M. Seibold. 2015. 'Transcription of malP is subject to phosphotransferase system-dependent regulation in *Corynebacterium glutamicum*', *Microbiology*, 161: 1830-43.

Kurokawa, T., and J. Sakamoto. 2005. 'Purification and characterization of succinate:menaquinone oxidoreductase from *Corynebacterium glutamicum*', *Arch Microbiol*, 183: 317-24.

Laloux, G., and C. Jacobs-Wagner. 2014. 'How do bacteria localize proteins to the cell pole?', *J Cell Sci*, 127: 11-9.

Lamanna, A. C., G. W. Ordal, and L. L. Kiessling. 2005. 'Large increases in attractant concentration disrupt the polar localization of bacterial chemoreceptors', *Mol Microbiol*, 57: 774-85.

Larisch, C., D. Nakunst, A. T. Huser, A. Tauch, and J. Kalinowski. 2007. 'The alternative sigma factor SigB of *Corynebacterium glutamicum* modulates global gene expression during transition from exponential growth to stationary phase', *BMC Genomics*, 8: 4.

Leaver, M., P. Dominguez-Cuevas, J. M. Coxhead, R. A. Daniel, and J. Errington. 2009. 'Life without a wall or division machine in Bacillus subtilis', *Nature*, 457: 849-53.

Lee, D. S., J. S. Park, Y. Kim, and H. S. Lee. 2014. '*Corynebacterium glutamicum* sdhA encoding succinate dehydrogenase subunit A plays a role in cysR-mediated sulfur metabolism', *Appl Microbiol Biotechnol*, 98: 6751-9.

Lee, J. K., M. H. Sung, K. H. Yoon, J. H. Yu, and T. K. Oh. 1994. 'Nucleotide sequence of the gene encoding the *Corynebacterium glutamicum* mannose enzyme II and analyses of the deduced protein sequence', *FEMS Microbiol Lett*, 119: 137-45.

Lee, Jung-Kee, Moon-Hee Sung, Ki-Hong Yoon, Jae-Gu Pan, Ju-Hyun Yu, and Tae-Kwang Oh. 1993. 'Cloning and Expression of the Gene Encoding Mannose Enzyme II of the *Corynebacterium glutamicum* Phosphoenolpyruvate-Dependent Phosphotransferase System in Escherichia coli', *Journal of Microbiology and Biotechnology*, 3: 1-5.

Lenarcic, R., S. Halbedel, L. Visser, M. Shaw, L. J. Wu, J. Errington, D. Marenduzzo, and L. W. Hamoen. 2009. 'Localisation of DivIVA by targeting to negatively curved membranes', *Embo j*, 28: 2272-82.

Lengeler, J. W. 2000. 'Metabolic networks: a signal-oriented approach to cellular models', *Biol Chem*, 381: 911-20.

Lengeler, J. W., and K. Jahreis. 2009. 'Bacterial PEP-dependent carbohydrate: phosphotransferase systems couple sensing and global control mechanisms', *Contrib Microbiol*, 16: 65-87.

Letek, Michal, Efrén Ordóñez, José Vaquera, William Margolin, Klas Flärdh, Luis M. Mateos, and José A. Gil. 2008. 'DivIVA is required for polar growth in the MreB-lacking rod-shaped actinomycete *Corynebacterium glutamicum*', *Journal of bacteriology*, 190: 3283-92.

Levina, N., S. Totemeyer, N. R. Stokes, P. Louis, M. A. Jones, and I. R. Booth. 1999. 'Protection of Escherichia coli cells against extreme turgor by activation of MscS and MscL mechanosensitive channels: identification of genes required for MscS activity', *Embo j*, 18: 1730-7.

Lindner, S. N., G. M. Seibold, A. Henrich, R. Kramer, and V. F. Wendisch. 2011. 'Phosphotransferase system-independent glucose utilization in corynebacterium glutamicum by inositol permeases and glucokinases', *Appl Environ Microbiol*, 77: 3571-81.

Litsanov, B., M. Brocker, and M. Bott. 2012. 'Toward homosuccinate fermentation: metabolic engineering of *Corynebacterium glutamicum* for anaerobic production of succinate from glucose and formate', *Appl Environ Microbiol*, 78: 3325-37.

Llorente-Garcia, I., T. Lenn, H. Erhardt, O. L. Harriman, L. N. Liu, A. Robson, S. W. Chiu, S. Matthews, N. J. Willis, C. D. Bray, S. H. Lee, J. Y. Shin, C. Bustamante, J. Liphardt, T. Friedrich, C. W. Mullineaux, and M. C. Leake. 2014. 'Single-molecule in vivo imaging of bacterial respiratory complexes indicates delocalized oxidative phosphorylation', *Biochim Biophys Acta*, 1837: 811-24.

Lopez, D., and R. Kolter. 2010. 'Functional microdomains in bacterial membranes', *Genes Dev*, 24: 1893-902.

Lopian, L., Y. Elisha, A. Nussbaum-Shochat, and O. Amster-Choder. 2010. 'Spatial and temporal organization of the E. coli PTS components', *EMBO J*, 29: 3630-45.

Lucena, D., M. Mauri, F. Schmidt, B. Eckhardt, and P. L. Graumann. 2018. 'Microdomain formation is a general property of bacterial membrane proteins and induces heterogeneity of diffusion patterns', *BMC Biol*, 16: 97.

Lux, R., K. Jahreis, K. Bettenbrock, J. S. Parkinson, and J. W. Lengeler. 1995. 'Coupling the phosphotransferase system and the methyl-

accepting chemotaxis protein-dependent chemotaxis signaling pathways of Escherichia coli', *Proc Natl Acad Sci U S A*, 92: 11583-7.

Lux, R., V. R. Munasinghe, F. Castellano, J. W. Lengeler, J. E. Corrie, and S. Khan. 1999. 'Elucidation of a PTS-carbohydrate chemotactic signal pathway in Escherichia coli using a time-resolved behavioral assay', *Mol Biol Cell*, 10: 1133-46.

Maki, Kimika, Kanako Uno, Teppei Morita, and Hiroji Aiba. 2008. 'RNA, but not protein partners, is directly responsible for translational silencing by a bacterial Hfq-binding small RNA', *Proceedings of the National Academy of Sciences*, 105: 10332-37.

Martinac, B., M. Buechner, A. H. Delcour, J. Adler, and C. Kung. 1987. 'Pressure-sensitive ion channel in Escherichia coli', *Proc Natl Acad Sci U S A*, 84: 2297-301.

Matsumoto, K., J. Kusaka, A. Nishibori, and H. Hara. 2006. 'Lipid domains in bacterial membranes', *Mol Microbiol*, 61: 1110-7.

Mercier, Romain, Yoshikazu Kawai, and Jeff Errington. 2014. 'General principles for the formation and proliferation of a wall-free (L-form) state in bacteria', *eLife*, 3: e04629.

Mileykovskaya, E., and W. Dowhan. 2005. 'Role of membrane lipids in bacterial division-site selection', *Curr Opin Microbiol*, 8: 135-42.

Mileykovskaya, E., I. Fishov, X. Fu, B. D. Corbin, W. Margolin, and W. Dowhan. 2003. 'Effects of phospholipid composition on MinD-membrane interactions in vitro and in vivo', *J Biol Chem*, 278: 22193-8.

Moker, N., M. Brocker, S. Schaffer, R. Kramer, S. Morbach, and M. Bott. 2004. 'Deletion of the genes encoding the MtrA-MtrB two-component system of *Corynebacterium glutamicum* has a strong influence on cell morphology, antibiotics susceptibility and expression of genes involved in osmoprotection', *Mol Microbiol*, 54: 420-38.

Moon, M. W., S. Y. Park, S. K. Choi, and J. K. Lee. 2007. 'The phosphotransferase system of *Corynebacterium glutamicum*: features of sugar transport and carbon regulation', *J Mol Microbiol Biotechnol*, 12: 43-50.

Muchova, K., E. Kutejova, D. J. Scott, J. A. Brannigan, R. J. Lewis, A. J. Wilkinson, and I. Barak. 2002. 'Oligomerization of the Bacillus subtilis division protein DivIVA', *Microbiology*, 148: 807-13.

Mueller, N. S., R. Wedlich-Soldner, and F. Spira. 2012. 'From mosaic to patchwork: matching lipids and proteins in membrane organization', *Mol Membr Biol*, 29: 186-96.

Nakamura, J., S. Hirano, H. Ito, and M. Wachi. 2007. 'Mutations of the *Corynebacterium glutamicum* NCgl1221 gene, encoding a mechanosensitive channel homolog, induce L-glutamic acid production', *Appl Environ Microbiol*, 73: 4491-8.

Neidhardt, Frederick C., and Roy Curtiss. 1996. *Escherichia coli and Salmonella : cellular and molecular biology* (ASM Press: Washington, D.C.).

Nijland, J. G., E. Vos, H. Y. Shin, P. P. de Waal, P. Klaassen, and A. J. Driessen. 2016. 'Improving pentose fermentation by preventing ubiquitination of hexose transporters in Saccharomyces cerevisiae', *Biotechnol Biofuels*, 9: 158.

Norris, V., P. Gascuel, J. Guespin-Michel, C. Ripoll, and M. H. Saier, Jr. 1999. 'Metabolite-induced metabolons: the activation of transporter-enzyme complexes by substrate binding', *Mol Microbiol*, 31: 1592-5.

Nothaft, H., S. Parche, A. Kamionka, and F. Titgemeyer. 2003. 'In vivo analysis of HPr reveals a fructose-specific phosphotransferase system that confers high-affinity uptake in Streptomyces coelicolor', *J Bacteriol*, 185: 929-37.

Nottebrock, D., U. Meyer, R. Kramer, and S. Morbach. 2003. 'Molecular and biochemical characterization of mechanosensitive channels in *Corynebacterium glutamicum*', *FEMS Microbiol Lett*, 218: 305-9.

Oguiza, J. A., A. T. Marcos, and J. F. Martin. 1997. 'Transcriptional analysis of the sigA and sigB genes of Brevibacterium lactofermentum', *FEMS Microbiol Lett*, 153: 111-7.

Ozcan, N., C. S. Ejsing, A. Shevchenko, A. Lipski, S. Morbach, and R. Kramer. 2007. 'Osmolality, temperature, and membrane lipid composition modulate the activity of betaine transporter BetP in *Corynebacterium glutamicum*', *J Bacteriol*, 189: 7485-96.

Parche, S., A. Burkovski, G. A. Sprenger, B. Weil, R. Kramer, and F. Titgemeyer. 2001. '*Corynebacterium glutamicum*: a dissection of the PTS', *J Mol Microbiol Biotechnol*, 3: 423-8.

Patek, M., and J. Nesvera. 2011. 'Sigma factors and promoters in *Corynebacterium glutamicum*', *J Biotechnol*, 154: 101-13.

Perozo, E., and D. C. Rees. 2003. 'Structure and mechanism in prokaryotic mechanosensitive channels', *Curr Opin Struct Biol*, 13: 432-42.

Pike, L. J. 2003. 'Lipid rafts: bringing order to chaos', *J Lipid Res*, 44: 655-67.

Prosser, G. A., and L. P. de Carvalho. 2013. 'Kinetic mechanism and inhibition of Mycobacterium tuberculosis D-alanine:D-alanine ligase by the antibiotic D-cycloserine', *FEBS J*, 280: 1150-66.

Quinn, P. J. 1981. 'The fluidity of cell membranes and its regulation', *Prog Biophys Mol Biol*, 38: 1-104.

Ramijan, K., E. Ultee, J. Willemse, Z. Zhang, J. A. J. Wondergem, A. van der Meij, D. Heinrich, A. Briegel, G. P. van Wezel, and D. Claessen. 2018. 'Stress-induced formation of cell wall-deficient cells in filamentous actinomycetes', *Nat Commun*, 9: 5164.

Ray, M. K., G. S. Kumar, and S. Shivaji. 1994. 'Phosphorylation of membrane proteins in response to temperature in an Antarctic Pseudomonas syringae', *Microbiology*, 140 (Pt 12): 3217-23.

Reinscheid, D. J., S. Schnicke, D. Rittmann, U. Zahnow, H. Sahm, and B. J. Eikmanns. 1999. 'Cloning, sequence analysis, expression and inactivation of the *Corynebacterium glutamicum* pta-ack operon encoding phosphotransacetylase and acetate kinase', *Microbiology*, 145 (Pt 2): 503-13.

Renner, L. D., and D. B. Weibel. 2012. 'MinD and MinE interact with anionic phospholipids and regulate division plane formation in Escherichia coli', *J Biol Chem*, 287: 38835-44.

Rohwer, J. M., N. D. Meadow, S. Roseman, H. V. Westerhoff, and P. W. Postma. 2000. 'Understanding glucose transport by the bacterial phosphoenolpyruvate:glycose phosphotransferase system on the basis of kinetic measurements in vitro', *J Biol Chem*, 275: 34909-21.

Rohwer, J. M., P. W. Postma, B. N. Kholodenko, and H. V. Westerhoff. 1998. 'Implications of macromolecular crowding for signal transduction and metabolite channeling', *Proc Natl Acad Sci U S A*, 95: 10547-52.

Rothe, F. M., C. Wrede, M. Lehnik-Habrink, B. Gorke, and J. Stulke. 2013. 'Dynamic localization of a transcription factor in Bacillus subtilis: the LicT antiterminator relocalizes in response to inducer availability', *J Bacteriol*, 195: 2146-54.

Ruffert, S., C. Lambert, H. Peter, V. F. Wendisch, and R. Kramer. 1997. 'Efflux of compatible solutes in *Corynebacterium glutamicum* mediated by osmoregulated channel activity', *Eur J Biochem*, 247: 572-80.

Russell N.J., Sandercock S.P. 1980. 'The regulation of bacterial membrane fluidity by modification of phospholipid fatty acyl chain length.' in Arnisa Kuksis Morris Kates (ed.), *Membrane Fluidity: Biophysical*

Techniques and Cellular Regulation (The Humana Press, inc.: Clifton, New Jersey).

Russell, Nicholas J. 1984. 'Mechanisms of thermal adaptation in bacteria: blueprints for survival', *Trends in Biochemical Sciences*, 9: 108-12.

Saier, M. H., Jr., and T. M. Ramseier. 1996. 'The catabolite repressor/activator (Cra) protein of enteric bacteria', *J Bacteriol*, 178: 3411-7.

Sasaki, M., H. Teramoto, M. Inui, and H. Yukawa. 2011. 'Identification of mannose uptake and catabolism genes in *Corynebacterium glutamicum* and genetic engineering for simultaneous utilization of mannose and glucose', *Appl Microbiol Biotechnol*, 89: 1905-16.

Schafer, A., A. Tauch, W. Jager, J. Kalinowski, G. Thierbach, and A. Puhler. 1994. 'Small mobilizable multi-purpose cloning vectors derived from the Escherichia coli plasmids pK18 and pK19: selection of defined deletions in the chromosome of *Corynebacterium glutamicum*', *Gene*, 145: 69-73.

Schindelin, J., I. Arganda-Carreras, E. Frise, V. Kaynig, M. Longair, T. Pietzsch, S. Preibisch, C. Rueden, S. Saalfeld, B. Schmid, J. Y. Tinevez, D. J. White, V. Hartenstein, K. Eliceiri, P. Tomancak, and A. Cardona. 2012. 'Fiji: an open-source platform for biological-image analysis', *Nat Methods*, 9: 676-82.

Schroder, J., and A. Tauch. 2010. Transcriptional regulation of gene expression in *Corynebacterium glutamicum*: the role of global, master and local regulators in the modular and hierarchical gene regulatory network, *FEMS Microbiol Rev*, 34: 685-737.

Schumacher, M. A., G. Seidel, W. Hillen, and R. G. Brennan. 2007. 'Structural mechanism for the fine-tuning of CcpA function by the small molecule effectors glucose 6-phosphate and fructose 1,6-bisphosphate', *J Mol Biol*, 368: 1042-50.

Shah, A., B. Blombach, R. Gauttam, and B. J. Eikmanns. 2018. The RamA regulon: complex regulatory interactions in relation to central metabolism in *Corynebacterium glutamicum*, *Appl Microbiol Biotechnol*, 102: 5901-10.

Sieger, B., and M. Bramkamp. 2014. 'Interaction sites of DivIVA and RodA from *Corynebacterium glutamicum*', *Front Microbiol*, 5: 738.

Sieger, B., K. Schubert, C. Donovan, and M. Bramkamp. 2013. 'The lipid II flippase RodA determines morphology and growth in *Corynebacterium glutamicum*', *Mol Microbiol*, 90: 966-82.

Singh, K. D., M. H. Schmalisch, J. Stulke, and B. Gorke. 2008. 'Carbon catabolite repression in Bacillus subtilis: quantitative analysis of repression exerted by different carbon sources', *J Bacteriol*, 190: 7275-84.

Stahlberg, H., E. Kutejova, K. Muchova, M. Gregorini, A. Lustig, S. A. Muller, V. Olivieri, A. Engel, A. J. Wilkinson, and I. Barak. 2004. 'Oligomeric structure of the Bacillus subtilis cell division protein DivIVA determined by transmission electron microscopy', *Mol Microbiol*, 52: 1281-90.

Tanaka, Y., N. Okai, H. Teramoto, M. Inui, and H. Yukawa. 2008. 'Regulation of the expression of phosphoenolpyruvate: carbohydrate phosphotransferase system (PTS) genes in *Corynebacterium glutamicum* R', *Microbiology*, 154: 264-74.

Tauch, A., O. Kirchner, B. Loffler, S. Gotker, A. Puhler, and J. Kalinowski. 2002. 'Efficient electrotransformation of corynebacterium diphtheriae with a mini-replicon derived from the *Corynebacterium glutamicum* plasmid pGA1', *Curr Microbiol*, 45: 362-7.

Veldhuis, G., M. Hink, V. Krasnikov, G. van den Bogaart, J. Hoeboer, A. J. Visser, J. Broos, and B. Poolman. 2006. 'The oligomeric state and stability of the mannitol transporter, EnzymeII(mtl), from Escherichia coli: a fluorescence correlation spectroscopy study', *Protein Sci*, 15: 1977-86.

Viana, R., V. Monedero, V. Dossonnet, C. Vadeboncoeur, G. Perez-Martinez, and J. Deutscher. 2000. 'Enzyme I and HPr from Lactobacillus casei: their role in sugar transport, carbon catabolite repression and inducer exclusion', *Mol Microbiol*, 36: 570-84.

Wendisch, V. F., A. A. de Graaf, H. Sahm, and B. J. Eikmanns. 2000. 'Quantitative determination of metabolic fluxes during coutilization of two carbon sources: comparative analyses with *Corynebacterium glutamicum* during growth on acetate and/or glucose', *J Bacteriol*, 182: 3088-96.

Wendisch, V. F., M. Spies, D. J. Reinscheid, S. Schnicke, H. Sahm, and B. J. Eikmanns. 1997. 'Regulation of acetate metabolism in *Corynebacterium glutamicum*: transcriptional control of the isocitrate lyase and malate synthase genes', *Arch Microbiol*, 168: 262-9.

Woo, H. M., S. Noack, G. M. Seibold, S. Willbold, B. J. Eikmanns, and M. Bott. 2010. 'Link between phosphate starvation and glycogen metabolism in *Corynebacterium glutamicum*, revealed by metabolomics', *Appl Environ Microbiol*, 76: 6910-9.

Zhuang, K., G. N. Vemuri, and R. Mahadevan. 2011. 'Economics of membrane occupancy and respiro-fermentation', *Mol Syst Biol*, 7: 500.

Gustavo Martins

EDUCATION

2015 - 2019: PhD degree in Molecular Microbiology. LMU Munich, Germany

2012 - 2014: Master Degree in Plant Biology. Federal University of Espirito Santo, Brazil

2007 - 2011: Bachelor Degree in Biology. Federal University of Espirito Santo, Brazil

_____

EXPERIENCE

Apr 2015 - present date	PhD student - LMU Munich, Microbiology, Marc Bramkamp Lab
Jun 2014 - Dec 2014	Biology tutor. UP - Uniao de Professores High School
Sep 2013 - Feb 2014	Teaching assistant / tutor in the course Taxonomy of Cryptogams. Federal University of Espirito Santo, Brazil
Mar 2009 - Dec 2011	Scientific Initiation internship. Federal University of Espirito Santo, Brazil

_____

UNDERGRADUATE RESEARCH PROJECTS

2012 - Effects of nitrogen depletion on lipid and biomass production of three microalgae. Federal University of Espirito Santo. Master thesis project with Prof. Dr. Valéria de Oliveira Fernandes.

2010 - Epiphytic algae diversity of the coastal environment of Espirito Santo. Federal University of Espirito Santo. Scientific initiation / Bachelor thesis project with Prof. Dr. Diógina Barata.

2009 - Citogenetics of Ephemeroptera. Federal University of Espírito Santo. Scientific initiation project with Prof. Dr. Vander Calmon Tosta.

_____

PUBLICATIONS
Martins, G. B., Giacomelli, G., Goldbeck, O., Seibold, G. M., Bramkamp, M. 2019. Substrate-dependent cluster density dynamics of *Corynebacterium glutamicum* phosphotransferase system permeases. Mol Microbiol, 111(5):1335-1354

Martins, G.B., Fernandes, V.O. 2016. Effects of nitrogen depletion on lipid and biomass production of three microalgae. Iheringia, 71(2): 117-123.
_____

LANGUAGES
Portuguese: Native
English: Fluent
German: Intermediate
Italian: Intermediate